CHLORIDE CONDUCTANCE IN XENOPUS LAEVIS

SKELETAL MUSCLE MEMBRANE

by

Donald Doo Fuey Loo

B.Sc., University of British Columbia, 1970

M.Sc., University of British Columbia, 1972

A THESIS SUBMITTED IN PARTIAL FULFILMENT OF

THE REQUIREMENTS FOR THE DEGREE OF

DOCTOR OF PHILOSOPHY
in
THE FACULTY OF GRADUATE STUDIES

in the Institute

of Applied Mathematics and Statistics

and the Department of Physiology

We accept this thesis as conforming to the required

standard.

THE UNIVERSITY OF BRITISH COLUMBIA

September, 1978

In presenting this thesis in partial fulfilment of the requirements for

an advanced degree at the University of British Columbia, I agree that

the Library shall make it freely available for reference and study.

I further agree that permission for extensive copying of this thesis

for scholarly purposes may be granted by the Head of my Department or

by his representatives. It is understood that copying or publication

of this thesis for financial gain shall not be allowed without my

written permission.

Department of __Mathematics__

The University of British Columbia
2075 Wesbrook Place
Vancouver, Canada
V6T 1W5

Date __Oct, 11, 1978__

ABSTRACT

The chloride current-voltage characteristics of the membrane

of sartorius fibers from Xenopus laevis were studied using a three

microelectrode voltage clamp system.

In fibers with normal resting potentials (-70 to -90 mV) and

in fibers depolarized in 115 mM KCl (resting potential -20 mV) the

direction and degree of steady state rectification depended on extra-

cellular pH. In alkaline solutions (pH 8.4) the current rectified

outwards; with large hyperpolarizations the current recorded in normally

polarized fibers was sometimes seen to diminish as the voltage was

made extremely negative (the current-voltage relation exhibited a

negative slope). In the depolarizing region (in depolarized fibers)

the slope of the I-V relation became constant (limiting conductance)

in alkaline solutions. In acid solutions (pH 5.4) the current rectified

inwards with hyperpolarization and reached a limiting value with

depolarization.

Chloride currents decay ('inactivate') following changes of

membrane potential from the resting potential (for both polarized

and depolarized fibers). The kinetics of current relaxation exhibited

voltage-dependent time constants depending on the size of the voltage

step with a sensitivity of about -1.5 msec/mV but were independent

of absolute membrane potential and external pH.

Inactivation of chloride conductance was studied in two-pulse (conditioning (V_1) and test (V_2), pulses) voltage clamp experiments. In variable V_1 experiments the dependence of the initial current at the onset of V_2 was sigmoidally related to V_1 (inactivation relation). The slope of the inactivation relation was twice as steep in acid as in alkaline solutions, but was independent of the resting potential. In variable V_2 experiments, the current-voltage relation was linear over a wide voltage range and for different values of V_1, the instantaneous I-V relations converged in the outward current region; they also had zero-current potentials that became increasingly negative with respect to the holding potential as V_1 was made negative.

Instantaneous chloride currents and the kinetics of current relaxation were found to depend on initial conditions when the membrane potential was changed under non-stationary conditions. The inactivation and recovery of initial current had similar timecourses as did the prolongation and recovery of the time constants. Initial currents recovered from conditioning with an exponential or sigmoid timecourse. Relaxation time constants exhibited a similar recovery pattern. The decline of initial current was initially exponentially dependent on the duration of conditioning. The time constant increased sigmoidally, or exponentially as the duration of conditioning increased.

Using the data from variable conditioning step and variable test step experiments a manifold (or state space representation) was constructed that enables much of the current-voltage behavior of the chloride permeation system to be predicted. Currents recorded

in voltage clamp experiments can be visualized as time-dependent flows along trajectories that are determined by the voltage. The rectification of the steady state and instantaneous current-voltage relations are related to the dispersion of the trajectories. The dependence of time constants of current transients can also be accounted for by the manifold.

The results are examined in light of models for channel behavior. The instantaneous I-V characteristics exhibit some properties of channels of the electrodiffusion type. The steady state current-voltage relations are qualitatively similar to those of a model incorporating a particle within the chloride channel that either blocks or unblocks it depending on the extracellular pH. The dependence of relaxation kinetics on the size of the voltage step and on initial conditions suggest the participation of a molecule acting in a catalytic role controlling the relaxation of current transients.

ACKNOWLEDGEMENTS

I am deeply indebted to, and it gives me the greatest pleasure to thank Drs. P. Vaughan and J. McLarnon for their technical assistance with the experiments and whose comments and suggestions were most helpful during the writing of this thesis.

The intellectual stimuli and encouragement provided by my friend and advisor, Dr. P. Vaughan, are beyond thanks.

The financial support from the Muscular Dystrophy Association of Canada and the University of British Columbia is gratefully acknowledged.

Preface

In this thesis the mechanism of passive chloride transport across amphibian skeletal muscle fibers is examined.

At the resting membrane potential chloride is the most permeant ion in amphibian skeletal muscle membrane accounting for about two-thirds of the total ionic conductance (Hodgkin and Horowicz, 1959). It plays a physiologically important role in muscle in the regulation of the resting potential and during electrical activity, the repolarization of the membrane is greatly accelerated by the high conductance (Hutter and Noble, 1960; Horowicz, 1964).

When the trans-membrane potential is altered in voltage clamp experiments, chloride currents exhibit voltage and time dependent relaxations having a complex dependence on the pH of the bathing environment (Warner, 1972). Although the physiological significance of chloride relaxations is not understood, an increased appreciation of the physical and chemical processes involved in ion translocation across cell membranes can be gained from a study of the voltage and time dependence of chloride currents.

The dissertation has been divided into four parts. First the background and rationale for the investigation is presented. Experimental results are then described in Chapter 2. In the third chapter, a geometric representation of the data is presented and finally in Chapter 4, some theoretical models for chloride transport are examined.

TABLE OF CONTENTS

LIST OF TABLES

LIST OF FIGURES

LIST OF FIGURES (continued)

LIST OF FIGURES (continued)

LIST OF FIGURES (continued)

LIST OF FIGURES (continued)

Chapter I

Introduction and Methods

Background

Early studies on ion permeation showed that membranes in general behaved as though they have negative fixed charge and would permit the passage of cations and exclude anions (Michaelis, 1926). Observations on skeletal muscle were compatible with these views of low anion permeability since changes in external chloride concentration on substitution by various lyotropic anions produced small changes in the transmembrane potential (Hober, 1904 ; Fenn, 1936; Horowicz, 1964).

However, in their study of the distribution of potassium and chloride across frog skeletal muscle, Boyle and Conway (1941) found that the resting muscle was permeable to chloride and other anions of small ionic radius: the Nernst equation was satisfied for both potassium and chloride. Since this pioneering work of Boyle and Conway the chloride permeation system in frog twitch muscles has been extensively studied and three interesting properties have emerged. First, the presence of any one of the anions in the lyotropic series $(Br^-, NO_3^-, I^-, ClO_4^-$ and $CNS^-)$ reduces the fluxes of chloride (Harris, 1958; Adrian, 1961; Hutter and Warner, 1967c; Moore, 1969) and electrical conductance (Hutter and Padsha, 1957; Hutter and Warner, 1967a). These anions have been found to have very little or no effects on Na^+ and K^+ movements (Edwards, Harris and Nishie, 1957). The relative magnitude of the membrane resistance when the chloride in the Ringer's solution is replaced by the lyotropic anions Br^-, NO_3^- , and I^- is (Hutter and Padsha, 1959):

$$Cl^- : Br^- : NO_3^- : I^- = 1.0 : 1.5 : 2.0 : 2.3$$

Second, the chloride permeability is affected by variations in external pH: in acid solutions, the chloride permeability is low; in alkaline solutions it is high (Hutter and Warner, 1967a,b; Moore, 1969). The dependence of permeability on pH has been seen to be sigmoid (S-shaped) with the region of sharpest transition close to pH 7 (Hutter and Warner, 1967a). Variations in the pH of Ringer's solution from 5.0 to 9.8 caused a three fold increase in membrane conductance. The anion permeability sequence is also markedly affected by variations in external pH (Hutter, deMello and Warner, 1968; Hestenes and Woodbury, 1972; Woodbury and Miles, 1973): In alkaline solutions (pH 9.8) the sequence is $Cl^- > Br^- > NO_3^- > I^-$ and is reversed in acid solutions (pH 5.0) $I^- > NO_3^- > Br^- > Cl^-$ (Hutter, deMello and Warner, 1968). Third, the chloride conductance has been found to be voltage dependent (Hutter and Warner, 1972). Hodgkin and Horowicz (1959) and subsequently other workers (Adrian, 1961; Harris, 1963; Hutter and Warner, 1972) found that chloride movements in frog twitch fibers in neutral Ringer's solution (pH 7.2-7.4) could be empirically described by the constant field theory (Goldman, 1943; Hodgkin and Katz, 1949). Subsequently the constant field theory has been found to be inadequate to account for chloride permeation at other values of the pH. The dependence of the steady state chloride current on voltage is strongly dependent on the external pH: in alkaline solutions, the current reaches a limiting maximum value for large hyperpolarizations whereas in acid solutions, the current continues to increase with hyperpolarizing voltages (Hutter and Warner,

1972).

Attempts by different workers to study the pH dependence of anionic conductance and anionic interactions have yielded conflicting results:

From a study of the inhibitory effect of the metallic ions copper and zinc on chloride efflux and the near neutral pK of the pH-dependence of chloride conductance, Hutter and Warner (1967c) hypothesized that an imidazole group controls chloride permeability. However, this has been questioned recently by Stephenson and Wood-bury (1976) who found that the enthalpy of the imidazole group of histidine (+8 Kcal/mole) is much different from the enthalpy values (greater than -20 Kcal/mole) for the reaction: $HS \rightleftharpoons H + S$ (S is the binding site for chloride conductance).

Hutter, deMello and Warner (1969) attempted to account for the reversal in the anion selectivity sequences by the field strength theory (Eisenman, 1961). They postulated that the cationic field strength of the sites controlling anion permeation increases as the pH of the bathing solution decreases. The selectivity sequence in alkaline solutions is governed by a site with weak field strength and in acid solutions, by a site with strong field strength. For instance, if a monopolar electrode cationic site is assumed, then the ionic radius in acid solutions is less than .65 A^o and the ionic radius in alkaline solutions lies between .65-.87 A^o (Wright and Diamond, 1977; Fig. 15). In order to account for the impediment of chloride movement by other anions, the permeability of an ion through the membrane was assumed to decrease with the strength of its binding

to membrane sites. A prediction of this theory is that fluoride should be the most permeable anion in alkaline solutions, and chloride should interfere with fluoride movement. However, Hestenes and Woodbury (1972) obtained the selectivity sequence: $Cl^- > Br^- > I^- > F^-$ at pH 9 and fluoride was found not to interfere with chloride movement. Moreover contrary to Hutter, deMello and Warner(1969), Hestenes and Woodbury reported no changes in the selectivity sequence at pH 5.0. Interestingly, the selectivity sequence of anions $(Cl^- > Br^- > I^- \geqslant CH_3SO_4^-)$ in alkaline solutions in mammalian diaphragm fibers has been found to be similar to frog twitch fibers (Palade and Barchi, 1977). As in amphibian fibers, the conductance of all permeant anions was found to decrease when the bathing fluid is made acid. However the reduction of each anion conductance was proportional and the sequence remained unchanged, whereas Hutter, deMello and Warner (1969) reported a disproportionately larger reduction of the chloride conductance as compared to the other anions, hence their observation that selectivity sequence reverses in acid solutions. Since the work of Hutter, deMello and Warner (1969) is the only report of a selectivity sequence reversal with pH, further work is necessary for clarification of the different observations of Hutter et al (1969) and Hestenes and Woodbury (1972).

The two recent studies on chloride transport by Woodbury and Miles (1972) arrived at different conclusions concerning the mechanism of chloride transport.

Warner (1972) suggested that the pH dependent rectification of the steady state chloride current-voltage relations is analogous to that obtained by Sandblom, Eisenman and Walker (1967) for a model

incorporating mobile charged carriers. Other similarities between the chloride conductance and the model of mobile charged carriers include linear instantaneous current-voltage relations, the presence of 'after-current' after a conditioning voltage prepulse; and a disagreement between permeability coefficients obtained by electrical conductance methods and by flux measurements (Adrian, 1961; Hutter and Warner, 1967a).

Woodbury and co-workers (Hestenes and Woodbury, 1972,1973; Woodbury and Miles, 1973; Parker and Woodbury, 1976; Stephenson and Woodbury, 1976) have presented evidence supporting a channel or pore hypothesis: a family of organic ('benzoate-like') anions whose molecular structure indicates a hydrophobic region and a carboxylate group (for instance, benzoate, valerate, butyrate, proprionate, formate, acetate) was found to have permeability behaviour opposite to that of chloride--their permeability increased as the pH was decreased (Woodbury and Miles, 1973). The permeabilities of these organic anions are lower than any of the lyotropic anions but they did not block chloride movement. The correlation between the sizes of their hydrophobic moieties and their sequence of conductance led to the postulate that these ions interact with a hydrophobic region of the membrane near the site of a rate limiting step. As a result of the interaction, the penetration of 'benzoate-like' anions through the membrane is facilitated. Moreover, similarities in the inhibitory effect of zinc ions on chloride and 'benzoate-like' ions suggest that they use the same ionic channels (Woodbury and Miles, 1973).

In order to pursue a more detailed discussion of the mechanism of
chloride transport as well as to describe the objective of our
experiments, a brief review of ion transport mechanisms across mem-
brane is required.

Ion transport mechanisms

Early quantitative descriptions of ion transport across membranes
were based on the work of Nernst (1889) and Planck (1890) on the
diffusion of ions in electrolytes (Cole, 1968). The interiors of
membranes were idealized as homogenous, and isotropic with a position
independent dielectric constant, and ionic movement within them was
viewed as the resultant of two forces--a concentration dependent
diffusion current and an ionic current driven by the electric field
(Goldman, 1943; Teorell, 1953).

With our increasing understanding of the structure of the cell mem-
brane, and the recognition that it is a very poor conductor composed
principally of lipids (Singer and Nicholson, 1972) our views on
transport mechanisms have changed quite radically. Ion transport
across cell membranes is now postulated to be mediated by special
localized proteinaceous structures within the lipid mosaic. Although
no transport mechanism has been worked out in detail, there is much
evidence (Armstrong, 1975a) supporting the hypothesis that some of the
specialized protein subunits form 'pores' across membranes, or
alternatively, they can act as 'carriers' for the transport of ions.
Much of our present understanding of ion transport across cell mem-
branes has been gained from a study of model systems such as lipid
bilayers and the transport of ions across them by compounds that form

pores across the bilayer, and those that act as carriers of ions (Hladky and Haydon, 1972; Eisenman et al, 1978).

Pores and carriers exhibit many common electrical properties. Studies on compounds that form channels and those that act as carriers in artificial membranes (Haydon and Hladky, 1972; Eisenman et al, 1967) have shown that macroscopic conductance (conductance from a collection of channels or pores) can be a highly non-linear function of membrane potential (Latorre et al, 1975; Haydon and Hladky 1972; Bamberg and Lauger, 1973) and that conductances undergo relaxations when the transmembrane potential is suddenly perturbed (Frehland and Lauger, 1974; Latorre et al, 1975; Lauger and Stark, 1970; Laprade et al, 1974; Bamberg and Lauger, 1973; Neher and Stevens, 1977). All of these properties have been observed in natural membrane transport systems.

There are, at the present time, two available methods for the determination of whether a particular transport mechanism utilizes a carrier or a pore. The first method, introduced by Krasne, Eisenman and Szabo (1971) studies the temperature dependence of the permeation system and has been successfully applied to artificial lipid bilayer membranes (Krasne et al, 1971) but not to cell membranes. The membrane is 'frozen' to temperatures lower than the lipid transition temperature and since carrier mobilities within lipid membranes are very dependent on lipid motions, they are drastically reduced upon freezing the lipid. Transport of ions via pores, on the other hand, is relatively independent of the transition temperature of the lipids (Krasne et al, 1971). In the second method, the turnover number, that is, the maximum transport rate of an individual carrier or the maximum number of ions crossing a

single channel, is determined. In artificial membranes, in which

known concentrations of ion carriers have been dissolved, transport

numbers of the order of 10^4 ions/sec have been observed (Lauger, 1972).

In other systems where pores are known to form across membranes, the

transport numbers are of the order of 10^6 ions/sec (Armstrong, 1975a,b).

At the present time, the strongest evidence for a particular

transport process being via a carrier or a pore is the determination of

the turnover number. In order to determine the turnover number, an

estimate of the density of conducting units (Hille, 1970; Keynes,

Ritchie and Rojas, 1971; Colquhound et al, 1974; Almers and Levinson,

1975) is required. Alternately, direct measurement of a single unit

conductance (Hladky and Haydon, 1972; Krawczyk, 1978) or noise analysis

(Anderson and Stevens, 1973; Neher and Stevens, 1977) may be used.

However when the turnover number is unavailable, as is the case with

anions in amphibian twitch fibers, we have to rely on models that are

based on analogies between properties of the anion transport system

and the properties of transport systems that are known carriers or

pores. Unfortunately, this does not yield unique answers. For instance,

the carrier hypothesis for chloride was based on the similarities

between the rectifications of the instantaneous and steady-state current

voltage relations of chloride and mobile charged carriers (Warner, 1972;

Sandblom, Eisenman and Walker, 1967). On the other hand, chloride

movement is interfered with by the lyotropic anions (the mechanism of

this interaction is not known) and ionic interference and block has

been observed in the potassium (Hodgkin and Keynes, 1955; Chandler and

Meves, 1965a;Bezanilla and Armstrong, 1972; French and Adelman, Jr., 1976),

sodium (Chandler and Meves, 1965a,b; Hille,1971, 1975a, 1975b; Woodhull,

1973), calcium (Hagiwara and Takahashi, 1967; Hagiwara, Toyama, and

Hayashi, 1971) channels, and channels in lipid bilayer membranes (Hladky

and Haydon, 1972; Bamberg and Lauger, 1977; Eisenman et al, 1978).

Woodbury and Miles (1973) have postulated that hydrophobic interactions

play a role in determining the conductance sequence of the anion

channel in frog twitch muscle membranes similar to the apparently

accessible hydrophobic region of the membrane in the vicinity of the

inner mouth of the potassium channel (Armstrong, 1969, 1971; Armstrong

and Hille, 1972).

The energetic cost of ionic transport across membranes is

represented by a series of activation energy barriers with successive

equilibrium positions at potential energy minima (Glasstone, Laidler and

Eyring, 1941; Johnson, Eyring and Polissar, 1954 ; Parlin and Eyring, 1954;

Ciani, 1965; Lauger, 1973; Stark, 1973). When the transport mechanism is

a pore, these minima may be imagined as the places where the ion is in

an energetically favourable position with respect to one or several

coordinating ligands. The activating barrier between successive minima

may be electrostatic in origin such as the interaction of the permeating

ion with a charged or dipolar side group within the pore. In the event

that the transport mechanism is via a carrier, the sequence of activating

barriers could represent successively the activating energy of the

association between ion and carrier at the membrane surface, the

diffusion and migration of carrier-ion complex across the interior of

the membrane, and the dissociation energy of the ion-carrier complex.

Experimental aims and objectives.

The objective of our experiments was to investigate some of the implications of the channel hypothesis for chloride permeation theory in amphibian twitch fibers.

The available experimental evidence on chloride transport does not selectively support a channel (or alternatively, a carrier) hypothesis and exclude the other. However, a channel hypothesis is more likely in view of the interaction of anions (Harris, 1958; Moore, 1959) and the hypothesized action of the 'benzoate-like' anions (Woodbury and Miles, 1973). The motivating question for our experiments was the following: suppose chloride translocation is via a pore, what are some of the chemical and physical processes that occur within the pore? Even though the question is formulated in terms of a pore, an analogous formulation can also be applied to carriers.

Partial answers to these questions have been provided by Warner (1972), who found, using voltage clamp experiments, that the chloride conductance is time dependent. In response to hyperpolarizing voltage steps, the chloride currents also depended on external pH: in neutral and alkaline solutions, the current decayed from an instantaneous to a steady value whereas in acid solutions, the transients were biphasic, first exhibiting a fall which was then followed by a subsequent rise to a steady value.

If the transient properties are interpreted using a channel hypothesis, and since the decaying current transients have comparably large time constants (300 milliseconds, Warner, 1972) as compared with

ionic redistribution times within a channel (less than 1 millisecond), the current transients may be attributed to movement or re-orientation of macromolecules within a channel or alternatively, to the number of conducting channels changing with voltage and time.

In the study of electrical characteristics of biological and lipid bilayer membranes, rectification phenomena are commonly encountered (Katz, 1948; Hodgkin and Huxley, 1952; Adrian, 1969; Haydon and Hladky, 1972). Since membrane conductance may depend both on the number of conducting channels and the conductance of single channels, variations in the number of conducting channels or in the conductance of a single channel with voltage can result in non-linear current-voltage relations when current is measured from a family of channels. The dependence of the conductance of a single channel on voltage also depends on the profile of the sequence of activating energy barriers within the pore (Parlin and Eyring, 1954; Woodbury, 1971; Hille, 1975b). If the above qualitative points of view were adopted for the chloride permeating system, then on the application of hyperpolarizing voltage steps from a fixed reference potential (such as the resting potential), the instantaneous current- voltage relation indicates the dependence of a single channel on voltage. The subsequent current transients may reflect a decrease either in the number of conducting channels or the conductance of each channel or erhaps both. The nature of the relaxation processes involved in the chloride permeating systems may be studied by determining the voltage and time dependence of the current transients.

When two voltage pulses are applied in succession, the instantaneous currents corresponding to the second pulse (test pulse) indicate the state

of the channel at the termination of the previous conditioning pulse.

Finally, the state of the channel during transitions may be studied by applying voltage perturbations under non-stationary conditions such as during a fall (or a rise) in current. The dependence of the instantaneous current on voltage at the onset of the perturbation and its subsequent dependence on time and transmembrane voltage all serve as clues to the molecular nature of the kinetic processes involved in chloride transport.

In the experiments reported here, we have attempted to gain a broad perspective of the behavior of chloride conductance under conditions of different external pH and different chloride concentration gradients across the membrane. Since the variety of experimental conditions is vast, a detailed study of the chloride conductance under all conditions was impractical because of the time required. Rather than studying the conductance in detail at one pH and at a fixed concentration gradient, we felt a more comparative and extensive over-view is required before detailed studies be undertaken at one pH. The present experiments have given us a broad over-view of the behavior of chloride conductance. It will be seen that the experiments provide a comparative basis for a further detailed study of any one aspect of chloride conductance.

Methods

Laboratory raised Xenopus laevis, rather than Rana pipiens were used because the latter were often infected with parasites. The Xenopus specimens were obtained from the Amphibian Facility of the University of Michigan at Ann Arbor, or from Nasco Ltd., Guelph, Ontario.

The experiments were done at room temperature (20-22°C) on surface fibers of sartorius.

Voltage clamp

The experiments were carried out using the three microelectrode voltage clamp technique as first formulated by Adrian, Chandler and Hodgkin (1970a). The voltage clamp arrangement with the positioning of the three microelectrodes is shown in Fig.1.1. The electrodes had resistances between 5 and 10 megaohms and those at A and B, 500 and 1000 microns respectively from the pelvic end, were filled with 3 M KCl and had tip potentials of less than 5 mV. The current injecting electrode at C, 1100 microns from the pelvic end, was filled with 2 M potassium citrate.

The voltage control in our experiments was different from that used in other 3 microelectrode experiments. The fiber interior at A was held close to virtual earth and the potential at D, making contact with the bath via an Agar-Ringer bridge, was held at minus the membrane potential by a feedback follower arrangement as described by Eisenberg and Gage (1969a). The potential at D was re-inverted and

Figure 1.1.   Schematic of the voltage clamp circuit.
The positioning and function of the electrode is
described in the text.
Amplifier A1 is a Burr-Brown 3307/12C with an open-
loop gain of 106 dB: the inside of the fiber at A
is negligibly different from virtual earth potential.
Amplifiers A2 and A5 are Burr-Brown 3400A.
Amplifier A3 (the clamp amplifier) is a Burr-Brown
3010/25 and the driving amplifier (set at 10 x gain)
is a Burr-Brown 3138/25 (100 volt output).

phase

gain

V_{comm}

ΔV

V_m

A1 A2 A3 A4 A5

C   B   A   D

ℓ ℓ

15a
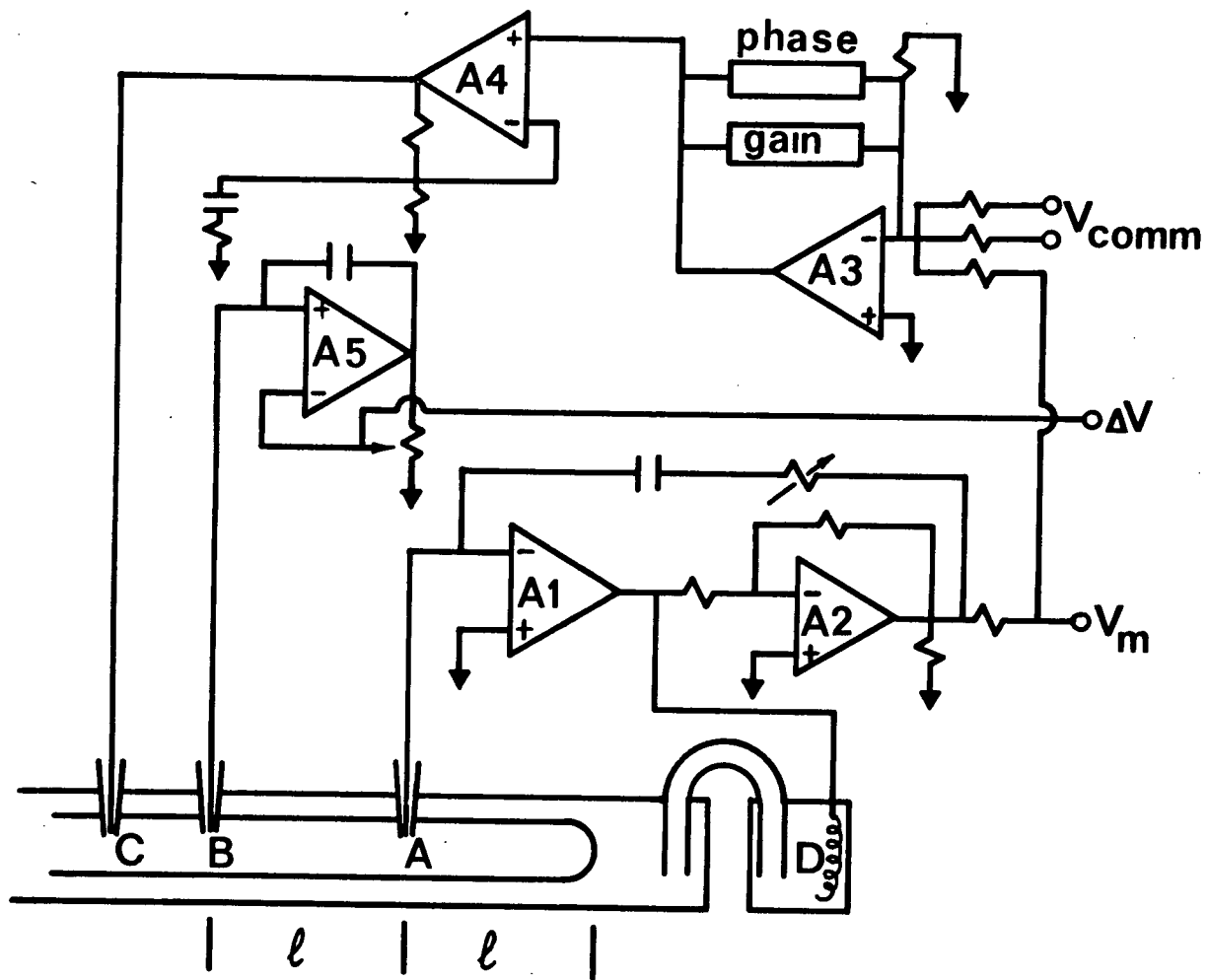
applied, together with a control voltage, to a summing amplifier (voltage clamp operating in the summing mode) the output of which injected current at C.

The axial voltage drop between A and B, denoted in our experiments by ΔV, was measured directly at B with a capacity compensated voltage follower referenced to earth potential. This method avoided the need for differential amplification to obtain ΔV.

The membrane current density I_m (Amp/cm^2) at A is related to ΔV by the relation (see Appendix)

$$(1) \qquad I_m \simeq \frac{d}{6 \, R_i \, \ell^2} \, \Delta V$$

R_i is the internal resistivity of the sarcoplasm; d is the fiber diameter, and ℓ is the distance between electrodes A and B. The error in this method is less than 5% (Adrian, Chandler and Hodgkin, 1970) if the separation (ℓ) between electrodes at A and B is less than twice the low frequency space constant.

The internal resistivity R_i was estimated in Xenopus laevis using conventional small signal cable analysis (Vaughan, 1975). A value of 163 ± 14 Ωcm was obtained in Ringer's solution. This value is in close agreement with the value obtained by Nakajima and Bastian (1974) in the iliofibularis muscle of Xenopus.

For the current calibration (ΔV) in our experimental records, the electrode separations were 500 microns (between A and B). The standard value of 170 Ωcm for R_i (Hodgkin and Nakajima, 1972) was used. A one millivolt difference in potential in a fiber with a diameter of 80

microns corresponds to a current density of 3.14 Amp/cm^2 of membrane area.

To bring the fiber under voltage control, the electrode closest to the pelvic end (position A, Fig.1.1) was first inserted into the fiber. Small hyperpolarizing constant current pulses were than passed through the citrate-filled electrode at C as it was lowered into the fiber. When the current injecting electrode and the electrode A were in the same fiber, electrode B in the solution recorded a potential minus that of electrode A. The electrode at B was then inserted between the current injecting electrode and position A. When all three electrodes were in the same fiber, the system was switched to voltage control and the clamp gain increased to minimize the rise-time to the command potential at B.

The holding potential, E_h, was always chosen equal (within 5 mV) to the resting membrane potential unless otherwise indicated.

Current and voltage were displayed on a Tektronix R5103N oscilloscope and photographed on 35 mm film for subsequent enlargement and analysis.

Sign convention

1. In all the experimental records inward current is shown as downward deflection of the oscilloscope trace unless otherwise noted.

2. All graphs are plotted with inward currents below the voltage axis.

3. All equations consider the sign of inward current to be positive.

Table I.1

Contents of solutions (mM/ℓ).

Soln	Na^+	K^+	Rb^+	Ca^{++}	Cl^-	SO_4^{--}	TTX gm/ℓ	sucrose	pH	buffer
A	119	2.5	–	1.8	121.1	–	10^{-5}	–	7.2	tris
B a	129	–	2.5	1.8	121.1	–	"	–	5.4	phosphate
b	119	–	2.5	1.8	121.1	–	"	–	6.7	tris
c	119	–	2.5	1.8	121.1	–	"	–	7.3	tris
d	119	–	2.5	1.8	121.1	–	"	–	8.4	tris
C a	154	–	2.5	8.0	–	84.25	"	–	5.4	phosphate
b	150	–	2.5	8.0	–	84.25	"	–	7.3	tris
c	150	–	2.5	8.0	–	84.25	"	–	8.4	tris
D	–	117	–	1.8	120.6	–	–	160	7.2	tris
D*	116	100	–	3.0	218	–	–	–	7.4	tris
D a	38	117	–	8.0	–	85.75	"	–	5.4	phosphate
d	34	117	–	8.0	–	85.75	"	–	8.4	tris
E a	38	–	117	1.8	120.6	–	"	160	5.4	phosphate
b	34	–	117	1.8	120.6	–	"	160	6.7	tris
c	34	–	117	1.8	120.6	–	"	160	7.3	tris
d	34	–	117	1.8	120.6	–	"	160	8.4	tris
E d*	34	–	117	1.8	120.6	–		400	8.4	tris
F a	38	–	117	8.0	–	85.75		–	5.4	phosphate
d	34	–	117	8.0	–	85.75		–	8.4	tris

Ions contributing to membrane current

Since the aim of the present experiments was to investigate the behavior of chloride currents, it was important that under experimental conditions contributions of other ions to the membrane current could be obviated or at least accounted for.

Chloride was the only anion in the solution except where small amounts of phosphate were introduced by the buffer system. Regenerative sodium currents were blocked by the addition of tetrodotoxin (10^{-5} g/ℓ) to the solutions.

An estimate of the rubidium conductance in rubidium-containing Ringer's solution (solutions B(a,b,c,d),Table I.1) at all pH was made by replacing the chloride with sulphate (solutions C(a,b,c)). The current voltage relations of the fibers in solutions C(a,b,c) were linear and were not influenced by pH. An averaged value of 20 µmho cm^{-2} (n=17) was obtained for the resting conductance of fibers in solutions C. Since sulphate does not permeate the membrane (Hodgkin and Horowicz, 1959; Hutter and Warner, 1972) this conductance is attributed to rubidium.

Solutions [Table I.1]

Solution A is Ringer's solution.

Solutions B(a,b,c,d) are standard Ringer's solutions with potassium replaced by rubidium and buffered at different pH's. Notice the slight differences in the sodium concentration depending on the buffer used. Trizma buffers (Tris(hydroxymethyl)aminomethane) were used at neutral and alkaline pH's and contributed no sodium.

The phosphate buffers used at pH's less than 6 were prepared from sodium salts.

Solutions C(a,b,c) are again standard Ringer's solutions but with sulphate replacing chloride. Additional calcium salt was added in order to maintain the level of ionized calcium at its normal level (Hodgkin and Horowicz, 1959). The number given is for total calcium.

Solution D is Ringer's solution containing high potassium (sodium replaced by potassium). This solution was used to permanently depolarize the fibers.

Solution D* is the depolarizing solution used by Hutter and Warner (1972, solution E).

Solutions D(a,d) were used to study the potassium conductance in depolarized fibers.

Solutions E(a,b,c,d) were used to measure chloride current in depolarized fibers. The potassium in solution D was replaced by the impermeant ion rubidium and the solution buffered to different pH's. Some of the solutions were osmotically unbuffered.

Solution Ed* was the hypertonic solution used in some depolarized fibers to prevent fiber contractions.

Solutions F(a,d) were the solutions used to test for Rb^+ and SO_4^{-2} permeation in depolarized fibers.

Further comments on the solutions will be provided for in the text.

Chapter II

Experimental Results

The membrane current accompanying hyperpolarizing voltage pulses
from the resting potential depended on the pH of the solution bathing the
fiber and the size of the voltage pulse. The current transients
were qualitatively similar to those reported by Warner (1972) for Rana
temporaria. In alkaline and neutral rubidium-containing solutions
(solutions Bc and Bd respectively), the membrane current decreased
monotonically from its initial (instantaneous) maximum, reaching
a steady value in 1.5 sec (Fig.2.0.1a). In acid solutions (solutions
B(a,b)) the current waveforms varied from fiber to fiber and three
types of responses could be described. Some fibers showed an initial
decay in current from its initial maximum (like those in alkaline and
neutral solutions) but the initial decrease was followed by an
exponential increase to the steady value (Fig.2.0.1b). In other
fibers, the initial decrease of current became smaller and more rapid
and for hyperpolarizations greater than -50 millivolts from the
resting potential, only a monotonic increase could be seen. Finally,
a third groups of fibers had current waveforms that rose monotonically
from initial to steady state at all voltages (Fig.2.0.1c).

In Ringer's solutions containing rubidium sulphate at different
pH's (solutions C(a,b,c)), these time dependent current responses
were not observed. If in the presence of chloride there is no
interaction among the cations, or between cations and chloride such
that they contribute a large fraction of the membrane current (and
there is no evidence to suggest that there is interaction), then the
currents described here may be attributed primarily to chloride.

Figure 2.0.1 Current waveforms recorded in response to hyper-
polarizing voltage steps. The numbers beside the
traces indicate the amplitude of the voltage steps (mV).
All currents were inward (corresponding to outward
chloride flux). Pulse duration was three seconds
in all cases.

a) Alkaline solution (pH 8.4, solution Bd). The
current always fell from the initial to the steady
state. Holding potential, -80 mV.

b) Acid solution (pH 5.4, solution Ba). Current
that fell and then rose. Traces recorded on a
digital averager. Holding potential, -70 mV.

c) Acid solution (pH 5.4, solution Ba). Waveforms
in which only a rising current was seen. Recorded
on the digital averager. Holding potential, -70 mV.
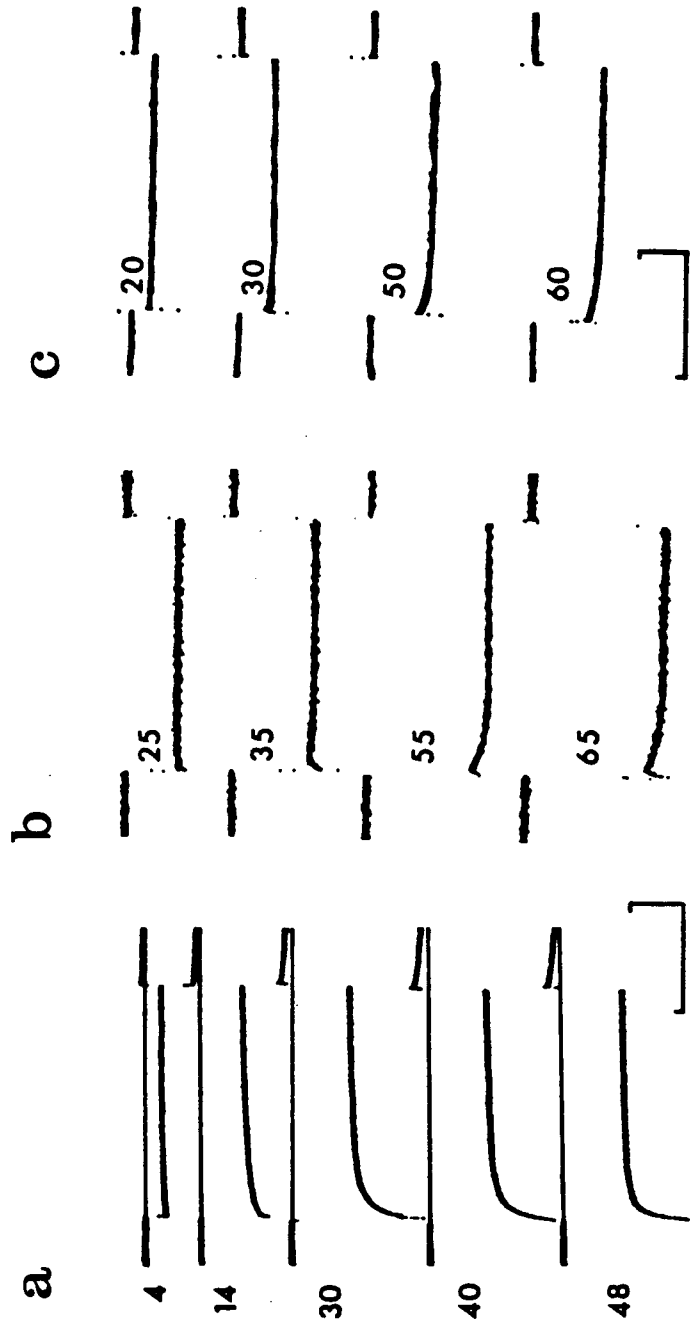
In the following section the response of the instantaneous
and steady state currents to hyperpolarizing voltage steps and also
the influence of the pH of the bathing solution will be described.
Instantaneous currents were estimated by analyzing the time course
of current relaxations (as will be described in Section I.1B) toward
the steady state from about 20 msec after the onset of the voltage
step and extrapolating to zero time as well as by direct reading from
the filmed record. The results obtained always agreed within 10%.

Since local contractures occurred with depolarizing voltage steps,
causing loss of impalement and fiber damage, only very small positive
voltage steps (less than 20 millivolts from the resting potential)
were applied. The amplitudes of the current transients were too
small for analysis, and subsequently will not be discussed.

Experimental Section I. The behavior of chloride currents in one

pulse voltage clamp experiments

I. Experiments on fibers with normal resting potentials

   A. The instantaneous and steady state current-voltage characteristics

Fibers in alkaline solutions (solution Bd, pH 8.4-8.8)

The current-voltage relations of 43 fibers bathed in alkaline

solutions were studied. Eleven fibers were held at -70 mV, thirty-one

were held at -80 mV, and one fiber was held at -90 mV. The resting

potentials of the fibers were within 5 millivolts of the holding

potential (average resting potential was -78 mV for 43 fibers).

The magnitude of the instantaneous current as a function of

the voltage was linear for hyperpolarizing potentials of less than

30 mV. For hyperpolarizing voltages that exceeded 50 mV the instan-

taneous currents appeared to reach a limit (Fig.2.1.1a). This is

in contrast to the fibers of Rana temporaria (Warner, 1972) where

instantaneous currents were linear as a function of voltage.

The steady state current-voltage relations for Xenopus laevis

fibers in alkaline solutions (pH 8) always became parallel to the

current axis for large hyperpolarizations. This is shown in Fig.2.1.1b

(solid circles) for 17 fibers that had the same holding potential

(-80 mV) and had the same steady state current density. For each

point, which represents the mean of a number of observations, the

sample size was less than 17 because the cells were not all studied

Figure 2.1.1 a) Instantaneous and steady state current-voltage relations of a fiber at pH 8.4 (solution Bd). As the membrane potential was made more negative the membrane currents reached limiting values. Open circles, instantaneous current; filled circles, steady state current. Holding potential, −80 mV. The currents include a contribution by rubidium.

b) Steady state current-voltage relations of populations of polarized fibers in solutions of pH 8.4 (filled circles) and 7.3 (open circles). Bars indicate standard errors of the means (for details, see text).
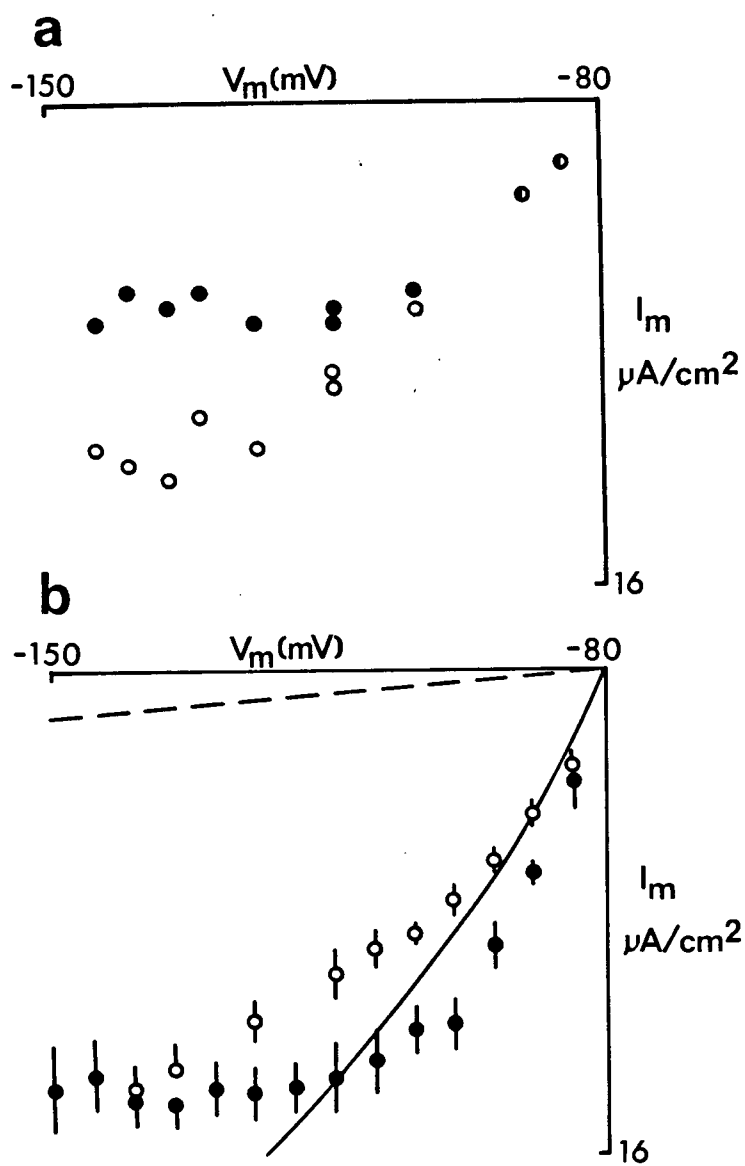
at the same voltages. The vertical bars depict standard deviations.

The dashed line in the figure indicates the currents recorded
in rubidium sulphate solutions (solution Cc). Since in general these
were done on different fibers, no attempt was made to subtract the
rubidium current from the steady state currents. However, it can be
seen that if the rubidium currents were subtracted, the chloride
current-voltage relations would be seen to have a negative slope
region. In several cells, negative slope conductance was observed
in RbCl solutions (solution Bd) without subtraction of the rubidium
current.

Fibers in neutral solutions (pH 7.3, solution Bc)

The current-voltage relations of 20 fibers were studied at
pH 7.3. Fifteen cells were held at -80 mV and five at -70 mV.
The average resting potential of the fibers was -78 mV. Both the
instantaneous and steady state current-voltage characteristics
were linear for a greater hyperpolarizing voltage range than the
fibers in alkaline solutions. For the largest hyperpolarizing voltages
applied (70 mV more negative than the holding potential) the conductances
(both the instantaneous and steady state) reach limiting values
(Fig.2.1.2). This is in contrast to fibers in more alkaline solutions
where the currents reach limiting values.

The circles of Fig.2.1.1b are averaged data for 15 cells at
pH 7.3. Here again, the same size and hence the contribution to the
vertical bars, was less than 15 (not all fibers were studied at the
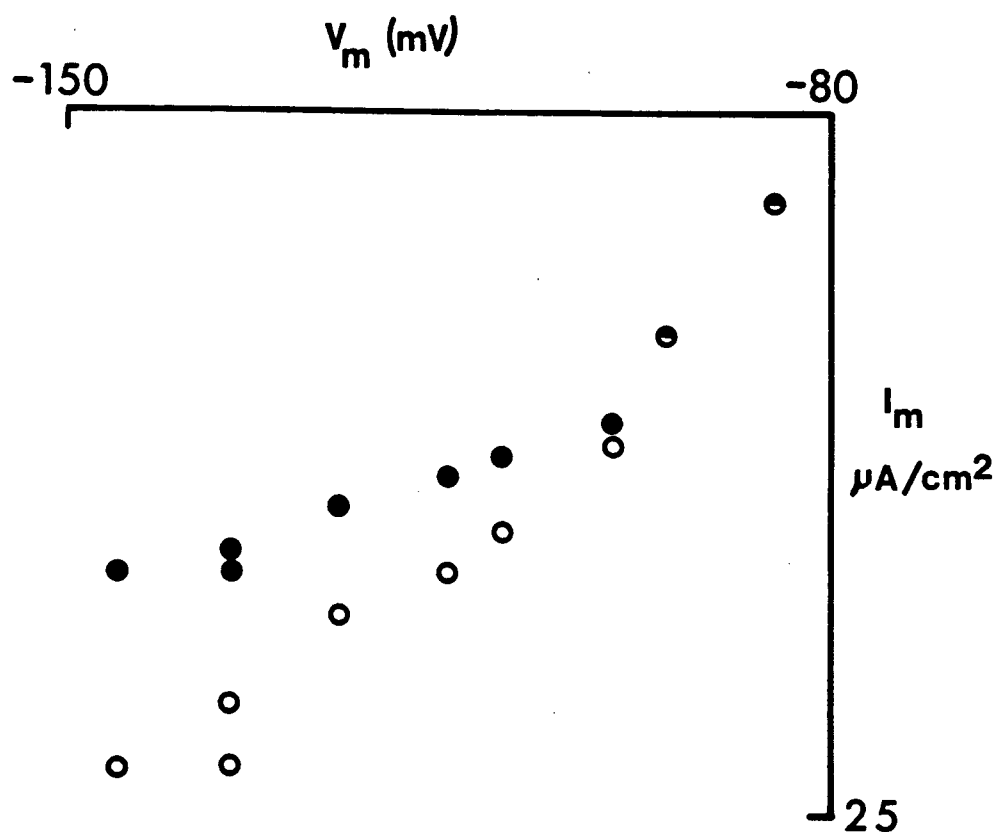
Figure 2.1.2 Instantaneous (open circles) and steady state
(filled circles) current-voltage relations for a
fiber at pH 7.3 (solution Bc). As the membrane
potential was made more negative the instantaneous
and steady state conductances reached a limiting
value. Holding potential, -80 mV. A contribution
by rubidium is included in the currents.

potentials).

The line shows the prediction according to the constant field

equation (Hodgkin and Horowicz, 1959; Hutter and Warner, 1972) with

a value of 8.0 X 10^{-6} cm sec^{-1} for P_{Cl}, the permeability coefficient.

It can be seen that in Xenopus laevis, even though the steady state

current-voltage relations reach a limiting conductance as in constant

field theory (Goldman, 1943), the rectification is greater than

predicted from the constant field theory.

Fibers in acid solutions (pH 5.4-6.7)

31 fibers were studied in this pH range: 15 fibers in solutions

of pH 6.4-6.7, and 16 fibers at pH 5.4-5.6. The average resting

potential for the fibers in the higher pH range was -75 mV and for the

fibers in the lower pH range was -70 mV.

The pattern of progressive linearization of the instantaneous

current-voltage curves with reduction in pH as described in the previous

sections continued in more acid solutions.

In the pH range (6.4-6.7) there was a large variability in the

behavior of the fibers. For instance, some fibers in solutions of

pH 6.4 exhibited instantaneous and steady state current-voltage curves

that were upwards concave as in alkaline and neutral solutions.

Other fibers at the same pH displayed linearity both in instantaneous

and steady state current-voltage curves that were upwards concave as in

alkaline and neutral solutions. Finally, some fibers showed typical

'acid' characteristics: linear instantaneous currents and steady state

currents that were downwards concave. This wide variety of behavior
might be due to a large variability in the pK of the pH dependent
titrable sites.

In the most acid solutions (pH 5.4) the instantaneous current-
voltage relations were always linear (up to the largest hyperpolar-
izations applied, -70 mV from the holding potential). This linearity
was independent of the transient behavior of the currents. The steady
state current-voltage relations at this pH were always downwards
concave for hyperpolarizing pulses as shown in Fig.2.1.3a.

The downwards concavity of the steady state current voltage
relations is due to the rising component of current transients. This
can be observed as follows: The rising component is the only con-
tributor to time dependent membrane current for fibers whose transients
increased monotonically to the steady state (filled circles, Fig.2.1.3a).
For fibers whose transients fell and then rose, since the time constants
of the fall were approximately 1/6 of the subsequent rise, the currents
can be approximated as being in a steady state after the initial fall,
before the rising component contributes any membrane current. When
the current was least, just before the delayed rise in current,
the current-voltage relations were linear, and the subsequent very
slight concavity of the steady state current-voltage relations in
Fig.2.1.3b was a result of this delayed rise in current (cf. Fig.2.1.3a).

Summary of the effect of pH on current-voltage relations and on
resting conductance

In alkaline and neutral solutions, the instantaneous and the

Figure 2.1.3 Instantaneous and steady state current-voltage
relations for fibers in the pH range 5.4 to 6.7.

a) Instantaneous (open circles) and steady state
(filled circles) relations in a fiber that demonstrated
monotonically rising currents. pH 5.4, holding
potential, -70 mV.

b) Relations for a fiber that gave a biphasic
current waveform. Open circles, instantaneous
current; filled triangles, current measured at
the local minimum where falling current gave
way to rising current; filled circles, steady
state current. The straight lines were fitted
by eye. pH 6.4, holding potential, -80 mV.

All currents in this figure contain contributions
by rubidium.
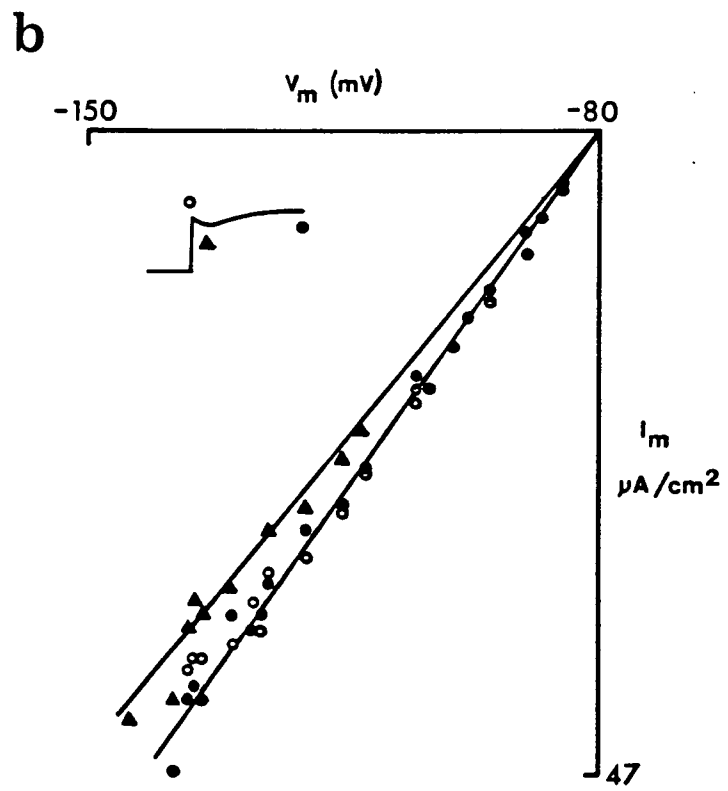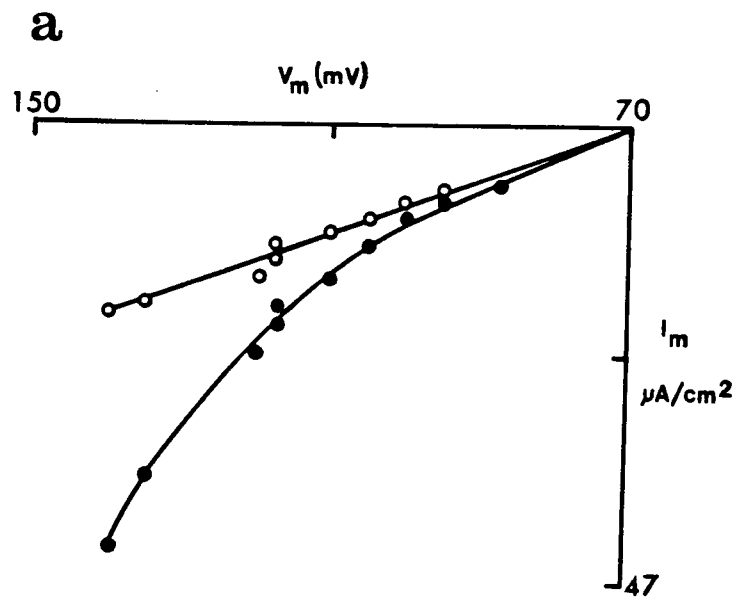
steady state current-voltage curves are concave upwards. The degree

of concavity and the slopes of the curves at the holding potential

decrease with decreasing pH, until ultimately the I-V relations are

linear   (around pH 6.4). The magnitudes of the current transients

also decrease as the current-voltage curves become linearized. This

pattern of linearization of I-V curves and decreasing magnitudes of

current transients depended continuously on pH until in acid solutions

there is a divergence of behavior by the introduction of a rising

component of time dependent current. In the simplest behavior the

instantaneous and steady state curves from alkaline and neutral

solutions coincide and as a result only an instantaneous linear current-

voltage relation is observed and the current rises monotonically to the

steady state. In more complex cases, the two curves do not coincide

completely and as a result the time dependent current first decreases

and then increases to the steady level.

In our studies on chloride conductance in Xenopus it was found

that there were large differences in the current densities and conduc-

tances from fiber to fiber even at the same pH. In spite of these

differences, the qualitative behaviors of the fibers at the same pH,

such as the direction of rectification, were similar. In order to

minimize this variability when the effects of pH on membrane conductance

are studied, experiments would have to be performed at different pH's

on the same fiber. Most of our information comes from pooled

measurements from a population of fibers. Table II.1.1 shows the

resting conductance obtained from the slope of the current-voltage

relations at the resting potential. In going from pH 8.4 to pH 6.4, the resting conductance decreased by a factor of 2. Fig.2.1.4 shows the result of an experiment where the solution bathing the fiber was changed from pH 6.4 to pH 8.4 with the three microelectrodes impaling the fiber. When the pH was changed from 8.4 to 6.4, the resting conductance decreased three times. These values are slightly less than reported by Hutter and Warner (1967a, 1972) in Rana temporaria.

Table II.1.1   Effect of pH on resting conductance

pH	resting conductance from current-voltage relations
5.4	2.1×10^{-4} mho cm^{-2}
6.4	3.75×10^{-4} mho cm^{-2}
7.4	4.0×10^{-4} mho cm^{-2}
8.4	7.35×10^{-4} mho cm^{-2}

B. The voltage dependence of chloride current transients

In the preceding section the qualitative behavior of the current transients in solutions of different pH was described. In response to hyperpolarizing voltage pulses, current transients are composed essentially of 3 components: a fast initial fall with time constants less than 100 msec; a slow 'creeping' fall to the steady state that required between 300-500 msec for completion; and a rising component that is observed only in fibers in acid solutions.

Figure 2.1.4   Steady state and instantaneous current-voltage
relations for a fiber in which voltage control
was maintained while the pH of the solution was
changed from 8.4 to 6.4. The open circles indicate
the instantaneous current at pH 8.4 and the filled
circles the steady state current at the same pH.
Instantaneous and steady state currents were
indistinguishable at pH 6.4 (filled squares).
Holding potential, -70 mV. Contributions of
rubidium current have not been subtracted.
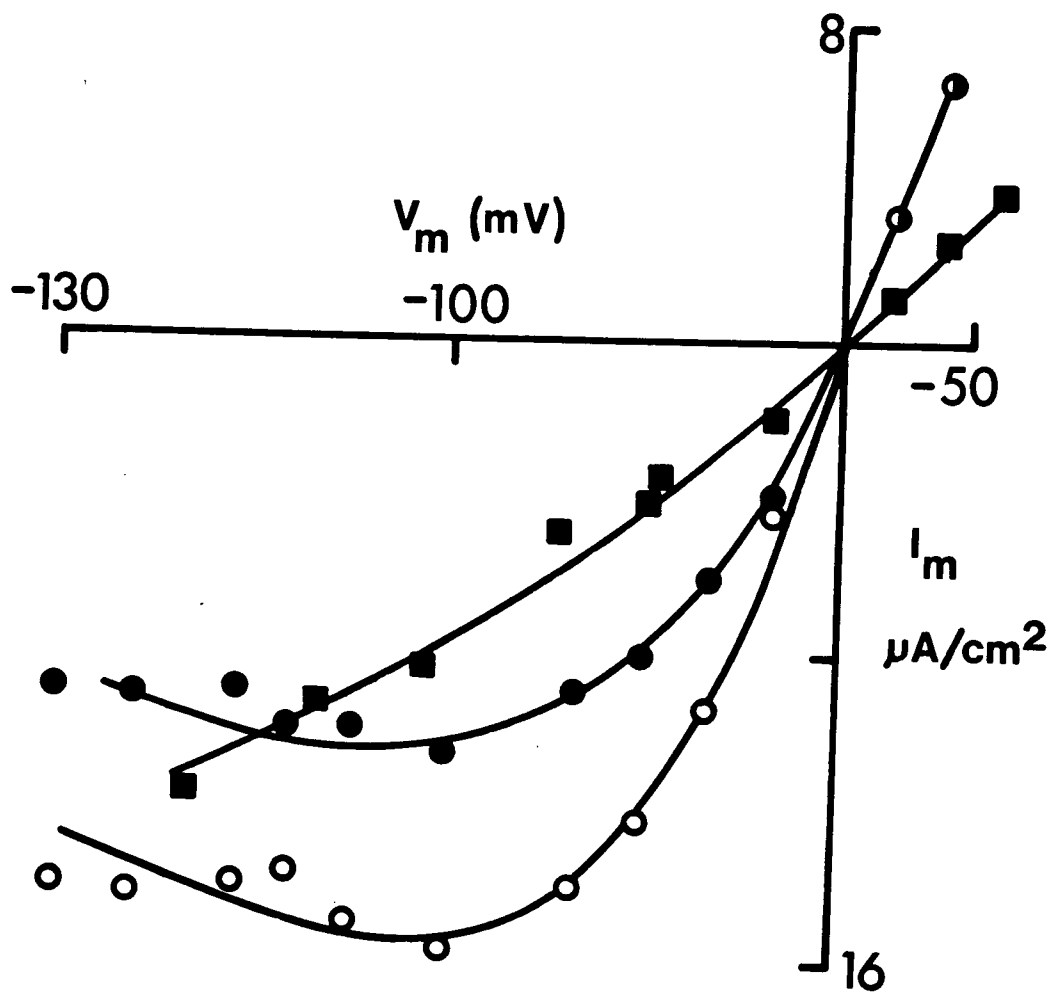
Analysis of current transients

The time constants of current transients were obtained as follows:

a) For increasing currents, Fig.2.1.5a. A logarithmic plot of the transient $(I_\infty - I(t))$ was made againt t, the time from the onset of the voltage pulse (Fig.2.1.5a), I_∞ is the steady current value. A straight line was drawn through the points by eye, as shown in Fig.2.1.5b.

b) For currents that decreased and then increased (at acid pH), Fig.2.1.5c. The time constant of the rising current transient and the contribution to total current made by the rising phase were estimated by method (a). When the rising current was subtracted from the total, the time constant of the falling phase was estimated from the line of best fit to the logarithmic plot of $(I(t)-I_\infty)$ against time Fig.2.1.5.d(i). The principal time constant of the falling phase was of the order of 50 msec, whereas the time constants of the rising phase exceeded 250 msec, allowing a simpler analysis to be used. In this method the local minimum between falling and rising phases was assumed to be the steady state current for the falling phase and the beginning (t=0) of the contribution of rising phase (Fig.2.1.5d(ii)). The differences between the results of the two methods were negligible and the simpler approach was generally used. But in situations were the two time constants were similar in magnitude, we were unable to resolve the current transients accurately.

Figure 2.1.5 Current waveforms and the analysis of transients.

a) Waveform of current recorded in response to a hyperpolarizing voltage step of 70 mV from a holding potential of -70 mV at pH 5.4. The trace was recorded from a digital averager and has been inverted by comparison with out usual records.

b) The rising transient of (a) is fitted by a single exponential.

c) Biphasic response from a different fiber at pH 5.4. The hyperpolarizing voltage step was 45 mV from a holding potential of -70 mV. The double arrow indicates the local minimum current.

d) The delayed rise in (c) is fitted by a single exponential (open circles). When this is projected to zero time and the resulting current subtracted from the total, the remaining falling current is fitted by a single exponential (filled circles). If the falling phase is analysed assuming a steady current at the level of the local minimum a slightly different time constant is obtained (open diamonds).

e) A current waveform that fell to a steady value. Holding potential, -80 mV, pH 7.4.

f) Currents that only decline were usually resolved into two time constants.

Current calibration (bar), 5 mV. The corresponding current density is 3.14×10^{-6} Amp/cm^2 per mV. In (b), (d) and (f) the abscissa is in milliseconds.
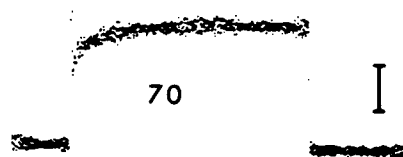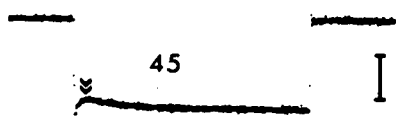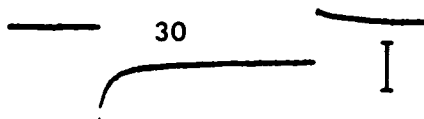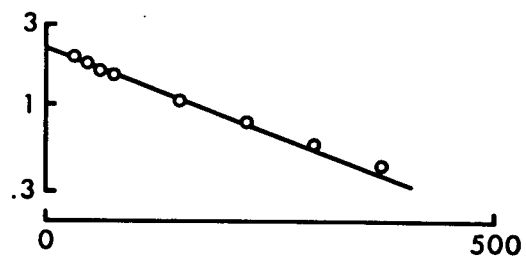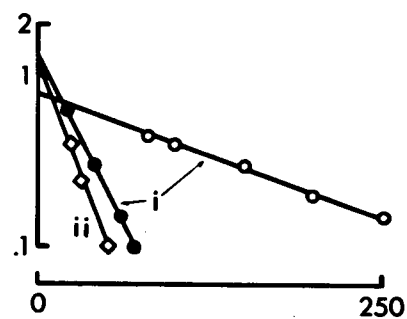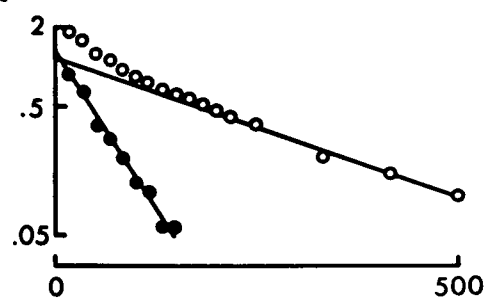
c) <u>Currents that decreased to a steady value, Fig.2.1.5e.</u> The
   logarithm of the transient component of the current was plotted
   against t, the time from the onset of the voltage step. The line
   of best fit was made by eye to the points between 200 and 400
   msec. This line had a time constant of about 500 msec. After
   subtracting this slow process from the total current transient,
   the difference was straight line with a time constant varying
   from 10 to 100 msec (Fig.2.1.5f).

The time course of the creeping decay of current appeared to consist
of a family of exponentials, possibly indicating the relaxation
spectrum of a distributive system. In the approximate analysis of
Fig.2.1.5f, the time period (200-400 milliseconds) was chosen because
the exponential approximation fitted the data for the longest time
interval and the current waveforms could consistently be resolved into
two components. The results that we describe were obtained by these
approximate methods.

The slow creeping fall in current to the steady state was found
not to depend on the membrane potential nor on the pH of the bathing
medium. Only the more rapidly evolving current transients were sensitive
to voltage. In the following section we will describe the voltage
dependence of the initial falling current in alkaline and neutral
solutions and the fall and subsequent rise in the current transients
in acid solutions.

Kinetics in acid solutions (pH 5.4-6.7)

The initial falling currents and the rising currents in acid solutions appeared to act independently. The voltage dependence of the rate of initial fall of current was independent of the subsequent kinetic behavior. That is, it did not depend on the existence of a subsequent rise. Likewise the time constants of the rising currents were independent of the presence of any preceding fall.

The time constants for the decrease in initial current depended linearly on the amplitude of the hyperpolarizing pulse as shown in Fig.2.1.6a. The slope of the line (obtained by regression) is -1.17 msec/mV. The abscissa of Fig.2.1.6a. represents the size of the hyperpolarizing voltage.

The time constants of the increasing component of current transients for fibers in acid solutions depended non-linearly on the hyperpolarizing voltage. For hyperpolarizing voltage steps greater than 50 millivolts, the time constant approached a limiting value of 250 milliseconds (Fig.2.1.6b).

Kinetics in neutral and alkaline solutions (pH 7.3-8.8)

A summary of the voltage dependence of the time constants of the initial decay of current is presented in Table II.1.2. It can be seen that in neutral and alkaline solutions, as in acid solutions, the time constants of the fall of initial current depended linearly on the hyperpolarizing voltage step.

Linear regression on data in neutral solutions (pH 7.3) gave slopes

Figure 2.1.6 The dependence of relaxation time constants on the
size of the membrane potential step in fibers bathed
in acid solutions (pH 5.4, solution Ba).

The holding potentials of the fibers studied were -70 mV.

a) The voltage dependence of the time constant of the
initial falling current transient.

b) The dependence of the time constant of the sub-
sequent rising phase.
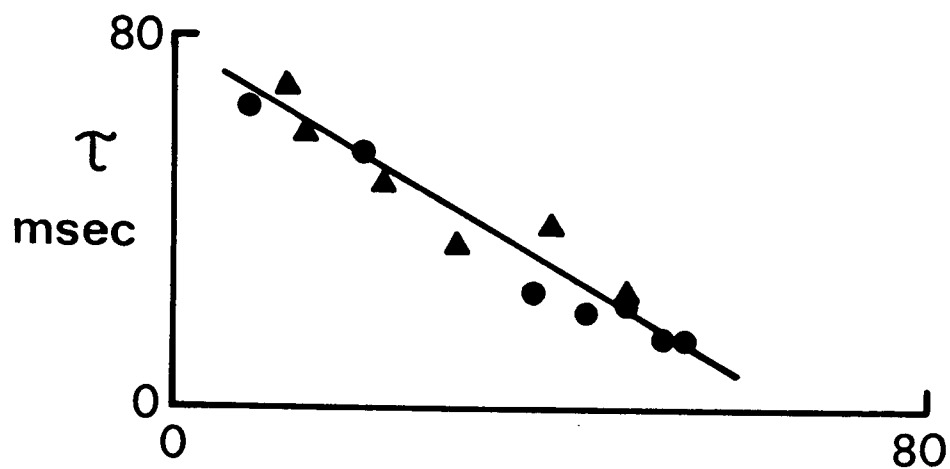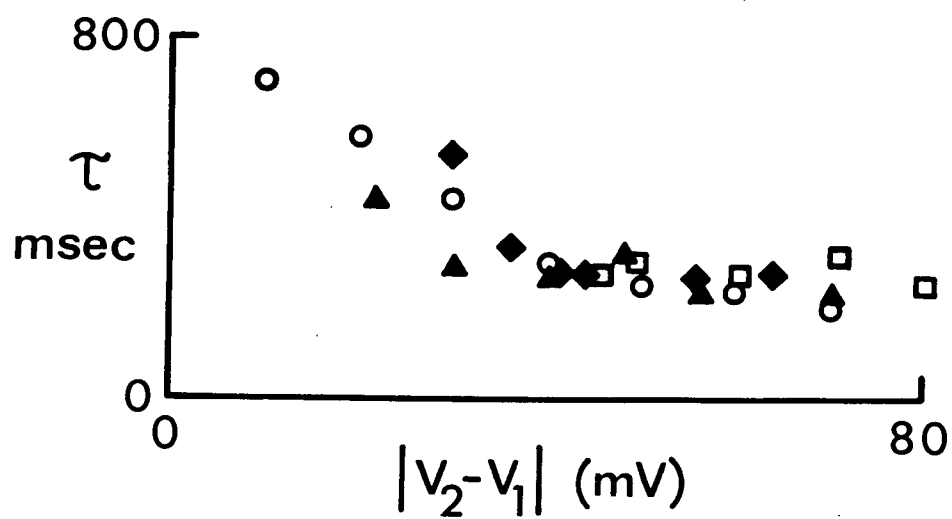
Table II.1.2

Summary of the voltage dependence of the fast time-
constants of relaxation of chloride current.

pH	Voltage dependence (msec/mV)	
5.4	−1.17*	
7.3	−1.55 ± 0.44 **	(n=8)
8.4	−1.56 ± 0.38 **	(n=4)

* Refer to Fig.2.1.6a.

** Standard deviation. In pH's 7.3 and 8.4, linear
regression was performed on data from individual
fibers and the slopes (voltage dependence of time
constants) were then averaged to obtain the mean
and standard deviation.

of -1.55 ± 0.44 (S.D. n=8) msec/mV and in alkaline solutions solutions
(pH 8.4) gave slopes of -1.56 ± 0.38 (S.D. n=4) msec/mV (Table II.1.2).

Comparison with Rana temporaria

Even though the qualitative behavior of the fibers in solutions
of different pH's was similar between fibers of Xenopus laevis and Rana
temporaria, there are quantitative differences between our results
and those reported by Warner (1972) for Rana. The decay of current
was resolved into a single time constant between 100 and 200 msec
(Warner, 1972) with a voltage dependence of -1.54 msec/mV in pH 9.8
and -1.33 msec/mV, for fibers in pH 7.4, whereas in our experiments,
current decays were resolved into two time constants, one pH and
voltage dependent (-1.55 msec/mV) but independent of pH.

Dependence of kinetics on the magnitude of voltage steps

In the previous section it was found that the time constants of
currents depended linearly on the hyperpolarizing voltage. However,
since the comparisons were made on different fibers with the same
holding potential, we can not distinguish whether this linear de-
pendence was on the absolute potential or on the size of the negative-
going voltage step. To differentiate between the two alternatives,
several experiments were conducted with the same fiber held
at different potentials. Fig.2.1.7 shows the results from
one fiber in solution of pH 7.3, held successively at -60, -70 and

Figure 2.1.7 Relationship between decay time constant and the
amplitude of hyperpolarizing voltage steps from the
holding potential at pH 7.3 (solution Bc), for three
holding potentials. Filled circles, open circles and
triangles are for holding potentials of -60 mV, -70
mV and -80 mV, respectively. The lines were fitted
by least squares linear regression. The abscissa is the
size of the hyperpolarizing voltage step and the
ordinate is the fast decay time constant, in milli-
seconds. The slow time constant found to be independent
of voltage.
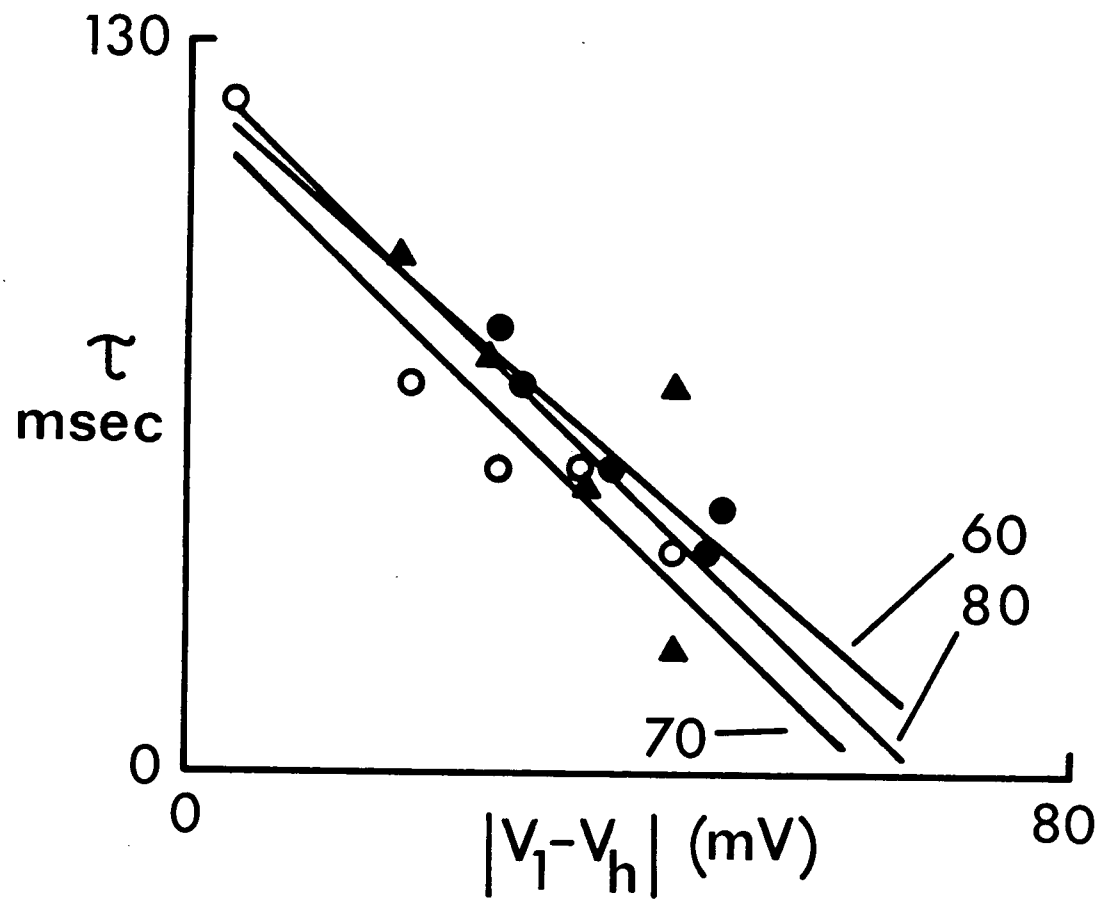
-80 mV. The abscissa is the size of the voltage step. The slopes of
the lines of best fit for data from each of the three holding potentials
for pulses between 10 and 50 mV amplitude are not significantly
different. That is the rate of the fast decay depends only on the
magnitude of the hyperpolarizing pulse and not on the holding potential
or the absolute membrane potential. This conclusion will be supported
by two pulse experiments and experiments on fibers with low resting
potentials.

Aftercurrents: changes in zero current potential with chloride passage across the membrane

On subsequent return to the holding potential after a hyperpolarizing
test pulse, the membrane current, instead of returning to the holding
current, was transiently outward. The magnitudes of the aftercurrents
were usually very small, making accurate analysis of their amplitudes
and time courses very difficult. However, it did appear that the
magnitudes of the instantaneous aftercurrents in fibers in neutral and
alkaline solutions (pH greater than 7) reached a limiting value for
large hyperpolarizations. This can be seen in Fig.2.1.8a. where a
sequence of voltage steps and associated aftercurrents from a fiber at
pH 7.3 is shown; the magnitudes of the instantaneous aftercurrents from
the same fiber but at two different holding potentials (open and filled
circles) is shown in Fig.2.1.8b.

Warner (1972) observed similar aftercurrents with hyperpolarizing
voltage steps in Rana temporaria and termed the phenomenon 'stored

Figure 2.1.8 Magnitude and direction of after-currents.

a) Outward after-currents, indicated by the arrows
on the right of the traces, recorded from a fiber at
pH 7.3 (solution Bc) following the stepping of the
membrane potential back to the holding potential from
a more negative potential (the numbers on the traces)
at which current had reached a steady state.

Resting and holding potential, -80 mV. Calibration:
abscissa, 1 second; ordinate, 5 mV. 1 mV = 3.14×10^{-6}
Amp/cm^2.

b) Initial after-currents plotted as a function of the
membrane potential during the preceding step. Data from
the same fiber as (a). Open circles are from a run in
which the holding potential was -60 mV and filled circles
are from a run in which it was -80 mV (the same as the
resting potential). Notice that abscissa is deviation
from holding potential. Calibration for the ordinate:
1 mV = 3.14×10^{-6} Amp/cm^2.
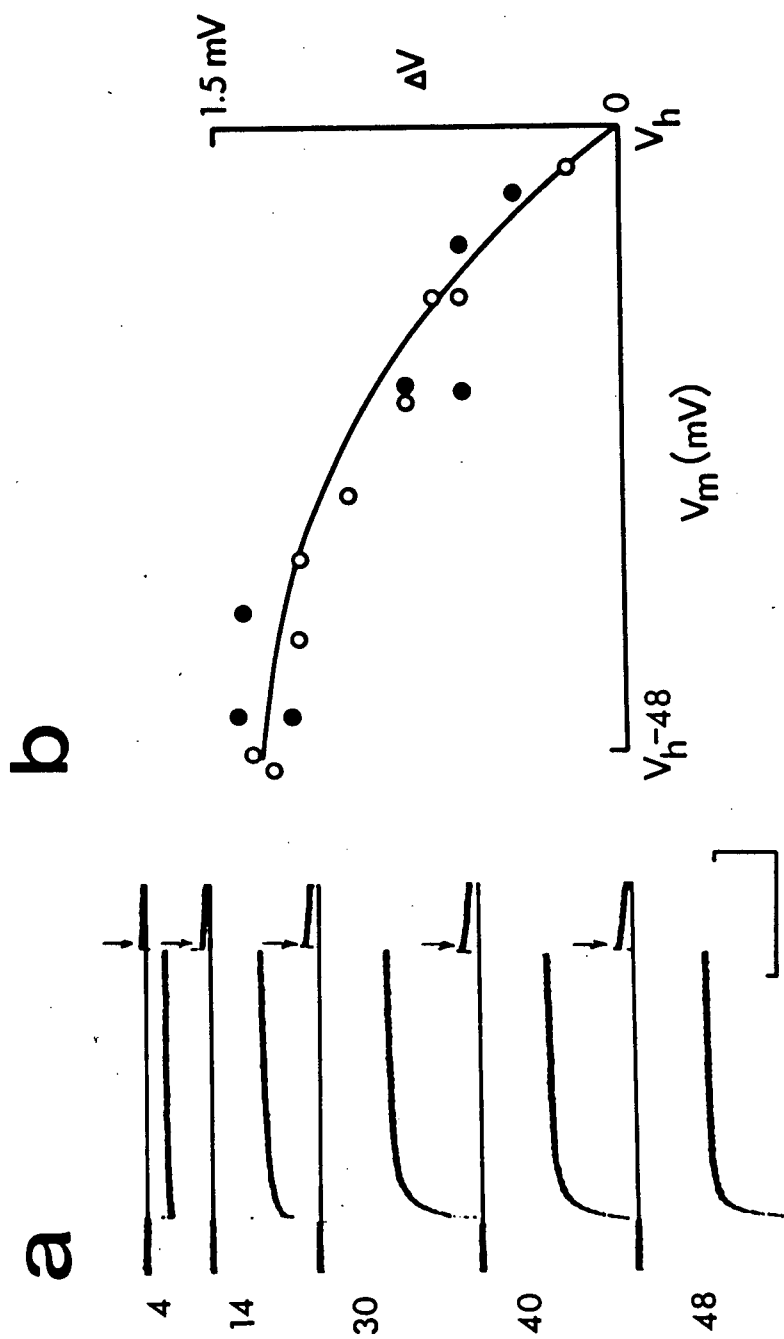
charge'. Such aftercurrents could be caused either by a depletion or
enhancement of chloride in a compartment in series with the electrical
pathway (an analogy would be the potassium depletion in the transverse
tubular system with hyperpolarizing pulses (Adrian, Chandler and
Hodgkin, 1970b; Almers, 1972a,b; Barry and Adrian, 1973)), or could be
due to a recovery of a membrane process that resulted in the decay of
current during the test pulse. The likelihood of both explanations
was investigated using fibers where the internal chloride concentration
was altered and also using two pulse experiments. This will be described
later.

II. Experiments on permanently depolarized fibers

Experimental rationale

In the preceding section, the pH dependence of chloride conductance
was described and some evidence was presented to support the dependence
of current transients on the size of the hyperpolarizing voltage step
rather than the absolute membrane potential. The experiments described
were conducted on fibers that had resting potentials between -70 and -90
millivolts. The chloride concentration ratio across the membrane is
given by Nernst's equation $Cl_o/Cl_i = \exp(-FV/RT)$, and varies between
16.0 (-70 mV) and 35.3 (-90 mV) at $20^{\circ}C$.

In this section, experiments performed on fibers where the
concentration ratio was lowered by permanently depolarizing the fibers
will be described. The internal chloride concentration was increased
while the external chloride concentration was kept constant at the same

value as fibers with high concentration ratios. These experiments were performed for several reasons:

The dependence of conductance on concentration provides us with information on the possible mechanisms of chloride permeation. For instance, Warner (1972) suggested that chloride might permeate the membrane via mobile charged carriers of the type studied by Sandblom, Eisenman and Walker (1967). A prediction of this model is that the degree of current-voltage rectification depends on the asymmetrical distribution of chloride across the membrane. Similarly, Hodgkin and Horowicz (1959) in describing the dependence of chloride currents on membrane potential by the constant field equation, suggest that the rectification is caused by the concentration gradient across the membrane (Chapter IV). If this were the case in neutral solutions, then it is important to determine whether there is any contribution of concentration gradients to the current-voltage characteristics in acid and alkaline solutions. In order to understand the effect of pH on conductance, the possible causes of rectification such as concentration gradients (if there are any) and pH must be clarified.

In fibers with high resting potentials, because of contractures, only very small depolarizing steps could be applied. Hence there is very little information on the response of the chloride permeation system to depolarizing pulses. In permenently depolarized fibers, a much wider range of potentials could be applied because the contraction mechanism is inactivated.

Another reason to study permanently depolarized fibers was to study

the nature of current transients and their voltage dependence. Some evidence has been presented that kinetics depend on the hyperpolarizing voltage step rather than on the absolute membrane potential.

Finally, in connection with current transients, it was found that for the long 'creeping' decays to the steady state in neutral and alkaline solutions, the currents were independent of voltage and pH. A plausible explanation for these currents is that they could arise as a result of depletion or enhancement of chloride in a compartment in series with the current pathway; if this were the case, then an alteration of the chloride concentration would influence the slow current transients.

The muscles were dissected as usual in standard Ringer's solutions (A). The muscle was slowly depolarized by gradual addition of depolarizing solution (solution D). The depolarization was kept slow to prevent the fibers from contraction. The muscle was finally soaked for 4 hours in solution D, then transferred to a solution in which the potassium in the solution was replaced by rubidium (solution E(a,b)) and allowed to equilibrate for about 30 minutes before recording began.

Resting potentials of depolarized fibers

Holding potentials for depolarized fibers, which were within 5 millivolts of the resting potential, were generally near -20 mV. However, in some instances, especially for fibers in alkaline solutions,

resting potentials as high as -30 mV were recorded. In an isotonic

solution containing 117 mM K^+, the internal potassium concentration

is 195 mM (refer to section on 'a comment on the solutions') hence

a membrane potential of -13 mV is anticipated from the Nernst equation.

Since solution D, which was used to depolarize the fibers, was

not traditionally used to depolarize muscle preparations (this solution

was used to maintain the external chloride concentration in depolarized

fibers the same as in polarized fibers) membrane potentials were

measured in a number of fibers in solution D and another solution

D*, used by Hutter and Warner (1972). This acted as a check on the

effect of solution D. The results, in pH 7.4, are summarized in

Table II.1.3.

Table II.1.3 Resting potentials of depolarized fibers

solution	resting potentials
D	-13.8 ± 1.1 (S.D.) mV; n=16
D*	-17.0 ± 2.1 (S.D.) mV; n=21

The results of Table II.1.3 indicate that the mean resting potentials

of fibers in solutions D and D* differ by less than 5 mV and that

the resting potentials are as predicted by the Nernst equation.

In solution D, the internal concentrations of potassium and

chloride (from the Nernst equation) are:

$$K_i = 205 \text{ mM} \quad , \quad Cl_i = 70 \text{ mM}$$

and in solution D*,

$$K_i = 193 \text{ mM} \quad , \quad Cl_i = 112 \text{ mM} \quad .$$

The potentials shown in Table II.1.3 for fibers in solution D

are slightly less negative than some of those to be reported below,

especially for experiments in alkaline solutions.

When potassium chloride was replaced with 117 mM rubidium chloride

slightly higher resting potentials (around -18 mV) were obtained.

When the depolarized fibers were placed in normal Ringer's solution

(solution A), repolarization of the membrane potential was very

slow: even after 25 minutes of washing, fibers that had been depolarized

(in 117 mM K^+) did not repolarize to membrane potentials more negative

than -25 mV.

This observation has also been reported previously by Adrian

(1964) who found that fibers loaded with chloride usually failed

to repolarize or repolarized only very slowly when placed in solutions

of low K^+.

Value of the internal resistivity (R_i) in depolarized fibers

Calibration of membrane current density (measured as ΔV, as

described in Methods), requires knowledge of the longitudinal resistance

of the sarcoplasm (see equation 1 of Chapter I).

As previously described, there is ample evidence to suggest that a reasonable value for this quantity in normally polarized fibers (resting potential, -80 mV) is 170 Ωcm and we have obtained data from cable measurements indicating that this resistance is independent of extracellular pH. In depolarized fibers, however, since the intra-cellular concentration of chloride may be greatly increased, the sarcoplasmic resistance may be greatly altered.

A set of experiments was performed to determine the internal resistivity (R_i) in depolarized fibers. Since it was difficult to measure fiber radius accurately, first an apparent radius was calculated for normally polarized fibers using a value of 170 Ωcm. The muscle was then depolarized with either solution D or solution D^* and a new set of cable data recorded (input resistance and d.c. length constant). Using the equivalent radius estimate from the first set of measurements, a value of R_i in the depolarized condition was established. It is interesting to note (Table II.1.4) that in solution D^*, in which intracellular $K^+ = Cl^-$ is 305 mM (see section on resting potential of depolarized fibers), R_i is significantly lower than in solution D (in which $K^+ + Cl^-$ is 265 mM). The value of 140 Ωcm has been routinely used to calibrate membrane current in depolarized fibers in solutions of high chloride content.

Contribution of cation currents

The contribution of the cation currents to the total membrane current was again checked in depolarized fibers to ensure that they

Table II.1.4

Cable constants in depolarized fibers.

Solution D

Muscle	V_m (mV)	R_o (x10^5ohm)	λ(x10^{-6}m)	a(x10^{-3}cm)	R_i(ohm.cm)
7.6.78	−82.6±3.7	2.1±1.1	2200±512	5.8±1.9	170
	−14.2±2.8	0.43±0.12	875±380	(5.8)	126±64
10.6.78	−85.6±4.8	1.57±0.18	2775±380	6.9±0.9	(170)
	−14.9±2.2	0.41±0.13	1036±175	(6.9)	110±69
12.6.78	−82.6±1.9	1.65±0.48	1880±293	5.7±1	(170)
	−13.9±2.4	0.51±0.17	706±118	(5.7)	171±45

Overall mean R_i in depolarized cells 140±56 (n=21)

Solution D*

Muscle	V_m (mV)	R_o (x10^5ohm)	λ(x10^{-6}m)	a(x10^{-3}cm)	R_i(ohm.cm)
14.6.78	−80.6±4.1	1.68±0.40	1467±219	4.9±0.7	(170)
	−14.6±0.5	0.75±0.18	838±145	(4.9)	86±48
16.6.78	−84.6±3.4	1.39±0.15	2996±785	7.6±1.3	(170)
	−17.6±0.6	0.25±0.05	1067±166	(7.6)	88±26

Overall mean R_i in depolarized cell 87±37 (n=27).

V_m = resting potential, R_o= input resistance, λ= d.c. space constant, a = fiber radius , R_i= internal resistivity .

contributed no significant current. The muscles were bathed in a

solution containing potassium sulphate at different pH's (solutions

D(a,d)). Results for 4 cells from different pH's are shown in Fig.2.1.9.

The potassium currents were not influenced by pH, and showed typical

inward-going rectification (Katz, 1948; Adrian, 1969). When potassium

was replaced by rubidium (solutions G(a,d)) currents obtained were

very small but not time-independent. In current-clamp experiments

the voltage record showed a large 'creep' and in voltage-clamp

experiments, although the currents were very small and initial currents

difficult to measure, they were of the order of 1.5 to 2.0 times the

steady state current. Rubidium current did not exceed 10% of the

chloride content.

A comment on the solutions

In initial experiments on depolarized fibers, due to the extremely

low rubidium conductance, we considered it unnecessary to add osmotic

buffer to the solutions. The fibers did not show any signs of swelling

even after 8 to 12 hours in the unbuffered solutions. The resting

membrane potential was monitored continuously in several experiments

and it was found that the resting membrane potential did not change for

periods of up to 4 hours in unbuffered solutions. However, the

possibility exists that some of the data might be artifacts of fiber

swelling (Speralakis and Schneider, 1968), and consequently some

experiments were repeated with the rubidium containing solutions

osmotically buffered with sucrose (solutions E(a,b,c,d)). The current-
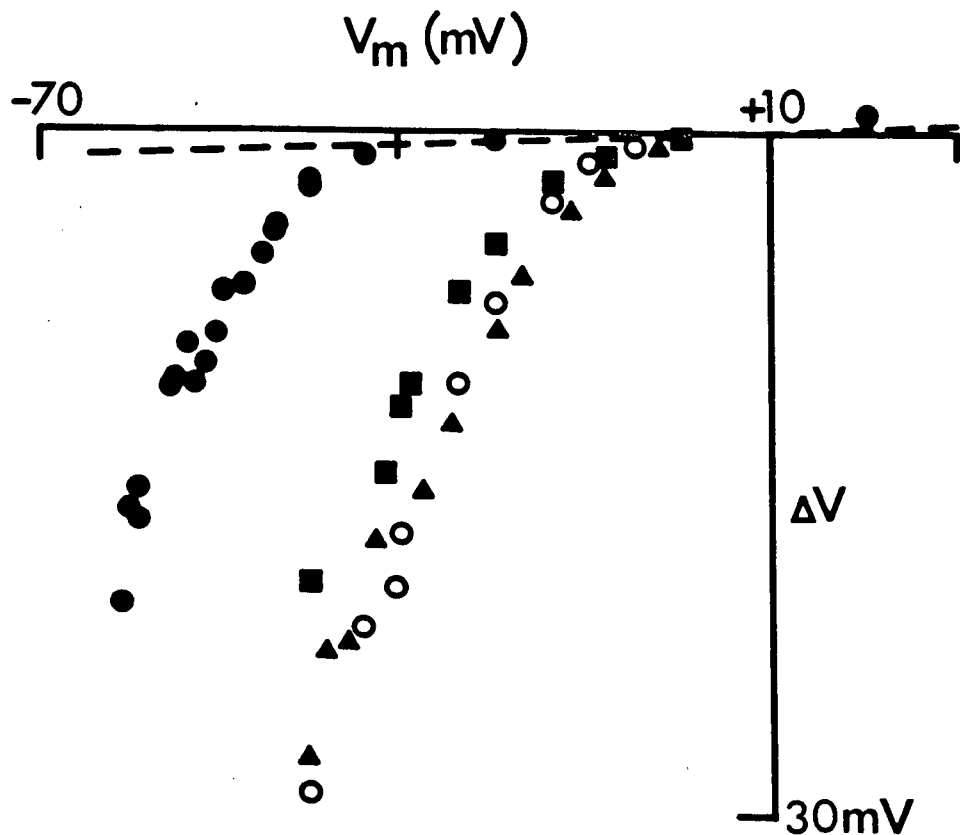
Figure 2.1.9 Steady state current-voltage relations for fibers
bathed in 117 mM K_2SO_4 solution (solution D(a,d)).
Very small currents were recorded when the pulses were
positive-going from the holding potential (+10 mV).
The dashed line indicates the envelope of records made
in 117 mM Rb_2SO_4 (solutions F(a,d)). Calibration:
1 mV = 3.79 x 10^{-6} Amp/cm^2.

voltage relations obtained were similar to those obtained in the unbuffered solutions. In the results to be presented, no distinction will be placed on the fibers that are either in osmotically buffered or unbuffered solutions unless otherwise discussed.

The components of the depolarizing solutions were calculated as follows:

At -90 mV the membrane potential is described by the Goldman-Hodgkin-Katz equation (Hodgkin and Katz, 1949) using a sodium to potassium permeability ratio of .01 (Hodgkin and Horowicz, 1959) the internal potassium concentration is:

$$K_i = \exp(V_m F/RT) \times (2.5 + .01 \times 120)$$
$$= \exp(.09 \times 96500/8.3 \times 295) \times (2.5 + .01 \times 120)$$
$$= 128 \text{ mM}$$

From the Nernst equation $Cl_i = 3$ mM .

If an intracellular sodium concentration of 10 mM is assumed, then the intracellular fixed negative charge concentration is 135 m.eq./ℓ . The osmolality of normal Ringer's solution is 227 m.osm/ℓ (measured by freezing point depression), thus giving a mean osmotic coefficient of 0.96. If intracellular inorganic ions have the same osmotic activity, then the osmotic activity of the internal fixed charge would be 92 m.osm/ℓ . In 117 KCl (solution D), from Donnan equilibrium,

$$K_i = 195 \text{ mM} \quad \text{and}$$
$$Cl_i = 70 \text{ mM}$$

and by assumption , $Na_i = 10$ mM.

Using an osmotic coefficient of 0.96, this yields 265 m.osm/ℓ   and

the internal fixed charge yields 92 m.osm/ℓ . Therefore the total

osmolality of the intracellular compartment is 357 m.osm/ℓ . The

ions in the external solution give an osmolality of 225 m.osm/ℓ .

Therefore for isotonicity with Ringer's solution, 132 m.osm/ℓ is

required. The solutions D and E(a,b,c,d) were slightly hypertonic

as 160 mM/ sucrose was added.

In response to both hyperpolarizing and depolarizing voltage

steps from the holding potential (usually -20 mV) the chloride transient

current waveforms in depolarized fibers in different solutions whose

pH varied from 5.4 to 8.4 always decreased monotonically to the steady

state. The current transients were found to be composed of two phases:

an initial decay with a time constant of 100 milliseconds and then

a much slower 'creeping' fall (300-500 msec time constant) to the

steady state. There were several differences between the instantaneous

and steady state current-voltage relations and the current transients

observed in depolarized fibers compared with those of polarized fibers.

The steady state and instantaneous properties are described first,

in this section.

A. The steady state and instantaneous current-voltage relations in
fibers that have been permanently depolarized

Fibers in acid solutions (pH 5.4, solution Ea)

The average resting potential of the fibers studied in this pH

was -14 millivolts (n=9). Both the instantaneous and steady state current-

voltage relations were downwards concave for hyperpolarizing voltage pulses. In the depolarization direction, the behavior was of two types: in some fibers, mainly those exhibiting very small current densities, the instantaneous and steady state currents reached a limiting value for the largest depolarizing voltages applied (+50 mV) whereas for fibers that had higher current densities, the instantaneous and steady state currents continued to increase with depolarizing voltage (Fig.2.1.10). In spite of these variations, it was clear that in acid solutions, the chloride permeation system exhibited inward rectification--the conductance for inward current (chloride efflux) was greater than for outward current (chloride influx).

It is important to notice the difference between the current-voltage relations in polarized and in depolarized fibers. In polarized fibers, the instantaneous relations were linear, and steady state rectification, although in the same direction as in depolarized fibers, is caused by the rising component of the current transients (see Fig.2.1.3). In depolarized fibers, the downwards concavity of the steady state relations is caused by the fall in current. There was a very small rise in current in some fibers for large hyperpolarizations (greater than -50 mV hyperpolarization) but the amplitude of the rise was less than 5% of the total steady state current. In depolarized fibers, the magnitude of the current transients (the difference between instantaneous and steady state current) was much larger than in polarized fibers.

Fibers in solutions of pH range (6.7-7.3) (solution Eb,c)

In this pH range, the current voltage rectification in permanently depolarized fibers changed from upwards concave ('alkaline' behavior) to

Figure 2.1.10   Instantaneous (open circles) and steady state
(filled circles) current-voltage relations in a
depolarized fiber in acid solution (pH 5.4). Holding
potential= -20 mV. In depolarized fibers in acid
solutions the current always fell to the steady
state.
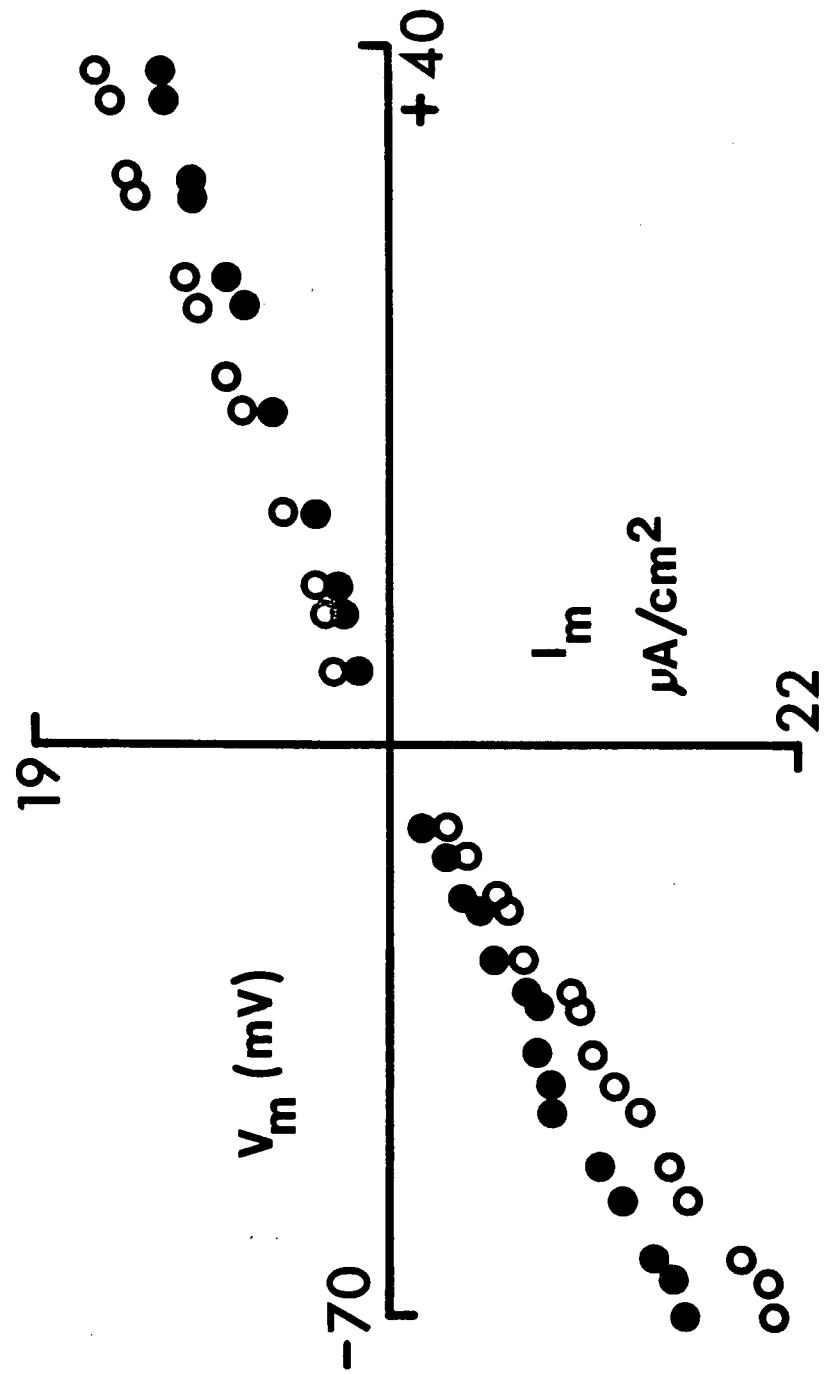
downwards concave ('acid' behavior).

Fig.2.1.11 shows the current-voltage relations from two fibers with the same resting potential (-20 mV). One was bathed in a solution of pH 6.7 (Fig.2.1.11a) and the other in a solution of pH 7.3 (Fig.2.1.11b). The unfilled and filled symbols represent the instantaneous and steady state currents, respectively. It is of interest to note that as was the case for depolarized fibers in acid solutions (see Fig.2.1.10) the instantaneous and steady state current-voltage curves rectify in the same direction.

Fibers in solutions of pH 8.4-8.8

The current-voltage relations of depolarized fibers in this pH range are difficult to interpret. The membrane current was continually reduced in response to hyperpolarizing voltages from the holding potential. As a result, the current voltage curves exhibited several branches. This phenomenon, which we have called 'variable conducting states', was seen in all cells studied in this pH range (average resting potential -19 mV, no. of cells = 20).

The steady state current voltage relations of the fibers had a region of negative slope which was much more pronounced than was ever seen in polarized fibers (Fig.2.1.1c).

Shown in Fig.2.1.12 are the current-voltage relations from a fiber held at -30 mV. The points are numbered according to the order in which the pulses were applied. For large hyperpolarizations the membrane current was very small. In this fiber, five hyperpolarizing runs (not all shown) were applied. The slope conductance (both

Figure 2.1.11   Instantaneous (open symbols) and steady state
(filled symbols) current-voltage relations for
fibers in pH 6.7 (a, solution Eb) and pH 7.3
(b, solution Ec). The resting and holding potential
of each fiber was -20 mV.

Calibration: ordinate, 1 mV = 3.79 x 10^{-6} Amp/cm^2.
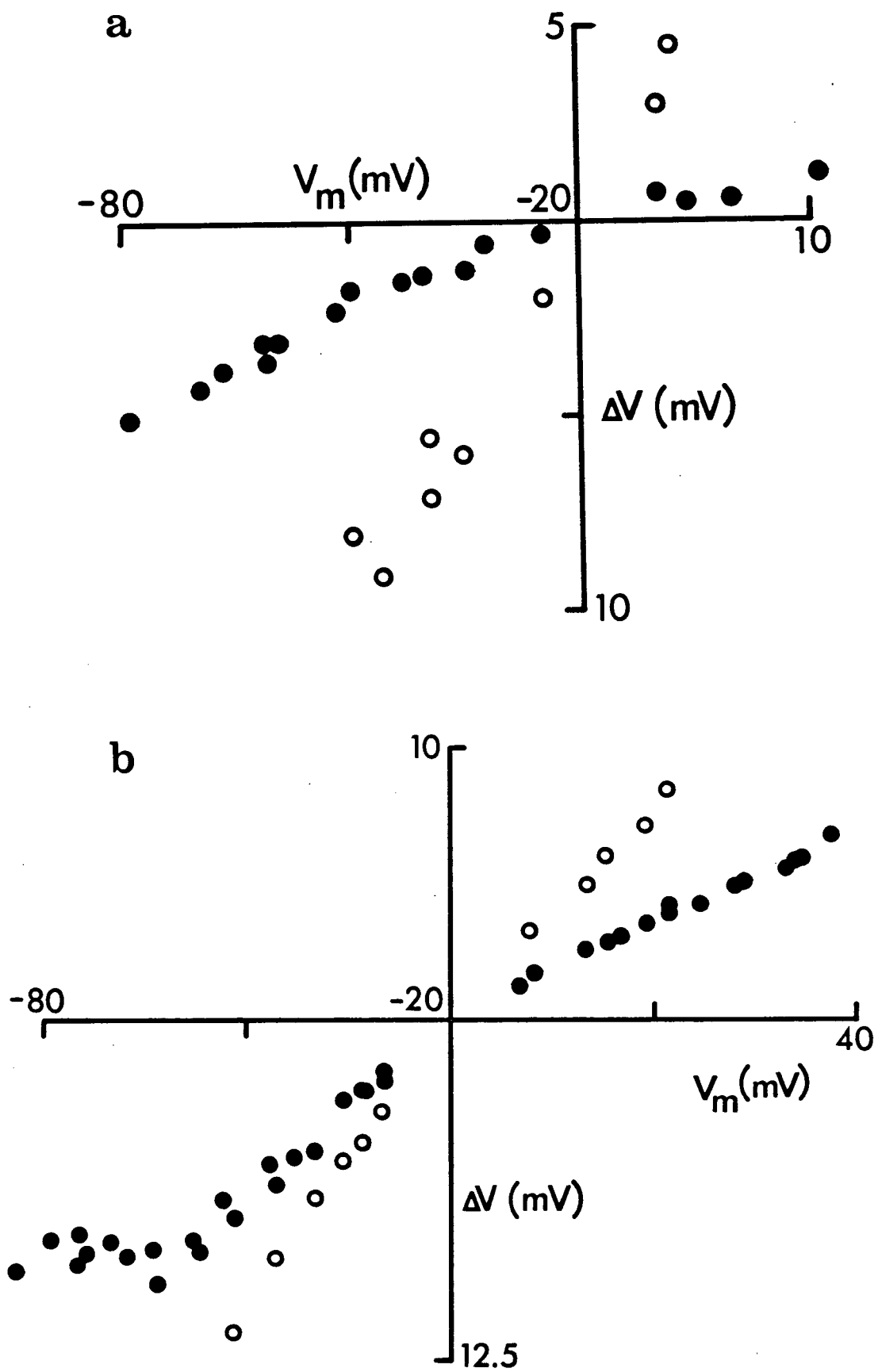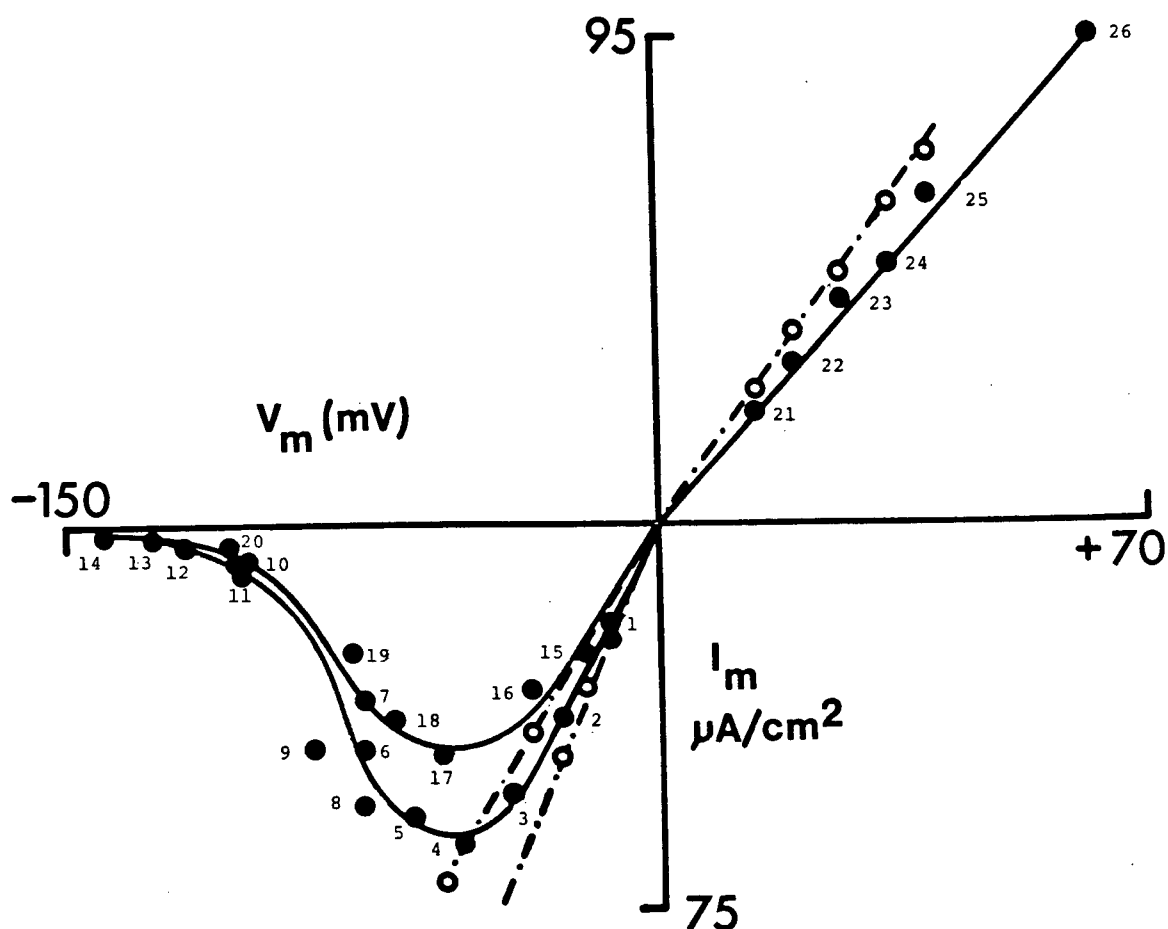
Figure 2.1.12   Instantaneous (open symbols) and steady state
(filled symbols) current-voltage relations of a
depolarized fiber in alkaline solution (pH 8.4).
The numbers beside the points indicate the order
in which the pulses were applied. Five hyperpolarizing
runs were conducted on this fiber, but not all of them
are shown on this graph. The dashed lines are the
instantaneous current-voltage relations.

instantaneous and steady state) at the holding potential for the different states are tabulated in Table II.1.5. For each state, the ratio of the instantaneous and steady state conductance is given. The constancy of this ratio is suggestive that a variable fraction of the membrane's chloride channels may be operational at any time or that the conductance of each channel may vary.

The experiments described in Fig.2.1.12 were performed on osmotically unbuffered solutions. Because of the complex behavior, it is possible that some of these effects might be due to fiber swelling, as the fibers were not in osmotic equilibrium. Consequently, the experiments were repeated with fibers in isotonic solutions. Here, the instantaneous I-V relations appeared to be linear and steady state relations saturated at large negative potentials and on repeated polarization, the membrane conductance was continually reduced. In these fibers, the return to the holding potential after large hyperpolarizations re-activated the contractile system and local contractures sometimes occurred, indicated by sharp 'wobbles' on the current record. These contractions could not always be seen in the stereomicroscope. To try to obviate any difficulty or error that might be introduced by contractions fibers were placed in a hypertonic solution (solution Ed*). In hypertonic solutions, the fibers were shrunken, easily damaged and impalement was difficult. The currents were too large for the preparations be adequately voltage clamped, so no results are available from these preparations.

As we have repeatedly noted, the instantaneous current in depolarized fibers in alkaline solutions (pH 8.4-8.8) is a linear function of the voltage. This is in contrast to polarized fibers (resting potential=

Table II.1.5

Instantaneous and steady state conductances
at the holding potential for 5 conducting
states in a depolarized fiber at pH 8.4.

The data is given as mV:
        (current scale/mV (membrane potential))
and the values in brackets $(mho.cm^{-2})$.

Run	Instantaneous conductance (a)		Steady state conductance (b)		$\dfrac{b}{a}$
1	0.6	(21.7×10^{-4})	0.5	(18.1×10^{-4})	.83
2	0.425	(15.4×10^{-4})	0.313	(11.3×10^{-4})	.73
3	0.35	(10.5×10^{-4})	0.30	(10.9×10^{-4})	.86
4	0.40	(14.5×10^{-4})	0.30	(10.9×10^{-4})	.75
5	0.325	(11.8×10^{-4})	0.288	(10.4×10^{-4})	.87

-80 mV) where the instantaneous current-voltage relations were found
to rectify in the same direction as the steady state relations (Fig.1.1a).

In alkaline solutions, the current-voltage relations appeared to
inflect near the holding potential: in general the outward-current
conductance was less than the inward for small polarizations from the
holding potential. That is, polarizations sufficiently small that in
the hyperpolarizing direction, the steady state current-voltage relation
was linear.

Summary of the effect of pH on resting conductance of depolarized fibers

Table II.1.6 summarizes the effect of pH on the resting conductance
of depolarized fibers. As with polarized fibers, the magnitude of the
resting conductance of depolarized fibers exhibited large variations.
However, it can also be seen (Table II.1.6) that the resting conductance
is reduced by at least 50% when the pH is reduced from 8.4 to pH 5.4
(as in the case of polarized fibers, Table II.1.1).

An interesting observation is that the resting conductance of
fibers in the neutral range (6.7-7.0) was similar to those in alkaline
solutions, suggesting that the pK of the pH titratable site might be
lower in depolarized fibers than in polarized fibers, and perhaps that
there is a dependence of pK on resting potential (Parker and Woodbury,
1976). This appears also to be true in Rana temporaria (Hutter and
Warner, 1972, Fig. 4 A,B). However the sample size of our experiment
(in Table II.1.6) is too small for this conclusion to be confirmed and
in view of the large variability between fibers, experiments need to be

performed on the same fiber at different pH's.

Comparison of the current-voltage relations in polarized and depolarized fibers

We summarize the similarities and differences in the current-voltage relations between polarized and depolarized fibers in solutions of different pH:

acid solutions	instantaneous	steady state
polarized	linear	downwards concave
depolarized	downwards concave	downwards concave

neutral solutions	instantaneous	steady state
polarized	conductance limited	conductance limited
depolarized	conductance limited	conductance limited (*)

alkaline solutions	instantaneous	steady state
polarized	saturating	saturating; and in some fibers, negative slope conductance
depolarized	linear; conductance reduced with repeated polarization	saturating; conductance reduced with repeated polarization resulting negative slope conductance

(*) In depolarized fibers in neutral solutions, even though the instantaneous and steady state current-voltage relations were both conductance limited as in polarized fibers in the same pH, the relations in the depolarized fibers appeared to be linear for a greater hyperpolarizing voltage range.

Table II.1.6

Effect of pH on resting conductance in depolarized fibers.

pH	resting conductance from current-voltage relations
5.4	3.0×10^{-4} mho cm^{-2}
6.7-7.0	6.7×10^{-4} mho cm^{-2}
8.4*	7.5×10^{-4} mho cm^{-2}

* Because fibers in alkaline solutions exhibited several conducting states, this value is the highest conducting state.

B. Voltage Dependence of Current Transients in Depolarized Fibers

As we have described in the preceding section, in response to
hyperpolarizing voltage steps from the holding potential, the current
waveforms in depolarized fibers in solutions of different pH's (solutions
E) were qualitatively the same: current transients always fell to the
steady state in two phases--an initial decay with a time constant of
100 msec and then a much slower 'creeping' fall (300-500 msec) to the
steady state.

The hyperpolarizing current transients were resolved into two
components using the same approximation procedure adopted for polarized
fibers. The slow component in depolarized fibers, as we have found for
polarized fibers, was independent of voltage.

Table II.1.7 summarizes the voltage dependence of the time constant
of the fast component. It can be seen that the voltage dependence of
the time constants in solutions of different pH is very similar.

The current transients in depolarized fibers in alkaline solutions
were more complex as they exhibited a wide range of time constants for
their rapid transients. These variations existed not only between
fibers, but between runs in a single fiber when the fiber went from one
conducting state to another. When a cell was in a highly conducting
state, currents were large and the time course of the rapid transients
was very brief (as short as 10 msec for a 50 mV pulse). In lower
conducting states the kinetics of the initial phase of relaxation were
slower. In Fig.2.1.13, the fast time constants for two cells (cell 2.6.2
and cell 2.10.3) for which data for only one conducting state are

included, are plotted as a function of the amplitude of the voltage step.
Despite the differences in the values of the time constants, their
voltage dependence remained constant. It can be seen from Table II.1.7
that the mean of the voltage dependence of the fast decays of initial
current in alkaline solutions is similar to those recorded at other pH's.

Depolarizing voltages

For depolarizing pulses from the holding potential, current always
fell to the steady level in solutions of low to high pH's. A family of
pulses is shown inFig.2.1.14 from a fiber in a solution of pH 8.4
(solution Ed). The time constants of current decay were 100 to 300
milliseconds. It was clear that the larger the depolarizing voltage, the
more rapid the transient but the data obtained were too scattered for
the voltage dependence of the time constant to be determined.

Priming of the membrane conductance with conditioning pulses in depolar-
ized fibers in alkaline solutions

Some depolarized fibers in alkaline solutions exhibited very complex
time and voltage dependent current transients that could be induced by
conditioning the membrane with very large hyperpolarizations. These
conditioning pulses greatly influenced the membrane conductance.
Fig.2.1.15 shows the results of one experiment in whcih the membrane
potential of a depolarized fiber was stepped from -30 mV to -118 mV.
This large priming pulse (of duration 3 msec) was followed by a sequence
of test pulses to -72 mV, applied 17 seconds apart. As the effects of
priming dissipated, the time course of the slow processes settled back

Table II.1.7

Summary of the voltage dependence of the fast
time-constants of relaxation of chloride current
in depolarized fibers.

pH	Voltage dependence (msec/mV)	
5.4	-1.82 ± 0.70 *	n=4
6.4	-1.67 ± 0.43	n=3
8.4	-1.52 ± 0.24	n=6

* Standard deviation.

Figure 2.1.13   Dependence of relaxation time constants on the size
                of the membrane potential step for two depolarized fibers
                at pH 8.4 (solution Ed).   Triangles are for cell 2.6.2,
                the open and closed symbols representing two different
                conducting states.   All depolarized fibers in alkaline
                solution exhibited at least two conducting states,
                but data for only one are included here for cell
                2.10.3 (filled circles).   The slopes of the two
                regression lines are not significantly different.
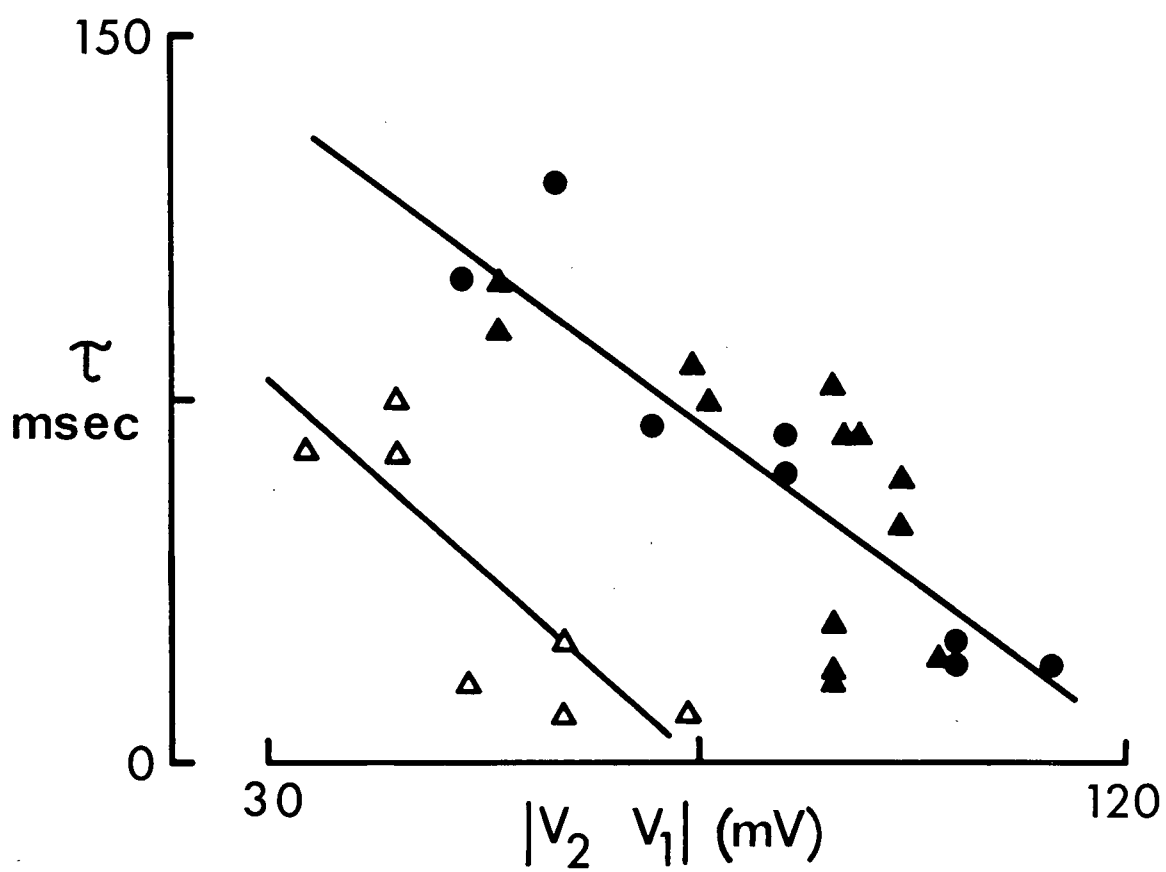
Figure 2.1.14 Waveforms of outward currents in response to
depolarizing pulses in a depolarized fiber at
pH 8.4 (solution Ed). The numbers on the traces
indicate the amplitudes of the voltage steps from
the holding potential (-20 mV). Note the large
inward aftercurrents following large pulses.
Calibration: one second, 10 mV. 1 mV = 3.79 x 10^{-6}
Amp/cm^2.

65

50

30

15
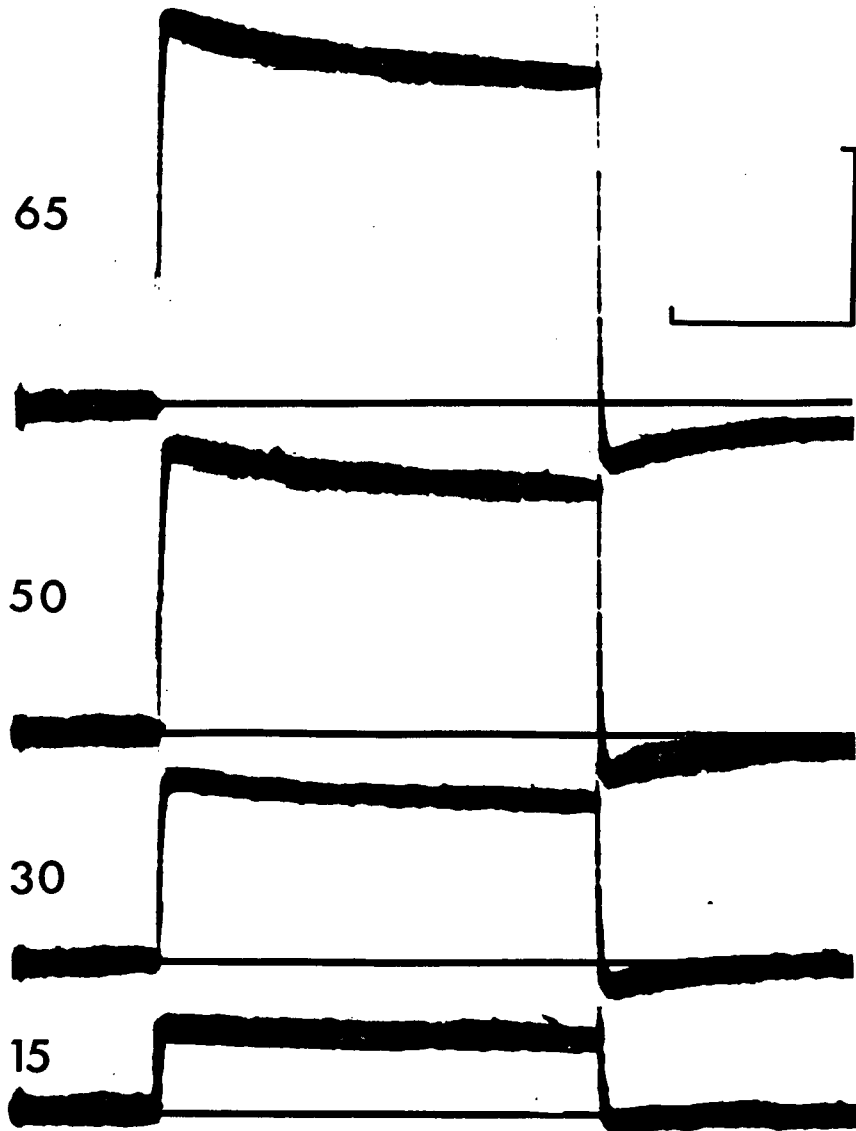
Figure 2.1.15 Currents recorded in a priming sequence. The protocol is described in the text. The upper panel shows the current recorded during the priming pulse. Note the large inward aftercurrent. Lower panel: currents recorded in response to test steps applied 17 seconds apart in the sequence 1,2,3,4. Note that even though the conductance is still very high at the end of the first test pulse the aftercurrents are always outward. Calibration: 500 msec, 5 mV. 1 mV = 3.79 x 10^{-6} Amp/cm^2. Holding potential, -30 mV. Solution Ed (pH 8.4).
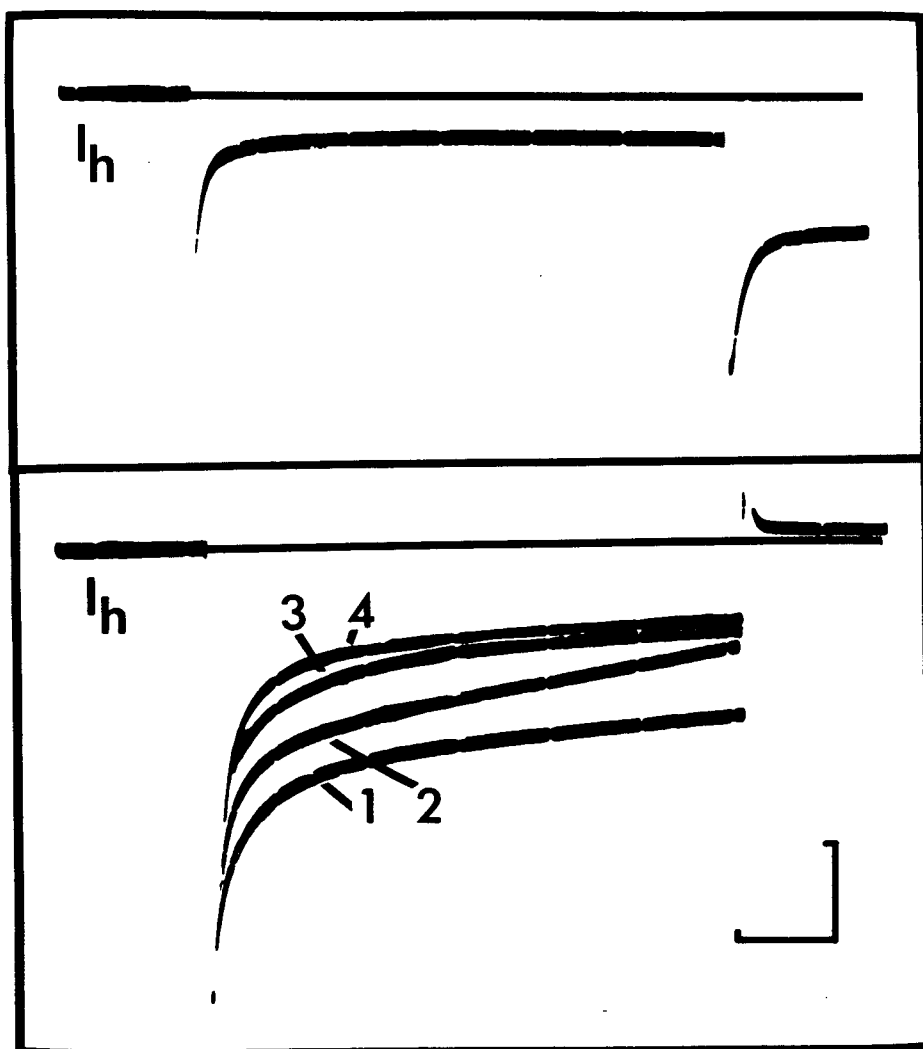
toward the initial values. The time constants of both the initial
rapid and the slower, priming-sensitive phases are listed in Table II.1.8
for each of the current records in Fig.2.1.15. Trace 4 (the current
recorded during the test step applied 68 seconds after the priming pulse)
is the same as was recorded before priming. Since the effects of
priming were so long-lasting and the resetting of initial conditions
involved very long waiting periods, we have not been able to establish
the time and voltage dependence of the onset of priming nor the time and
voltage dependence of its disappearance.

Instantaneous after-currents in depolarized fibers

In depolarized fibers, as in polarized fibers, the direction of the
after-current after returning to the holding potential from a preceding
hyperpolarization or depolarization was opposite to that during the
preceding pulse. However, its magnitude was much larger than in
polarized fibers.

Regardless of the external pH, with depolarizing conditioning
pulses, the instantaneous after-currents always reached a saturating
value with large depolarizations (greater than 50 mV from the resting
potential). This observation is especially of interest in view of the
different rectification behavior of the steady state current voltage
relations of the preceding pulse, thus suggesting that the after-
currents were independent of the preceding steady state current.

With hyperpolarizing conditioning pulses, the after-currents in
fibers in alkaline solutions also showed a tendency to reach a maximum

Table II.1.8

Time dependence of the recovery of time constants
after priming.

Time*	Fast time constant	Slow time constant
17 seconds	160 msec	4.25 seconds
34 seconds	160 msec	2.25 seconds
51 seconds	160 msec	800 msec
68 seconds	160 msec	550 msec

* Time after the beginning of the (three second) conditioning pulse.

value whereas in acid solutions, the observations were variable: some fibers showed saturation whereas others did not (Fig.2.1.16).

Discussion

Steady state current-voltage relations

The steady state current-voltage relation for chloride ions in Xenopus muscle membrane is similar to that for Rana temporaria (Hutter and Warner, 1972): the steady state characteristics depend on the extracellular pH, with a transition near pH 7. The relations show upward concavity in the hyperpolarizing segment for pH greater than 7 and upward convexity (inward-going rectification) in the same region in acid solutions. This behavior has been seen to be independent of the resting potentials of the fibers, except that when chronically depolarized fibers are investigated in alkaline solution there is a negative slope region for large hyperpolarizations that is not as pronounced in normally polarized cells. Negative slope conductance has not been observed in Rana temporaria (Warner, 1972; Hutter and Warner, 1972).

The negative slope conductance observed in our experiments is not as pronounced as that reported by Palade and Barchi (1977) for chloride conductance in normally polarized fibers from rat diaphram. Replacement of chloride by methylsulphate in the mammalian muscle alters the degree of negative slope conductance: indeed for 75% replacement the current-voltage relation becomes linear (Palade and

Barchi, 1977). Our experiments were performed before the work of Palade

and Barchi (1977) appeared in the literature and we have not attempted to

confirm this observation on our preparation: however we have observed

that replacing most of the chloride in solution with sulphate in

depolarized fibers neither significantly reduces steady state current nor

abolishes negative slope behavior.

Instantaneous current-voltage relations

The instantaneous current-voltage relations in Xenopus laevis

differ from those reported in Rana temporaria (Warner, 1972) and for rat

diaphram (Palade and Barchi, 1977). In both the above works, the

instantaneous current-voltage relations were linear at all pH's, whereas

in Xenopus, the instantaneous current-voltage relations usually rectify

in the same direction as the steady state relations in polarized fibers

and become more linear in depolarized fibers. It is not clear what

the difference between Xenopus and Rana might be due to: whether it is

due to an actual difference in the membranes or in the methods used

to estimate the instantaneous currents.

Relations between the instantaneous and steady state properties in

polarized and depolarized fibers

The different rectification curves that are observed in fibers

held at different resting potentials and at different pH's raise some

difficulties in the interpretation of the effects of variations in the

chloride concentration gradient.

In acid solutions the steady state current-voltage relations of
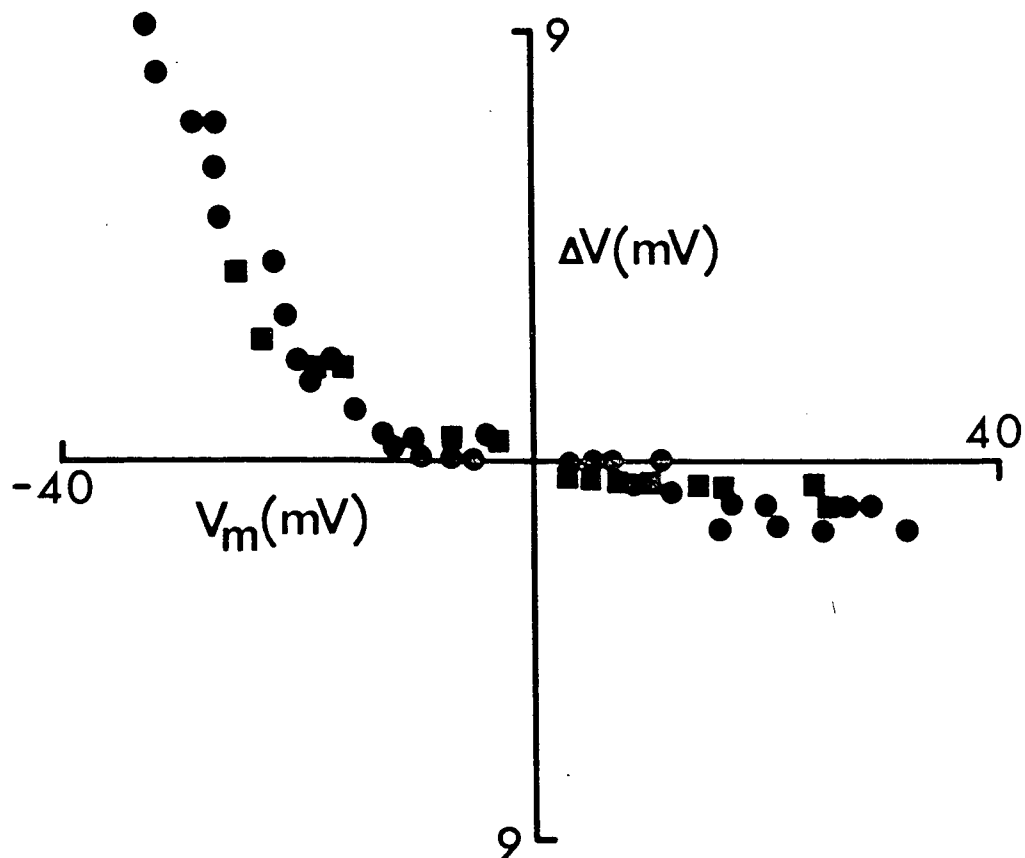
Figure 2.1.16   Instantaneous aftercurrents recorded in two
depolarized fibers in acid solutions plotted as a
function of the amplitude of the preceding voltage
step.   The fibers were held at -20 mV.
Calibration: 1 mV = 3.79 x 10^{-6} Amp/cm^2.

both polarized and depolarized fibers rectify in the same direction but the causes of the rectification appear to be different: in polarized fibers, it is caused by a rising current (Fig.2.1.3 of chapter II) whereas in depolarized fibers, the rectification is caused by the initially falling transient current.

In polarized fibers in acid solutions, the current transients are composed of two components: an initial fall and a subsequent rise, whereas in depolarized fibers, the rise is negligible. Since the current transients of the fall have the same voltage dependence in polarized as in depolarized fibers, it is reasonable to conclude that they represent the same component. The steady state current-voltage relation in polarized fibers with the rising component removed is linear (Fig.2.1.3a), whereas it is downwards concave in depolarized fibers. The instantaneous current voltage relations are linear in polarized fibers and downwards concave in depolarized fibers.

In contrast in alkaline solutions, the instantaneous and steady state relations rectify in the same direction in polarized fibers, both reaching a saturating current and in some instances negative slope conductance. In depolarized fibers, the steady state current-voltage relations also exhibit saturating currents and in many fibers, a pronounced negative slope conductance. In depolarized fibers, the instantaneous current-voltage relations are linear over a much larger voltage range than in polarized fibers.

Dependence of chloride conductance on concentration

In the experiment on Xenopus, the resting chloride conductance has

been found to be independent of the chloride concentration at all
pH's. This is a puzzling result as it is at variance with previous
observations on the dependence of chloride currents on chloride
concentration in neutral solutions. Since the constant field theory has
been found to approximate chloride currents in neutral solutions
(Hodgkin and Horowicz, 1959a; Adrian, 1961; Adrian and Freygang, 1962;
Harris, 1963; Hutter and Warner, 1972), the voltage dependence of the
current-voltage rectification and the magnitude of the resting
conductance should increase significantly with a tenfold increase in
internal chloride concentration. This was not observed in Xenopus,
and it is not clear what the causes of this difference might be. The
only possible cause is an inaccurate determination of the internal
resistivity (see equation 1, chapter I) and hence an incorrect calibra-
tion of the current density. However, the data obtained on the
internal resistivity of depolarized fibers suggest that there is a
very small change in the internal resistivity with a ten-fold increase
in internal chloride concentration.

The pH sensitivity of fast transients

The only aspect of chloride current transient behavior that is
pH-dependent is that in polarized fibers in acid solutions there is
a rising component of the current in response to a single hyperpolarizing
voltage step. It is not seen elsewhere. The presence of this
component does not alter the voltage dependence of the rate of any
preceding fall.

Aftercurrents and slow transients

Slow transients, or 'creep', in ionic currents under voltage clamp conditions and non-zero aftercurrents have been attributed to enhancement or depletion of ionic concentration in restricted or unstirred spaces in electrical continuity with the inside of the fiber and the bulk extracellular space. For example, potassium current creep in frog muscle fibers with hyperpolarization (Adrian, Chandler and Hodgkin, 1970b; Almers, 1972a,b; Barry and Adrian, 1975) is thought to be due to a depletion of potassium in the lumen of the transverse tubular system. The available evidence in the literature suggests that there is no chloride conductance in the T-system (Hodgkin and Horowicz, 1959; Gage and Eisenberg, 1969a). Therefore if such an explanation were to be invoked for the slow decay of chloride current and non-zero aftercurrents, the existence of another internal (external) space where local depletion (enhancement) of chloride concentration occurs, during transmembrane flux, would have to be demonstrated. Strong evidence against this comes from experiments in depolarized fibers in chloride-rich media. The changes in concentration gradients across membranes in these conditions would be minimal, yet the amplitudes of the initial aftercurrents were at least as large in these as in normally polarized fibers. Additionally, aftercurrent amplitudes have seen to saturate under conditions where the preceding steady state currents are still increasing with membrane potential.

Experimental Section 2. Two Pulse Voltage Clamp Experiments

In this section the nature of the fall in membrane conductance with hyperpolarizing potentials ('inactivation') is investigated further by two pulse experiments.

First, conditioning potentials (V_1) of varying amplitude were applied and the conductance at the end of the conditioning pulse was examined by applying a fixed test potential (V_2). The instantaneous current at the beginning of the test potential, $I_2(0)$, was used as an indication of the degree of 'inactivation' at the end of the conditioning pulse.

I. Instantaneous current-voltage relations

A. Experiments where the conditioning potential was varied

The qualitative behavior of all fibers studied was independent of the external pH and the resting membrane potential. When V_1 was more negative than V_2, the test currents rose to the steady state values, whereas for V_1 more positive than V_2, the test currents fell (Fig.2.2.1a). When V_1 was large and negative (or positive), the initial test current $I_2(0)$ approached an asymptotic minimum (or maximum). For intermediate values of V_1, instantaneous test current $I_2(0)$ was found to be sigmoidally related to the conditioning potential. This is shown in Fig.2.2.1b for a typical cell in alkaline solution (resting potential, -80 mV, pH 8.4, solution Bd). The open circles represent the steady state current during the test pulse and the filled circles, $I_2(0)$. The abscissa is the membrane potential during the conditioning step (V_1). The observations

Figure 2.2.1   a) Traces from a two-pulse experiment in alkaline
                solution showing the experimental protocol and test
                current transients, I_2. Holding potential = -70 mV.
                Solution Bd. Current calibration: 1 mV = 3.14 x 10^{-6}
                Amp/cm^2.

                b) Instantaneous currents ($I_2(0)$) (filled circles)
                recorded at the onset of a step to -130 mV (V_2) from
                various conditioning potentials (V_1). The open circles
                indicate the steady state current at V_2 for each pulse.
                Resting potential = -80 mV. pH 8.4 (solution Ed).

                c) Normalized data from two cells plotted against the
                amplitude of the conditioning step. The filled circles
                are obtained from (b).

a

$5\,mV$

$I_1(1)$ $I_2(1)$

$I_1(2)$ $I_2(2)$

I_h

V_h

$1\,sec$

$20\,mV$

$V_1(1)$ V_2

$V_1(2)$

b

$V_m(mV)$

-160 -80

$I_2(0)$

$20\,mV$

c

$V_1\,(mV)$

-140 -80

$I_2(0)$

1
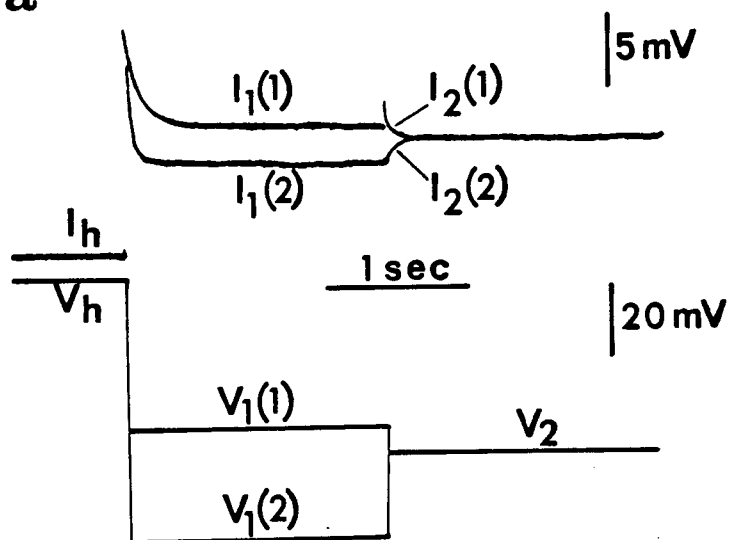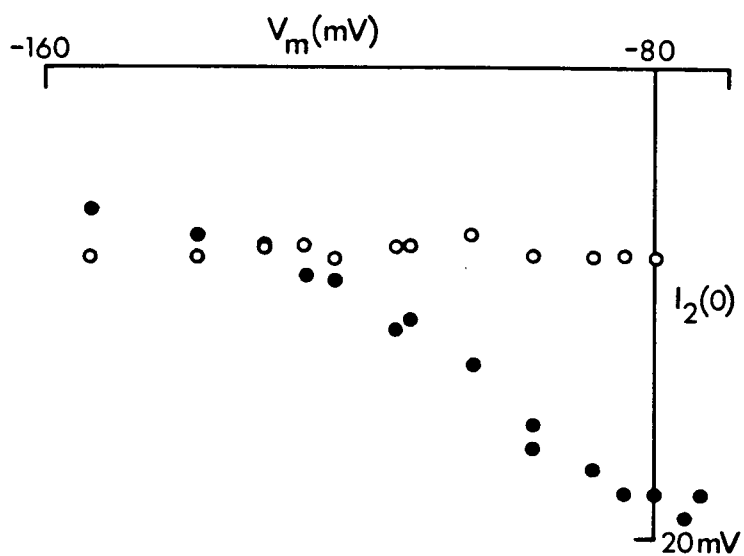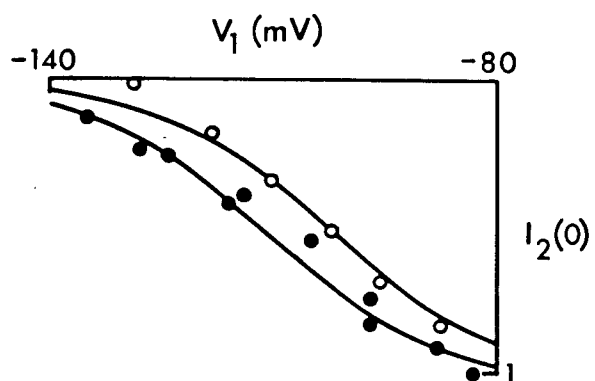
are similar to those made in alkaline solutions in Rana temporaria

(Warner, 1972, Fig. 5A).

Normalization procedures: comparison of data from different fibers

Since cells exhibited different maximum and minimum saturation

currents, a normalization procedure was adopted to compare the effects

of pH on different cells. The relation

$$(2.1) \qquad I_2(0)^{normalized} = (I_2(0) - I_2(0)^{min}) / (I_2(0)^{max} - I_2(0)^{min})$$

was used. $I_2(0)^{max}$ and $I_2(0)^{min}$ are the asymptotic maximum and minimum

recorded values of $I_2(0)$, respectively. The procedure is equivalent

to making the minimum asymptotic value zero and the maximum inward

current, one.

Fibers in alkaline solutions

Normalized data for two polarized fibers in alkaline solution is

plotted in Fig.2.2.1c. The filled circles are derived from Fig.2.2.1b

for which cell V_2 was -130 mV; the open circles are for a fiber in

which V_2 was -104 mV. In both cases, the normal holding potential was

-80 mV. The measured currents differed greatly in amplitude, the steady

state value of I_2 in one (V_2 = -130 mV) being almost three times than

in the other (V_2 = -104 mV). Similar differences were seen in the measured

value of $I_2(0)$.

The curves were fitted to the data points in Fig.2.2.1c using the

distribution function

$$(2.2) \qquad I_2(0)^{normalized} = 1/(1 + \exp(-k(V_1-V*)))$$

where $k=zF/RT$ (z=valence, F is the Faraday constant, R is the gas

constant, and T is the absolute temperature), k is the shape parameter

and V* is the half-saturation voltage. A good fit of the distribution

function to all data from all fibers, whether polarized or depolarized,

in alkaline solutions was obtained with k=.087 (z≃2).

Fibers in acid solutions

The only difference between the results in alkaline and acid

solutions was the value of the slope parameter k. Normalized data

from three polarized fibers in acid solutions (pH 5.4) is shown in

Fig.2.2.2a. Here k=0.188 (z≃4) and this value gave good fit to data

from all cells in acid solutions that showed a falling transient phase

with hyperpolarization, whether polarized or depolarized . In one cell

studied in which only rising transients were seen (with hyperpolarization,

for instance, see Fig.2.0.1c), the sign of k was found to be reversed

although its magnitude was not changed (i.e. the sigmoid curve was

inverted and had the opposite slope). Further experiments in these

fibers is required for an understanding of the rise in conductance with

hyperpolarization.

These observations suggest that at the onset of V_2, $I_2(0)$ is pro-

portional to the distribution of a charged species, between two states

that either enhance or impede the passage of ions through the chloride

channel. The sign of this effective charge cannot be determined, as

formally it is a consequence of the way in which the voltage term in the distribution function is written $((V-V^*)$ or $(V^*-V))$. The assumption of positive valency is consistent with the idea that it could become protonated in acid solution. The difference between acid and alkaline results is clearly demonstrated in Fig.2.2.2b in which the derived relationships are superimposed.

B. Experiments in which the test potential was varied.

We have observed that at the 'end' of a hyperpolarizing or depolarizing pulse, when the membrane potential was returned to the holding level, there was a tail of after-current, or equivalently, a shift of zero current voltage had occurred. This phenomenon was investigated in experiments in which, after a period of conditioning at a constant voltage, the membrane potential was stepped to a variable test level. An estimate of the zero current voltage could then be made from the intersection of the instantaneous current $I_2(0)$ with the V_2 axis.

Results from a depolarized fiber at pH 5.4 are depicted in Fig.2.2.3a. The filled circles represent steady state currents and the open circles initial currents recorded when the membrane potential was stepped from -80 mV to more positive voltages. The linearity of this relation was typical of all those for cells bathed in acid solutions and an example from an experiment on a polarized fiber in alkaline solution (pH 8.4) is shown in Fig.2.3.3b. Non-linearity was always seen as upward concavity (current tending to saturate) as would be expected from the behavior

Figure 2.2.2   a) Normalized data from variable V_1 experiments for
three polarized fibers (resting potential = -70 mV)
at pH 5.4 (solution Ba).

b) Difference between the distribution function for
fibers in acid solutions (a) and in alkaline solutions (b).

a

$V_1(mV)$

-130   -70

$I_2(0)$

b

120mV   0

b   a

$I_2(0)$
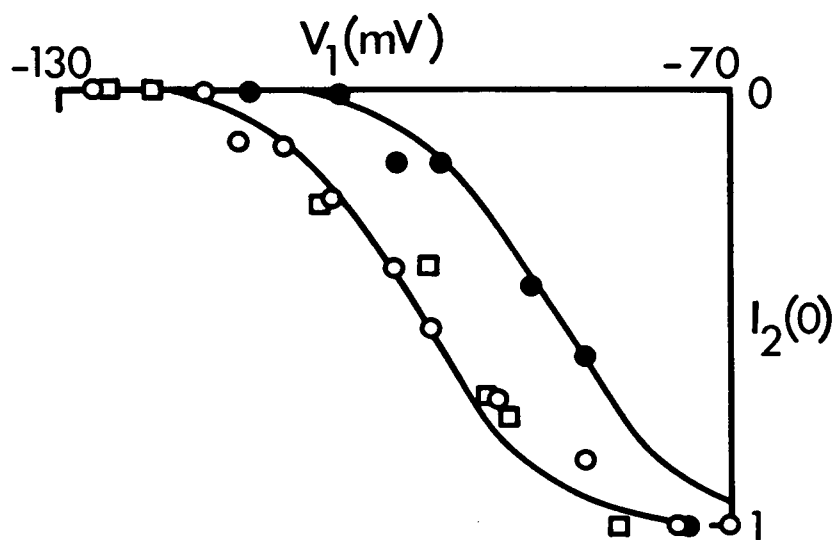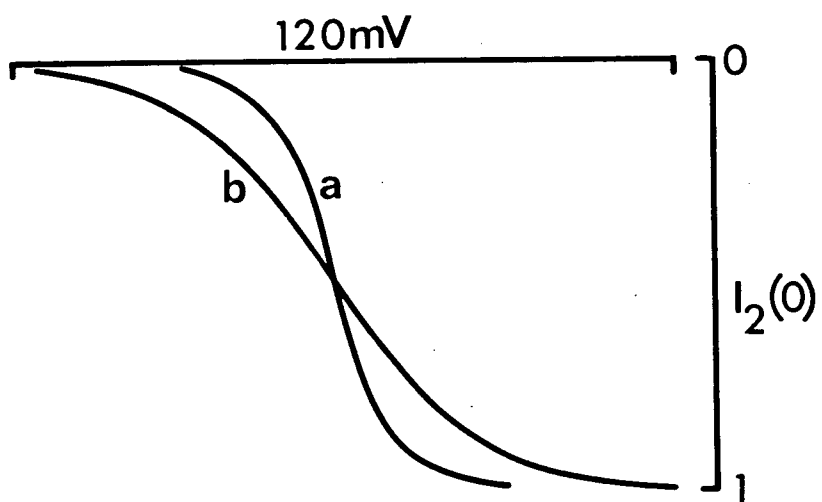
Figure 2.2.3 Steady state and instantaneous current-voltage relations
in two-pulse experiments.

The filled circles represent steady state current-
voltage curves and the open circles, the instantaneous
currents recorded when the membrane potential was
suddenly stepped to a variable test voltage from
a previously fixed conditioning potential (V_1).

a) Depolarized fiber (resting potential, -20 mV) at
pH 5.4 (solution Ea). V_1 = -80 mV.

b) Polarized fiber (resting potential, -80 mV) at
pH 8.4 (solution Ed). V_1 = -118 mV.

Current calibration: a) 1 mV = 3.79 x 10^{-6} Amp/cm^2.
b) 1 mV = 3.14 x 10^{-6} Amp/cm^2.
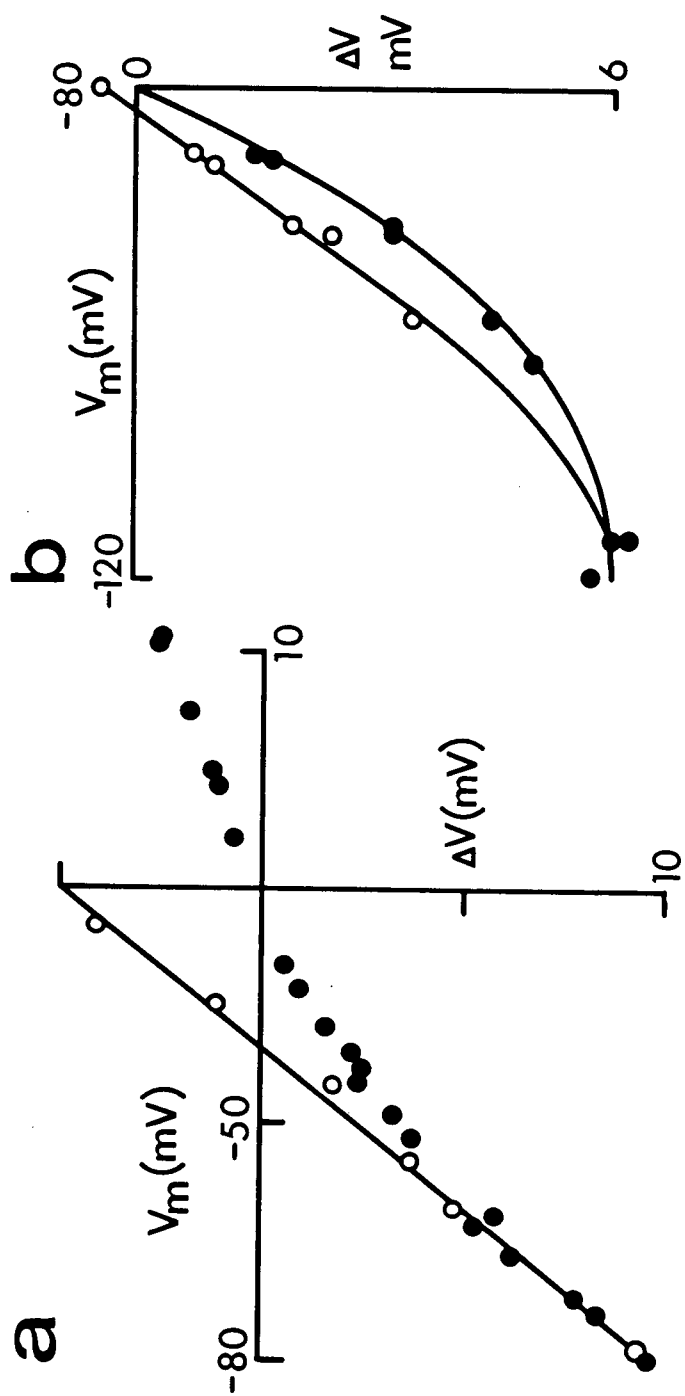
of currents at the onset of test steps from the holding potential. A

shift of zero current potential in a negative-going direction from the

resting potential after hyperpolarizing conditioning has been noted

by Warner (1972). In our experiments, this shift ranged from 0 to 25

millivolts.

The dependence of the magnitude of the voltage shift on the

conditioning voltage was investigated in depolarized fibers in alkaline

solutions. Results are displayed in Fig.2.2.4 for an experiment in

which three different values of V_2 were used over a range of V_1 from

-58 to +7 mV in a fiber in osmotically buffered solution. The variable

V_1 relations are plotted in Fig.2.2.4a (open circles, V_2=-38 mV; filled

circles, V_2=-47 mV; filled squares, V_2=-57 mV) in which the lines are

drawn according to equation 2.2 scaled between the minimum and maximum

currents for each V_2. The value of k that was used was the same as for

all other cells in alkaline solution (.087). Notice that the separation

of the relations is less at the left hand end (V_1 most negative) than at

the right-hand end (V_1 most positive), that the separation of the upper-

most line (least negative value of V_2) from the middle relation is almost

the same as that of the lowest relation (largest negative value of V_2).

This implies that for equal steps of V_2, the relations are equally spaced

on the current axis: there is no lateral shifting of these relations, as in

each case V^* is 9 mV more negative than the holding potential (i.e. -27

mV). In Fig.2.2.4b the points for V_1=-58 mV (smallest currents), V_1=-40 mV,

V_1=-33 mV, V_1=-13 mV and V_1=-3 mV (largest currents) are replotted on the

V_2 versus current ($I_2(0)$) plane. The lines through the points are drawn

Figure 2.2.4 a) Family of $I_2(0)$ versus V_1 relations obtained from
a depolarized fiber (resting potential, -18 mV) in
osmotically buffered alkaline solution (solution Ed).
The numbers on the lines indicate the absolute membrane
potential at V_2. The lines were fitted according to
equation 2.2, scaled to the maximum and minimum values
of $I_2(0)$.

b) Family of $I_2(0)$ versus V_2 relations replotted from
(a). The numbers adjacent to the lines indicate the
absolute membrane potential at V_1. The lines were
fitted by eye.

a

V_1(mV)

-58   -18   7

I_2(0)

$\mu A/cm^2$

-38
-47
-57

133

b

V_2(mV)

-58   -3

I_2(0)

$\mu A/cm^2$

- 58
- 40
- 33
- 13
- 3

133
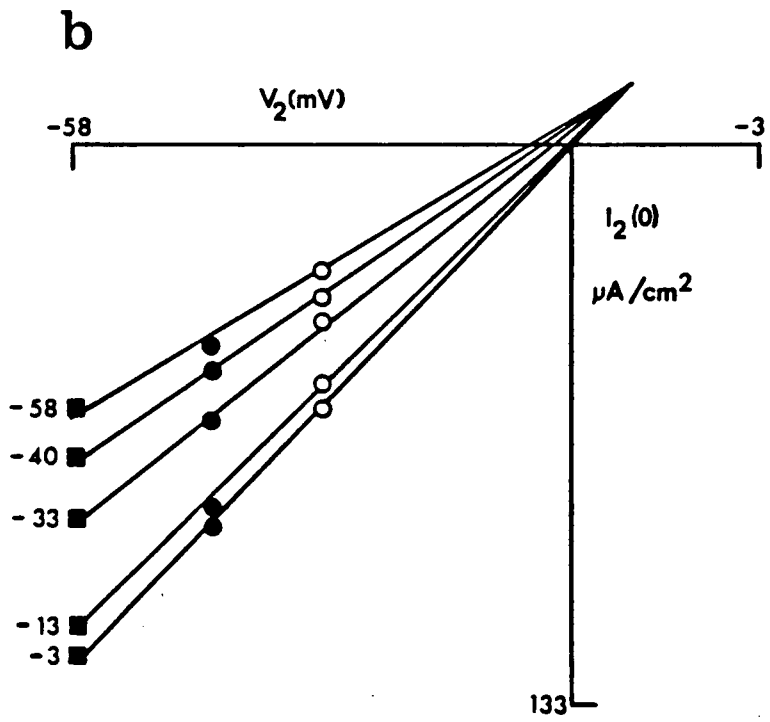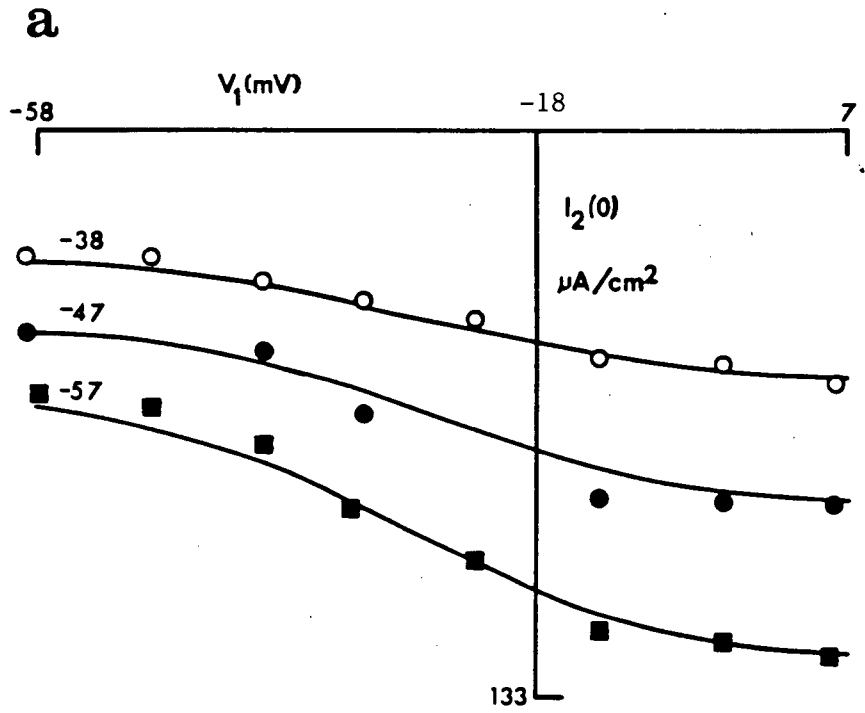
by eye and appear to meet in a point. The importance of this observation will become apparent in Chapter III. The rationale for drawing straight lines was that in an earlier run on the same cell, for a V_1 of -55 mV and a range of V_2 from -68 mV to +12 mV the relations was seen to be linear. It is not shown here because the currents recorded were slightly less than those for the runs shown and the relation fell outside the envelope of those included in Fig.2.2.4b.

II. The voltage dependence of chloride current transients in two pulse experiments.

The voltage dependence of current transients in response to hyper-polarizing voltage pulses from the holding potential has been found to depend only on the size of the voltage step. In this section, the voltage dependence of current transients in two pulse experiments is described. It will be seen that the voltage dependence of rising currents (when V_1 is more negative than V_2) and the falling currents (when V_1 is less negative than V_2) are both dependent on the size of the voltage step.

A. Dependence of time constants on the voltage step $|V_2-V_1|$

Depolarized fibers

When V_1 was less negative than V_2, the decay of the test current $I_2(0)$ was resolvable into either one or two time constants for fibers in both alkaline (pH 8.4) and acid (pH 5.4) solutions.

Fig.2.2.5 shows the time constants of the initial transients from a fiber with a two time constant decay. The open symbols represent the

fast time constants for the initial fall of current in experiments in which the conditioning pulse (V_1) was more positive than V_2. There was a slow time constant (not shown in the Figure) whose magnitude was 100 msec and was voltage independent. In other fibers, this slow time constant has been found to vary between 100 and 250 msec. The filled symbols represent the converse situation (V_1 more negative than V_2) in which rising currents were observed. The regression line relating the time constant to the absolute voltage difference has a slope of -1.46 msec/mV. This is similar to the voltage dependence in one pulse experiments (Table II.1.7).

For the fibers that exhibited only one time constant with current decay, the voltage dependence was greater. This is shown in Fig. 2.2.6 for a fiber at pH 5.4 and held at -20 mV. When V_1 was more positive than V_2, the falling transient I_2 was fitted by a single exponential with a time constant of 250-350 msec and a voltage dependence of -2.5 msec/mV. When the test currents rose (V_1 more negative than V_2) the regression line relating the time constants to the absolute voltage difference $|V_2-V_1|$ had a slope of -1.78 msec/mV for $|V_2-V_1|$ greater than 15 mV (otherwise the transients were too small for the time constants to be accurately resolved).

Polarized fibers

In acid solutions, the current transients were too small for accurate analysis.

Otherwise the conclusion about the dependence of current transients on the size of the voltage step was also found to hold in neutral and alkaline solutions.

(

Figure 2.2.5   Time constants of relaxation of the test currents
(I_2) in a two-pulse experiment, plotted as a function
of the absolute value of the difference between the
voltage steps. The data was obtained from two depolarized
fibers (resting and holding potential, -30 mV) in
alkaline solution (solution Ed). Filled triangles: fast
time constant for rising transients (V_1 more negative
than V_2). Open symbols: time constants of falling
currents (V_1 less negative than V_2). The triangles
(open and filled) are from the same fiber.
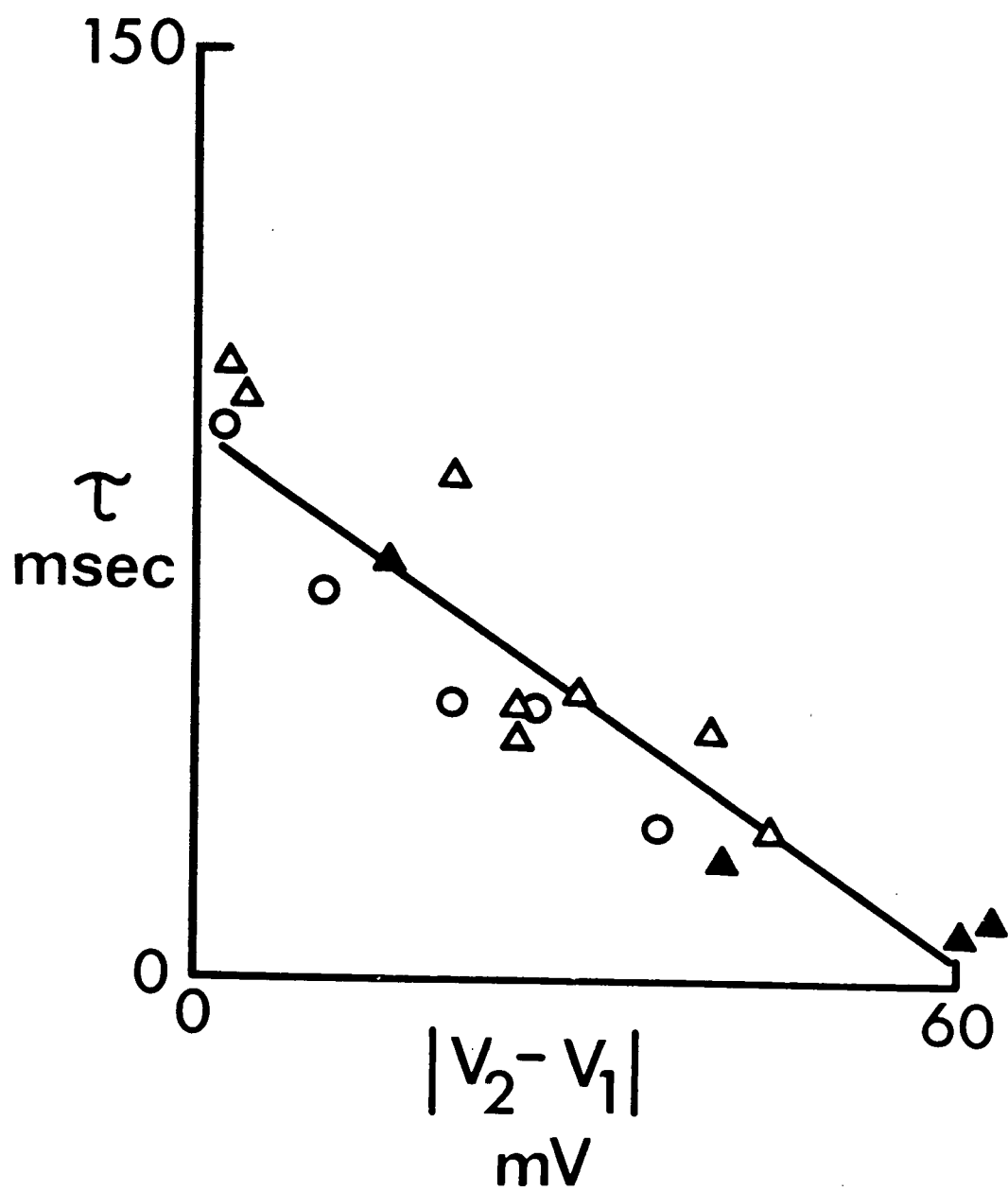
Figure 2.2.6 Top panel: data derived from a depolarized fiber
(resting potential, -20 mV) at pH 5.4 (solution Ea)
in an experiment similar to that of Figure 2.2.5.
Filled symbols are again the time constants of rising
transients and open circles are for falling transients.

Bottom panel: falling transients from an experimental
sequence (from the same fiber as the top panel) in
which the relaxation was resolved into only one time
constant.

time constant (msec)
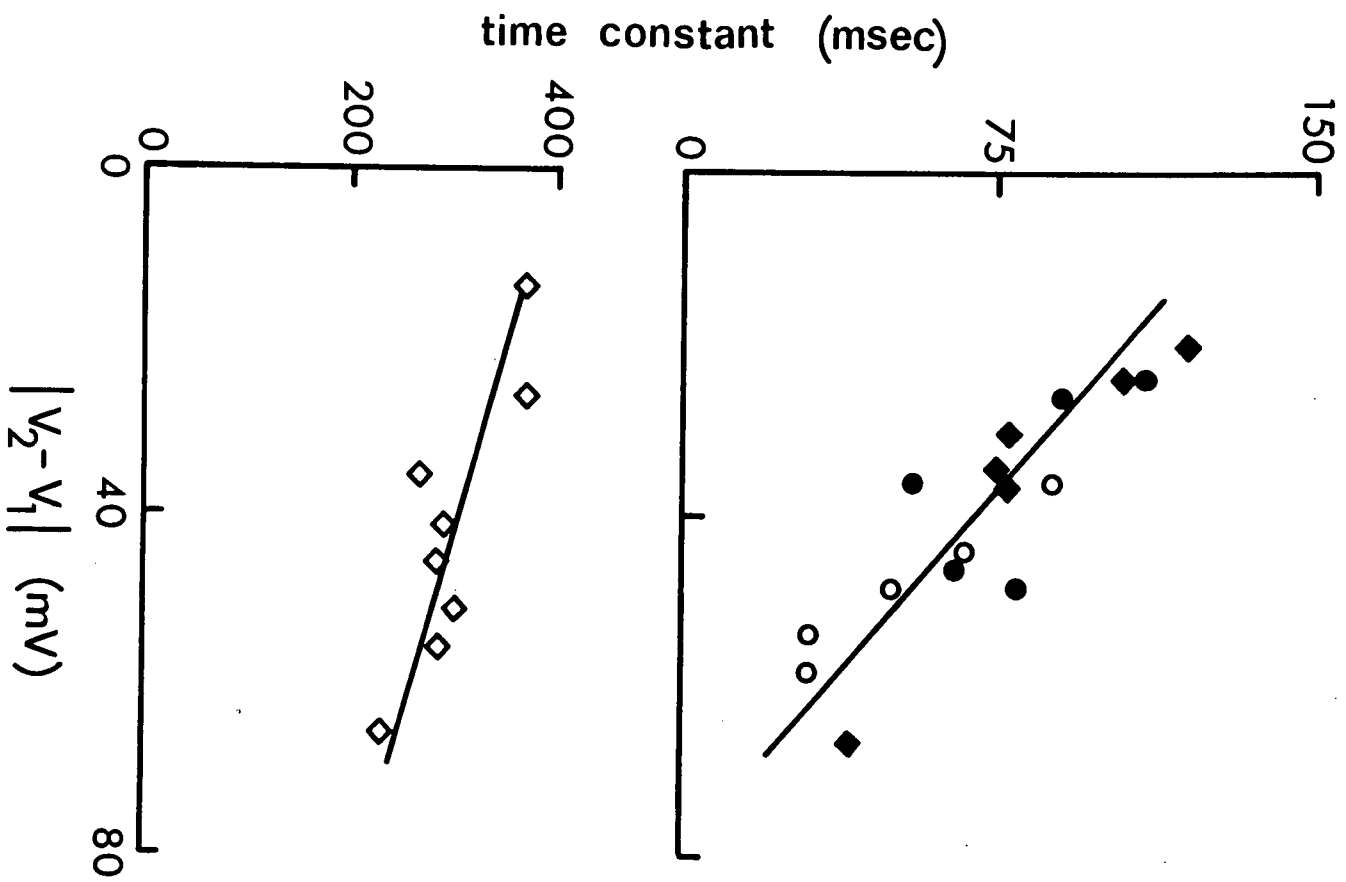
Summary of the voltage dependence of current transients

One and two pulse experiments on polarized and depolarized fibers
in solutions of different pH's (except in acid solutions when the cur-
rent transients exhibit only a rise) have revealed that the voltage
dependence of current transients may be summarized as follows:

When the conditioning and the test potentials are both more
negative than the resting potential the fast time constant depends on
the size of the voltage step, whether the currents rise (V_1 is more
negative than V_2) or fall (V_1 more positive than V_2).

For potentials that are more positive than the resting potential,
the current transients are two to three times longer than their
corresponding hyperpolarizations but the analytical expression for
their voltage dependence has not been obtained.

Appearance of a delayed (non-exponential) falling current

When the test current initially rose (V_1 more negative than V_2)
a delayed fall to the steady state was often seen in depolarized fibers
at all pH's and was particularly prominent in those fibers that
exhibited priming in alkaline solutions. The time-course of the delayed
fall was non-exponential and it exhibited complex voltage and time
dependence behavior. As V_1 was made increasingly negative and V_2 held
constant, the initial rate of rise of current became more rapid and
the delay before the fall to the steady state was reduced (Fig.2.2.7).

The initial rise in current was apparently due to chloride because
the time constant (of the rise in initial current) was found to have
the same voltage dependence on $|V_2-V_1|$. The magnitude of the

Figure 2.2.7 Changes in the waveform of I_2 in an experiment in
which V_2 was held constant at -35 mV. The amplitude
of V_1, in millivolts, is indicated on the left of
the traces. The horizontal line above each trace
indicates the holding current. Calibration:
abscissa; 1 second; ordinate; 5 mV (for the current
traces). 1 mV = 3.79 x 10^{-6} Amp/cm^2.

48

60

70

82
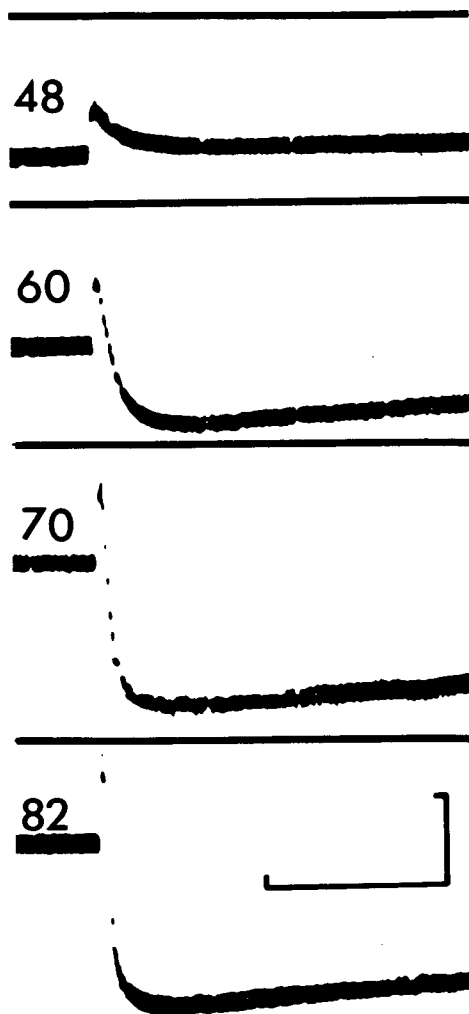
non-exponential component was found to increase with increasing V_2

(when the conditioning potential V_1 was held constant). It is

possible that the delayed non-exponential fall might be due to another

ionic component. This will be discussed in experimental section 3.

Discussion

The results presented in this section show that instantaneous

currents in Xenopus muscle membrane depend on the membrane potential

at which a steady state has been reached just prior to the application

of a voltage step as well as the magnitude of the step.

Observations that the minimal instantaneous test currents $(I_2(0))$

are not zero at all pH and for very large negative conditioning poten-

tials indicate that inactivation is not complete and that the probabi-

lity of a chloride channel opening at any transmembrane potential at

any time does not reach negligibly small values.

Shifting of the S-curves

A curious observation with the sigmoid curves in polarized and

depolarized solutions was that the mean of the distribution was always

between -9 and -30 mV with respect to the holding potential. This

suggests that some controlling moiety within the channel finds a minimum

free energy state under conditions of electro-chemical equilibrium of

the ions (chloride) normally conducted by the channel.

Relation between instantaneous and steady current values

Classical descriptions of ion transport across cell membranes

consider the driving force on an ion the deviation of the transmem-
brane potential from its equilibrium or Nernst potential. If this
view were adopted for chloride in Xenopus, then the current would be
expressed as: $I_{Cl} = g \cdot (V_m - V_{Cl})$, here g is the chord conductance with
respect to the equilibrium, (V_{Cl}), or holding potential (when the two
are the same). We have noted that the steady state current-voltage
relations rectify as a function of external pH. It is interesting to
note that the sigmoid curves ($I_2(0)$ versus V_1 relations) were observed
regardless of the previous steady state conductance. A quantitative
comparison of the differences can be made by defining the conditioning
steady state conductance $g(V_1, \infty)$ by:

$$g(V_1, \infty) = I(V_1, \infty)/(V_1 - V_{Cl})$$

and the instantaneous test conductance $g(V_2, 0)$

$$g(V_2, 0) = I_2(V_2, 0)/(V_2 - V_{Cl})$$

where $I(V_1, \infty)$ = steady state conditioning current density

$I(V_2, 0)$ = instantaneous test current density

For fibers bathed in acid solutions, $g(V_1, \infty)$ increased with
increasingly negative conditioning pulses whereas it decreased in alka-
line solutions. Since the instantaneous $I_2(0)$ (as a function of V_1)
relations were always sigmoid regardless of the slope of the steady
state current-voltage relations for currents that initially decrease,
it is qualitatively clear that steady state conductances are not equal
to the subsequent instantaneous conductances. Two quantitative com-
parisons of $g(V_1, \infty)$ and $g(V_2, 0)$ can be made. First, the instantaneous
test current $I(V_1, V_2, 0)$ is predicted from the conditioning steady

state current $I(V_1, \infty)$ using the relation

$$I(V_1, V_2, 0) = (V_2 - V_{Cl}) I(V_1, \infty) / (V_1 - V_{Cl})$$

and is compared with the experimentally measured instantaneous I_2 from variable V_1 experiments.

Conversely, the steady state (V_1) current-voltage relation is predicted from the measured instantaneous I_2 via

$$I(V_1, \infty) = (V_1 - V_{Cl}) I(V_1, V_2, 0) / (V_2 - V_{Cl})$$

The filled circles of Fig.2.2.8 are the measured currents and the open circles are the corresponding values predicted using the appropriate $I(V_1, \infty)$ or $I_2(V_2, 0)$.

Several conclusions can be drawn from these quantitative comparisons:

For both polarized and depolarized fibers in acid solutions, the measured instantaneous I_2 is always less than predicted from the previous steady state conditions (Fig.2.2.8b,d).

In contrast, measured instantaneous I_2 is always greater than predicted for polarized fibers in alkaline solutions (Fig.2.2.8f). Conversely, measured $I(V_2, 0)$ predict increasing steady state currents with increasingly negative V_1 rather than the limiting currents that were observed (Fig.2.2.8e).

For depolarized fibers in alkaline solutions, measured instantaneous I_2 is always less than predicted from the previous steady conditions (Fig.2.2.8h).

Finally, it is of interest to note that since the measured minimal instantaneous I_2 is near zero (holding current) for depolarized

fibers in both acid and alkali pH's, the predicted steady state (V_1) current-voltage relations always show a negative slope conductance (Fig. 2.2.8c,g), whereas in polarized fibers, the measured minimal $I(V_2,0)$ is much larger and under these calculations, increasing currents are always predicted with increasing V_1's (Fig. 2.2.8a,e).

The voltage dependence of the kinetics of current transients

The chloride permeation system responds asymmetrically to positive- and negative -going voltage steps from the resting potential. In the positive or depolarizing direction, the current transients are approximately three times slower than their corresponding hyperpolarizing voltage pulses. This asymmetric response is not predicted from the movement of a charged particle within the membrane phase.

Relaxation rates have been shown to have the same dependence on the voltage difference $|V_2-V_1|$ at all pH's and in polarized and depolarized fibers, at least when V_1 and V_2 are more negative than the resting potential. This is so in spite of the steady state current-voltage relations being very different under the different conditions imposed. The valence of a charged group associated with the control of the instantaneous currents in the chloride channel was derived from the slope of the sigmoid relations ($I_2(0)$ versus V_1). If this group were to relax from one state to another when the membrane potential is changed, one would expect the rate of relaxation (and therefore the speed of the current transients) to change by a factor of two in going from alkaline to acid solutions. This was not observed in experiments (despite the large variability of the relaxation rates).

We do not know whether this is due to the 'groups' involved in the control of initial currents and current transients being different or to the method of time constant extrapolation or approximation being inappropriate for this kind of analysis (for example, perhaps we should have been measuring an initial extremely fast transient that we could not resolved).

Finally, if current transients reflect a change of state of some controlling group or site, within the chloride channel, the present results indicate the site has no preferred, or minimum potential energy, state, and the rate of transition from one state to another depends linearly on the initial force applied (voltage step), over a wide range.

Figure 2.2.8   In this figure the filled circles represent data

obtained experimentally and open circles represent

points computed as described in the text. In (a)

the filled circles represent the steady state current-

voltage relation for a polarized cell in acid solution

(holding potential, -70 mV; solution Ba). Data was

used to compute the open circles in (b). Conversely,

the filled circles in (b) represent experimentally

derived values of $I_2(0)$ (ΔV) as a function of $V_1(V_m)$

and these data were used to obtain the open circles in

(a). Data in (c) and (d) are from a depolarized fiber

at pH 5.4 (holding potential, -20 mV; solution Ea) and

those in (e), (f) and (g), (h) are from polarized

(holding potential, -80 mV; solution Bd) and depolarized

fibers (holding potential,-30 mV; solution Ed) respectively

at pH 8.4.
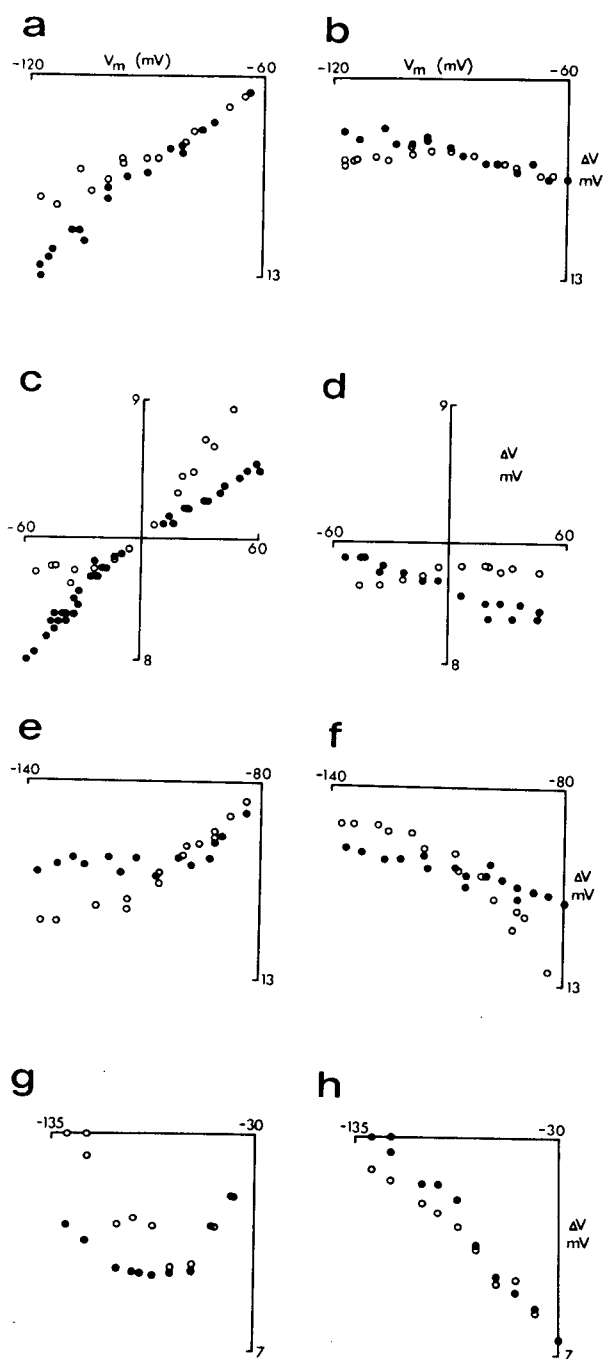
Experimental Section 3: The Inactivation and Recovery of Initial

Currents; Dependence of Kinetics on Initial Conditions

I. Recovery of Conductance

When a hyperpolarizing step was applied to a muscle fiber held

at the resting potential the current decreased to the steady state

in alkaline solutions and increased to the steady state in acid

solutions. Upon return of the hyperpolarizing voltage to the resting

potential transient aftercurrents were noted; these aftercurrents,

opposite in direction to the hyperpolarizing currents, reflect the

recovery of the membrane conductance to its original resting condition.

This recovery was studied by applying a second hyperpolarizing

constant (amplitude) test pulse at a variable period t after the

return of the first pulse to the holding potential.

Fig.2.3.1 shows the experimental protocol. The first pulse

set the membrane to a certain 'conditioned' state. When the voltage

was returned to the holding potential, the mechanisms responsible

for the observed changes in conductance began to be restored to their

initial, or 'unconditioned' state. The current at the beginning of

the second pulse $I_2(0)$, and the timecourse of relaxation of this

current (I_2) were used as indicators of the degree to which initial

conditions had been restored.

From observations that have described, some of the results may

be anticipated: For no time separation between the conditioning

and test pulses (conditioning step more negative than test step)

the test current I_2 rose to a steady state; if the two steps were

equal then the test current was constant $(I_2(0)=I_2(\infty))$. When the
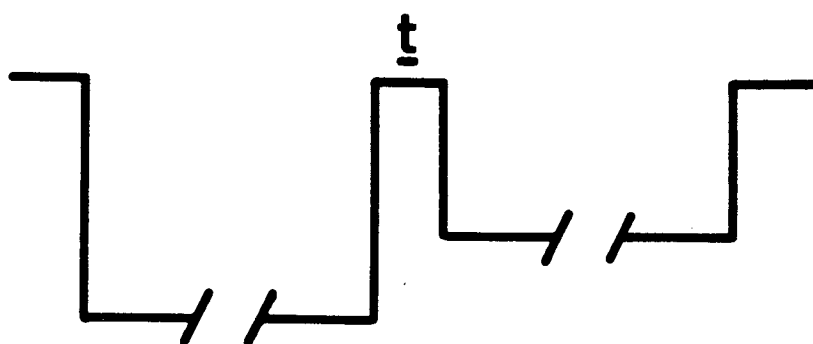
Figure 2.3.1   Protocol of recovery experiments. Two voltage pulses
about three seconds long were applied, the first,V_1,
set to a more negative potential than the second,V_2.
The two pulses are separated by a brief and variable
return to the holding potential ($\underline{t}$).

test potential was separated from the conditioning potential after

a long period of recovery at the holding potential, then the test

currents fell to the steady value regardless of the size of the con-

ditioning potential. Thus for t=0 a rise in test current is found

and for long t a fall is observed (with different time constants for

the two cases). Therefore as the time period of recovery was varied,

the initial currents and the time constants of their relaxations

to the steady value would be expected to depend on the duration of

the recovery at the holding potential.

A. Recovery experiments in polarized fibers

The results from fibers in neutral and alkaline solutions were

similar; the dependence of initial currents and dependence of time

constants on duration of recovery are illustrated in Fig.2.3.2.

Open circles are from a fiber in pH 7.3 and filled circles in pH 8.4.

The dependence of recovery of the initial currents on t appeared to

be sigmoid (S-shape) (Fig.2.3.2b). The rates of recovery of both

time constants (Fig.2.3.2a) and initial currents (Fig.2.3.2b) for

fibers in neutral and alkaline solutions were similar. These

results will be described in greater detail for depolarized fibers

(as they are similar to polarized fibers).

In acid solutions (pH 5.4-6.7) for the fibers that exhibited a

biphasic response with hyperpolarizations (Fig.2.0b) the transients

associated with the test pulses were very small and it was not

possible to analyze for time constants.

Fig.2.3.3 shows the waveforms from a fiber in acid solution

(pH 5.4) whose current rose with hyperpolarization. With increasing

durations of recovery at the holding potential, the magnitude of the

current transient increased (the amplitude of $I_2(0)$ decreased) and

the rate of rise to the steady state increased.

Clearly, in contrast to situations where a falling current transient

accompanied hyperpolarization from the holding potential, the monotonic

rise in current during conditioning caused an enhancement of $I_2(0)$. One

experiment from these fibers showed that when V_2 was fixed and V_1

was variable, initial I_2 depended sigmoidally on V_1, but the sigmoid

curves were inverted when compared with the result when conditioning

by negative-going voltages caused a diminution of $I_2(0)$. The occurrence

of sigmoid relations in both cases suggests that they are under the

control of similar mechanisms. This is reinforced by the present

observations that recovery of initial current and kinetics both

depend on initial conditions for fibers exhibiting normal or inverted

sigmoid ($I_2(0)$) dependence on conditioning potential V_1. However,

a difference does exist between them as the rising currents have

a different voltage dependence from the fall. No attempt was made

to investigate these details any further.

B. Recovery experiments in depolarized fibers

The recovery of conductance from a hyperpolarizing prepulse was

studied in more detail in depolarized than in polarized fibers

because the difference between the initial test current $I_2(0)$ and

steady state test currents $I_2(\infty)$ was much larger; consequently the

kinetics could be more accurately resolved. In the experiments the

test potential was always chosen more positive than the conditioning

potential. Recovery of initial current was then characterized by

the duration (t_o) of the period at the holding potential at which the

initial current had recovered to a value equal to the steady state

current ($I_2(\infty)$), although initial and steady states were sometimes

separated by non-steady currents. For t less than t_o, $I_2(0)$ was

less than $I_2(\infty)$ and for t greater than t_o, $I_2(0)$ was greater than

$I_2(\infty)$ (Fig.2.3.4). Both the dependence of initial current $I_2(0)$ on

t and the dependence of current transients of I_2 on t will be

described in the following.

Fibers in acid solution (pH 5.4)

The recovery of initial current showed both exponential

dependence on t (time constant varying from 15 to 25 msec) and

sigmoid dependence (Fig.2.3.5). Because of the sigmoid and exponential

dependence, the parameter t_o was found to be an adequate indicator of

the rate of recovery in different fibers. This rate of recovery

appeared to depend on the amplitude of V_1: the larger the conditioning

pulse the smaller the t_o and when recovery time-course followed an

exponential, the smaller the time-constant. These observations can

only be considered as preliminary as an insufficient number of

experiments was performed on the same fiber with different conditioning

potentials for the nature of this dependence to be resolved.

The dependence of the kinetics of I_2 transients on t can be

qualitatively observed in Fig.2.3.4. The fiber was in a solution

Figure 2.3.2 a) Recovery of relaxation time constants in two

polarized fibers. Open circles are from a fiber

studied at pH 7.3 (resting potential, -80 mV, solution

Bc). Filled circles are from a fiber in a solution

of pH 8.4 (resting potential, -80 mV, solution Bd).

In this experiment, both pulses (V_1 and V_2) were of the

same amplitude and hence only falling current transients

were observed.

b) $I_2(0)$ plotted as a function of $\underline{t}$ (period of

recovery at the holding potential (-80 mV)) in the

same experiment. The right hand ordinate is for data

from the fiber studied at pH 7.3 and left hand ordinate

is for the fiber studied at pH 8.4. The abscissa is

equivalent to the steady state current, 9.25 mV and

6.25 mV on the ΔV scale for the fiber at pH 7.3 and that

at pH 8.4 respectively. 1 mV corresponds to a current

density of 3.79 x 10^{-6} Amp/cm^2.
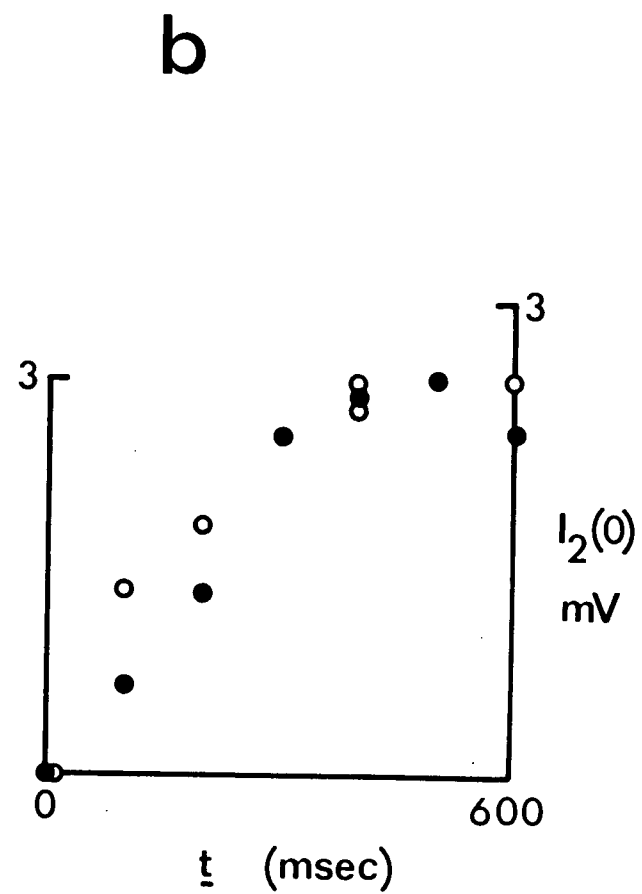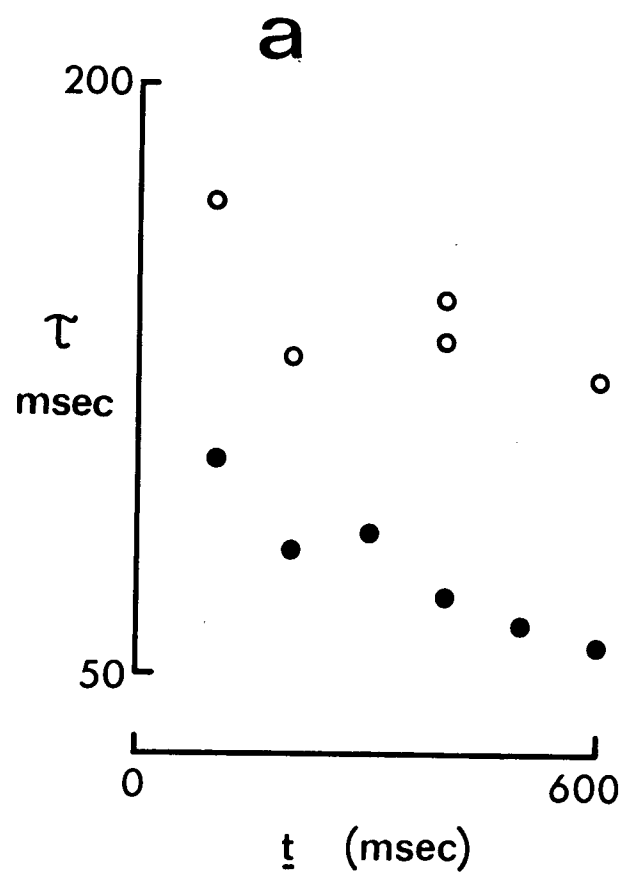
Figure 2.3.3 Current traces recorded during a recovery experiment
on a polarized fiber (resting potential, -70 mV) at
pH 5.4 (solution Ba). Note that as $\underline{t}$ increased,
the initial current $I_2(0)$ decreased. Both voltage
steps were of the same amplitude, -70 mV (absolute
membrane potential was -140 mV). The current traces
were inverted by the digital averager. The currents
are inward. Calibration: 5 mV. 1 mV = 3.14×10^{-6}
Amp/cm^2.

70

170

270
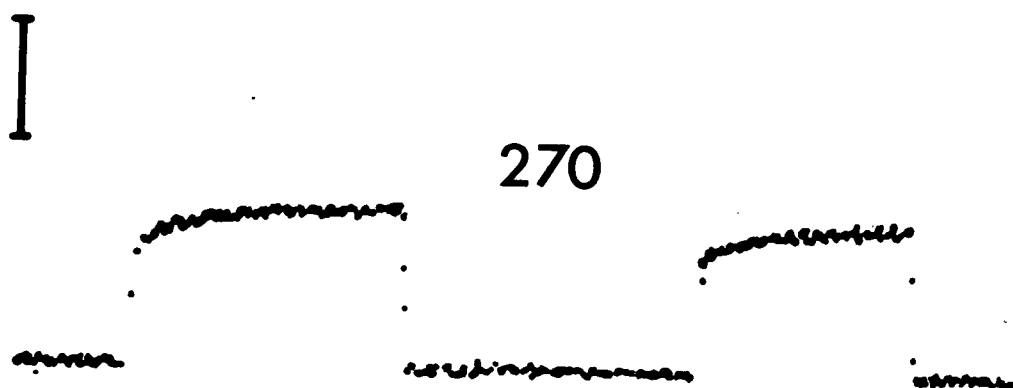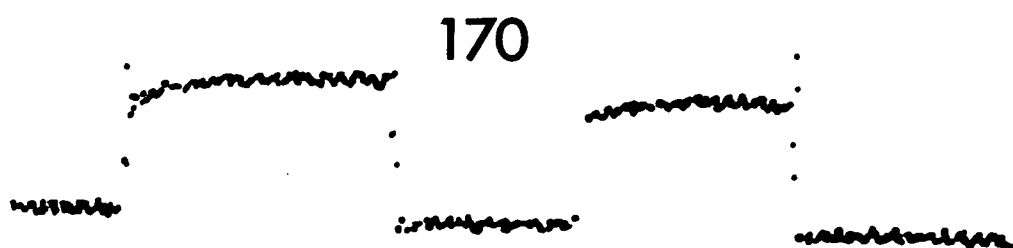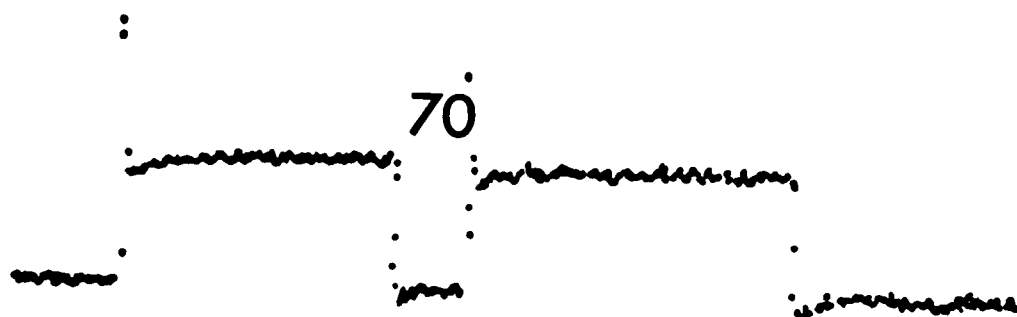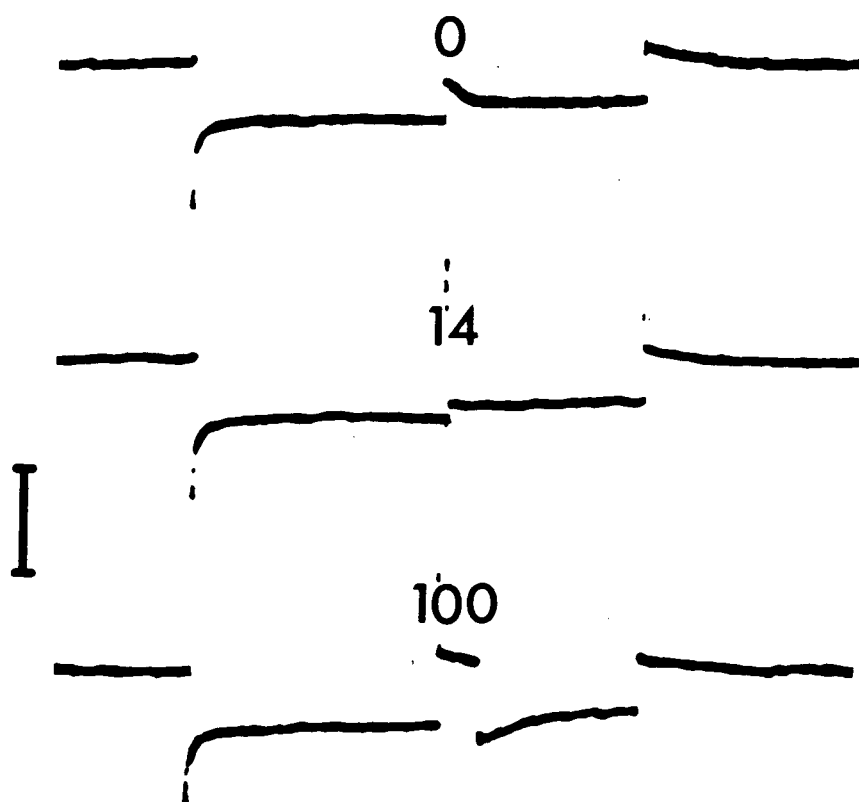
Figure 2.3.4 Waveforms seen as $\underline{t}$ is varied: as $\underline{t}$ is made longer
the initial current at the onset of the second pulse
($I_2(0)$) increases. When $\underline{t} = \underline{t}_o$, $I_2(0) = I_2(\infty)$.
The numbers on the traces indicate $\underline{t}$ in milliseconds.
For the fiber for which results are depicted here
(resting potential, -20 mV, pH 5.4, solution Ea) $\underline{t}_o$
was about   14 milliseconds (middle trace).
Calibration: 5 mV. 1 mV = 3.79×10^{-6} Amp/cm^2.

Figure 2.3.5 $I_2(0)$ as a function of $\underline{t}$ for two depolarized fibers

at pH 5.4.   Resting potentials of the fibers were

-20 mV.   Solution Ea.   In one fiber (filled circles)

recovery of initial current appeared to follow a sigmoid

timecourse, whereas in the other (filled squares) it

appeared to rise according to the function

$$I_2(t) = I_2(0)_{max}(1 - \exp(-\underline{t}/s)).$$

The solid line is a plot of the latter function with

s= 15 milliseconds.   The ordinate scale is normalized.
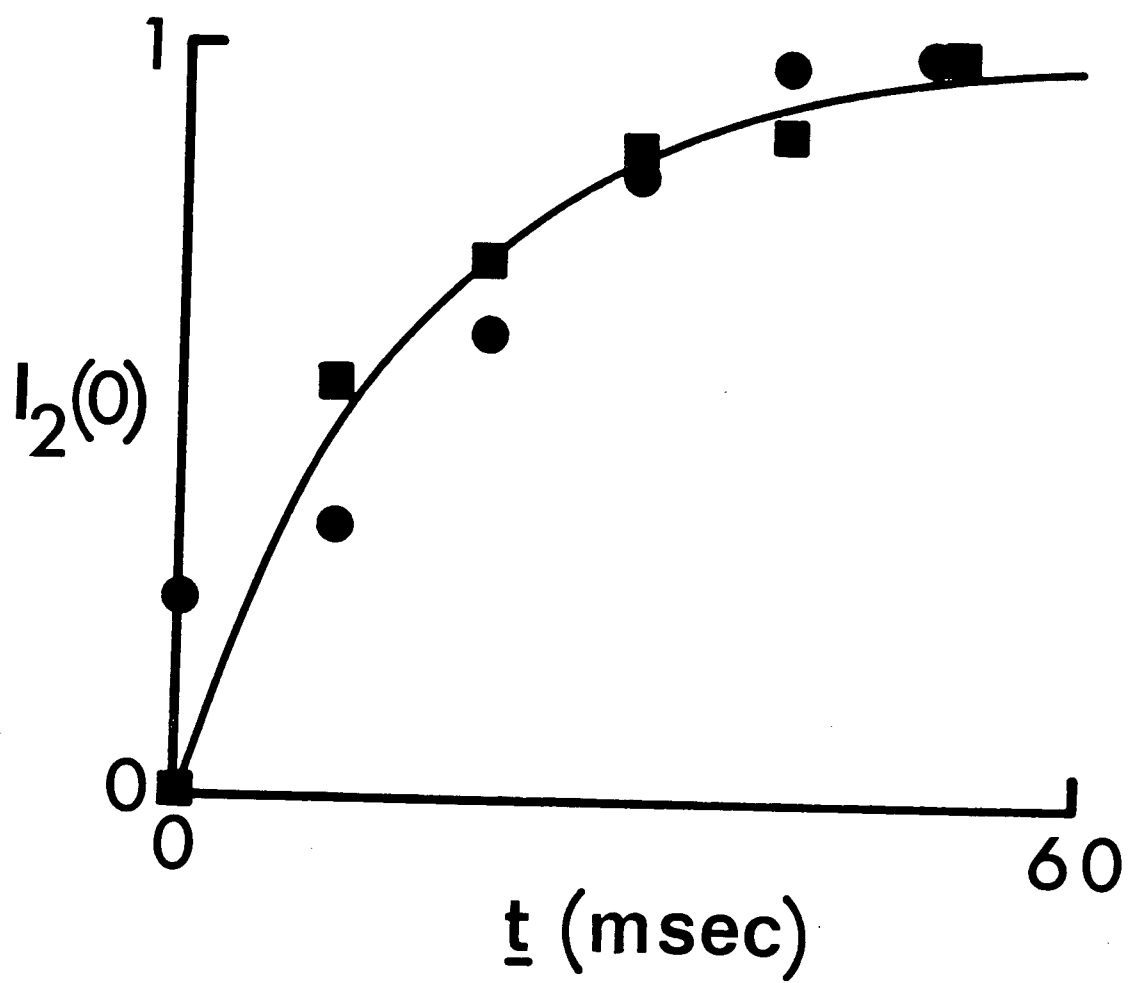
Figure 2.3.6 The dependence of the instantaneous test current
$I_2(0)$, and the time constant of the relaxation of
the test current to its steady state on the period
of recovery, $\underline{t}$, at the holding potential.

Open circles indicate the time constants of current
during the test pulse (right hand ordinate). When
$\underline{t}$ was less than 14 milliseconds, current initially
rose ($I_2(0)$ <$I_2(\infty)$) and the time constant decreased with
increasing durations of recovery. The filled circles
indicate the initial currents ($I_2(0)$). pH 5.4;
holding potential, -20 mV; solution Ea. The conditioning
potential, V_1 , was -60 mV (absolute membrane potential)
and the test potential, V_2 , was -40 mV (absolute
membrane potential).

Current calibration: 1 mV = 3.79 x 10^{-6} Amp/cm^2.
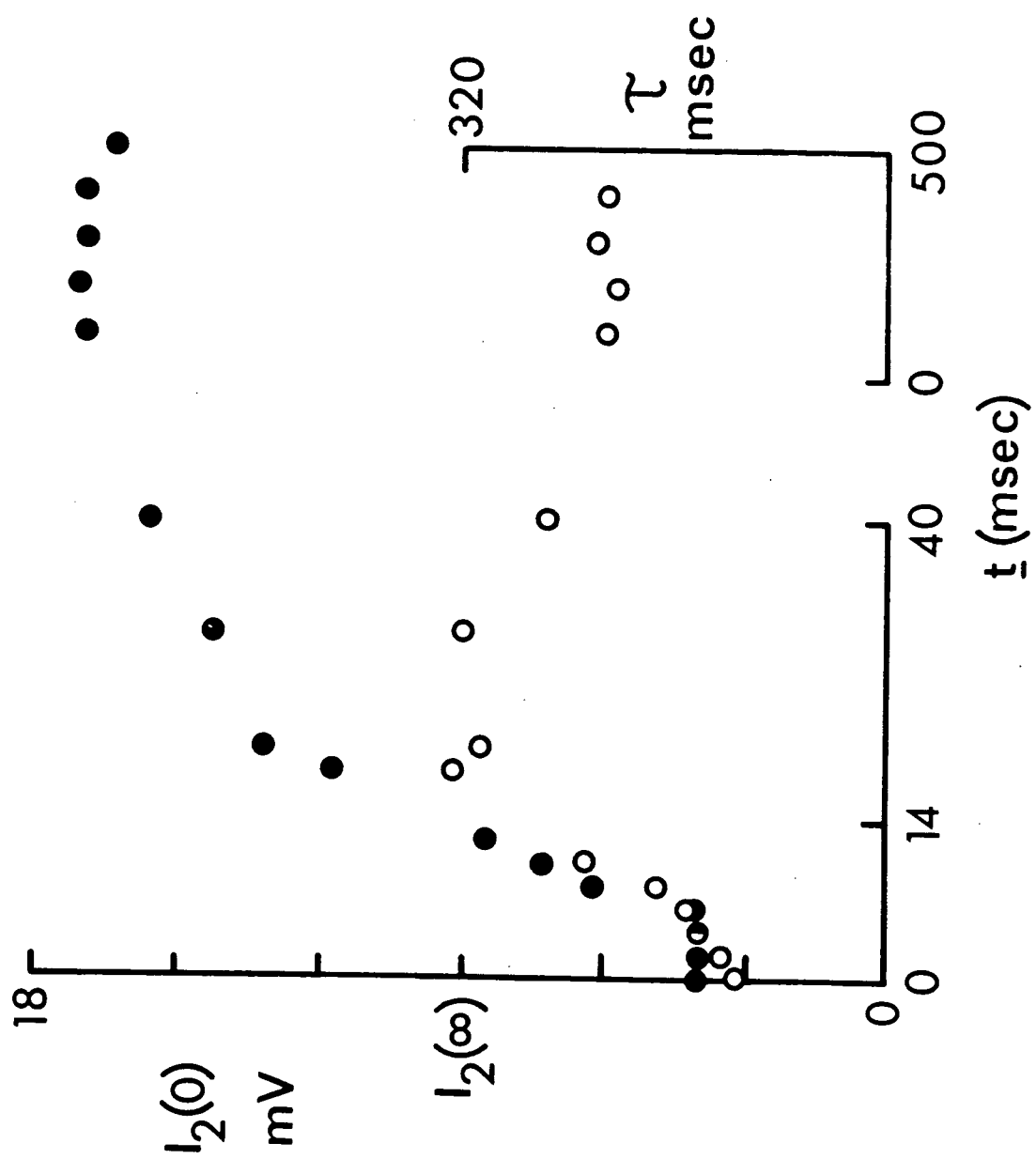
of pH 5.4 and had a resting potential of -20 mV. As the duration

of recovery t approaches t_0 (t_0 = 14 msec in this instance), the

rate of rise of the initial test current decreases. Increasing the

duration of recovery beyond t_0 in turn increases the rate of relaxation

(now an exponential decay) as shown in Fig.2.3.4.

The dependence of the time constants of the test current I_2 on

the duration of recovery at the holding potential (-20) from the

fiber of Fig.2.3.4 is shown in Fig.2.3.6. The open circles are the

time constants and also shown are the instantaneous or initial test

currents ($I_2(0)$ (filled circles)). The time constants for t

greater than 14 msec (t_0) are for falling currents.

Fibers in alkaline solution (pH 8.4)

The recovery of initial currents for fibers in alkaline solutions

was similar to those in acid solutions: fibers exhibited both

exponential and sigmoid dependence on t with approximately the same

rates of recovery. However, in alkaline solutions, the rate of recovery

in a group of fibers was found to be unusually rapid. An example is

shown in Fig.2.3.7 for current waveforms corresponding to steps from

the holding potential (-30mV) to -126 mV and then to -74 mV and

finally back to the holding potential. The steps to -126 and to -74 mV

were separated by variable duration steps (t) back to the holding

potential. When t was less than 5 msec the initial current ($I_2(0)$)

was very small and I_2 rose to a maximum after which current fell

non-exponentially. When t exceeded 6 msec the amplitude of $I_2(0)$

increased dramatically (relative to the amplitude at 5 msec) and decayed rapidly to a value about 2.5 times the steady level; thereafter the decay was slow and non-exponential. This waveform was similar to that described previously for I_2 following a conditioning pulse that 'primed' the membrane conductance. The sigmoid dependence of the initial currents on t for the fiber of Fig.2.3.7 is shown in Fig.2.3.8.

In fibers bathed at pH 8.4 that showed transitions from near-minimal $I_2(0)$ to near maximal initial currents over a range of t of a few milliseconds, the rising transients ($t<t_o$) could often be resolved into two time constants: an initial time constant of about 10 msec that did not vary with t and a slower time constant which became longer with t, up to t = 5 msec (Fig.2.3.9). Despite the rapid transitions, the dependence of time constants on t was similar to that for fibers in which the initial current transition was very much slower (cf. Fig.2.3.5). When t exceeded t_o (7 msec in Fig.2.3.8) transient I_2 was a non-exponential fall.

II. The Rate of Inactivation of Chloride Currents: Experiments in which the Duration of the Conditioning Step was varied.

Upon application of a hyperpolarizing pulse from the holding potential, the membrane conductance inactivates or falls. The objective of the experiments described in this section was to study the rate of this inactivation by applying a second test pulse before steady state for the conditioning pulse is reached. The initial current during the test pulse can be used as an indication of the state

Figure 2.3.7 Current waveforms recorded in a recovery experiment
on a depolarized fiber at pH 8.4 (resting potential,
-30 mV, solution Ed). As shown on the Figure, $\underline{t}$ was
0, 5, 6 and 7 milliseconds in the selected traces.
V_1 was 96 mV (to an absolute membrane potential of
-126 mV) and V_2 was 44 mV (to an absolute membrane
potential of -74 mV). Calibration: current = 5 mV.
1 mV = 3.79 x 10^{-6} Amp/cm^2. abscissa = one second.
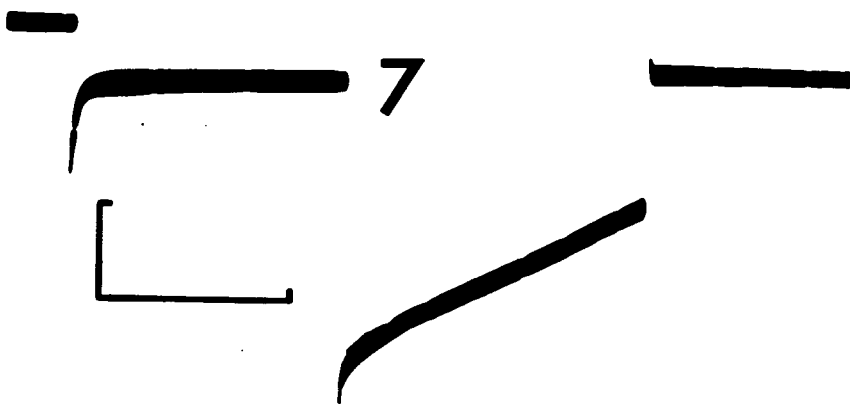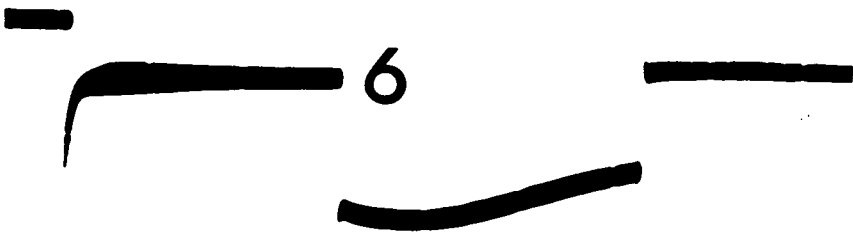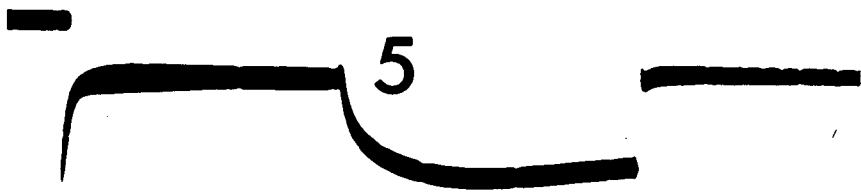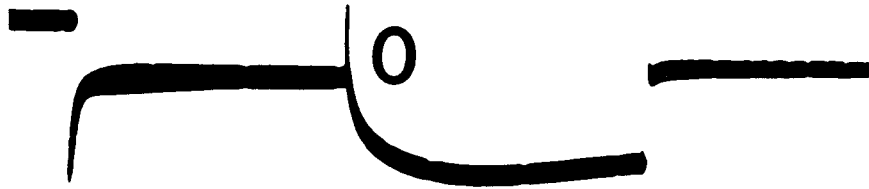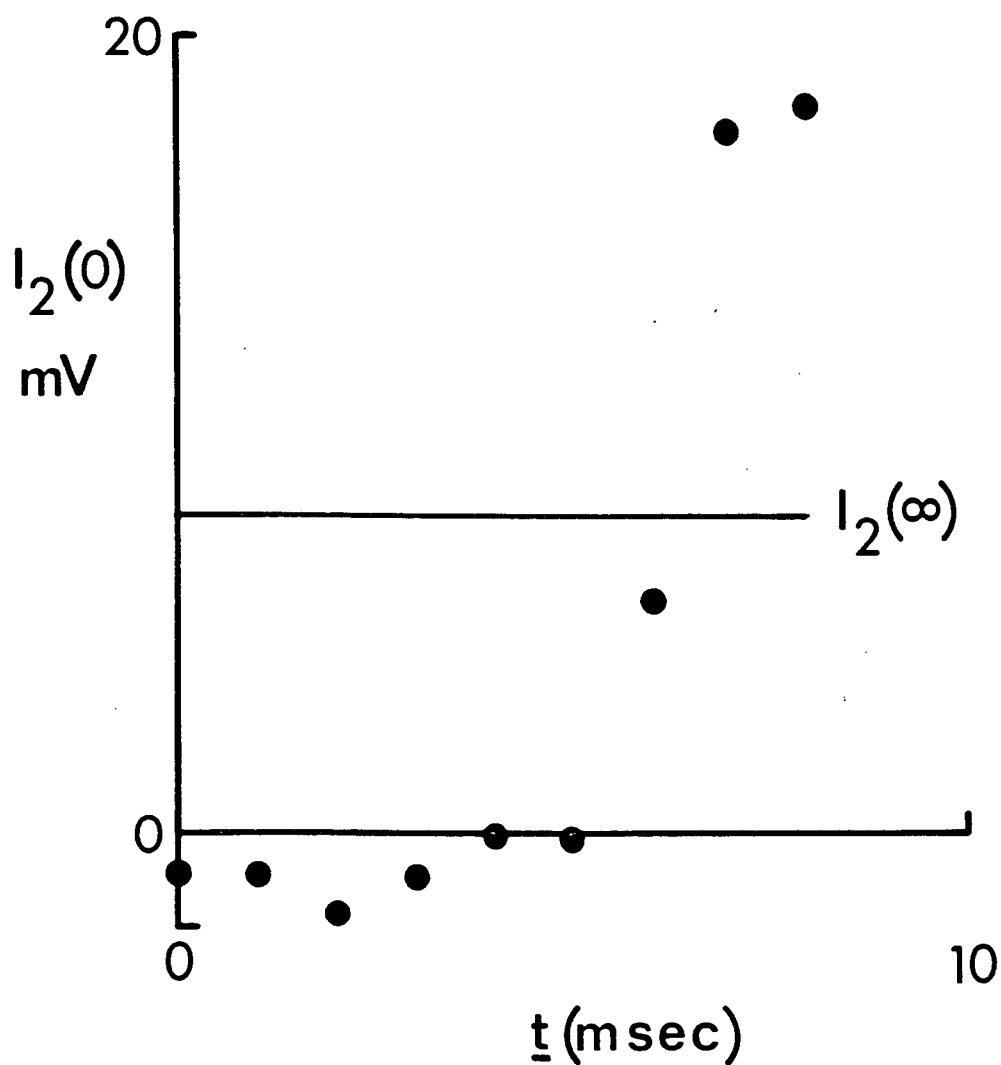
Figure 2.3.8 Dependence of $I_2(0)$ on $\underline{t}$ for the fiber on which the
waveform of Figure 2.3.7 were measured. Note that at
very short times the initial current was outward; the
transition to maximal inward current was extremely rapid.
Current calibration: 1 mV = 3.79 x 10^{-6} Amp/cm^2.
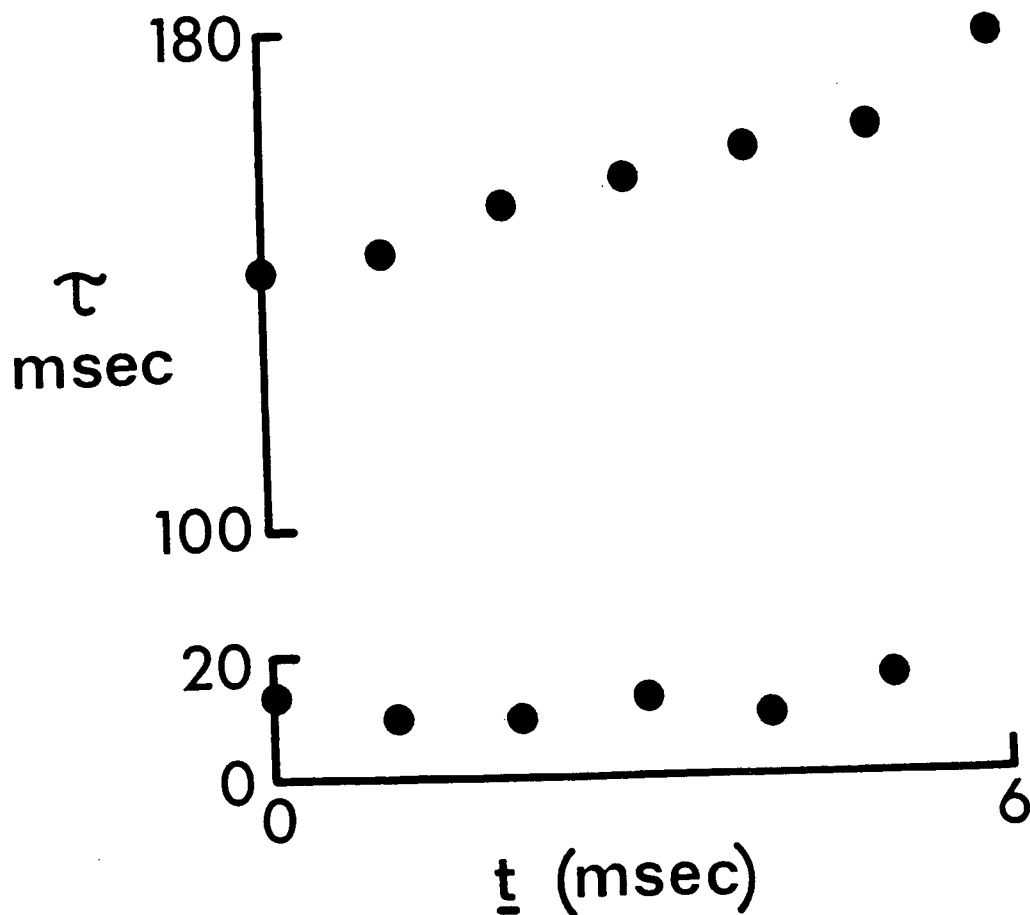
Figure 2.3.9 Time constants for rising currents in a fiber that
showed a rapid transition trom rising to falling currents
as a function of $\underline{t}$ in a recovery experiment at pH 8.4.
There were two time constants, one of about 10 msec that
was independent of $\underline{t}$ and a longer one that was time
dependent.

Figure 2.3.10   a) Current traces from a fiber held at -20 mV at
pH 8.4 (solution Ed). In this experiment the dura-
tion of V_1 was altered: the duration of V_1 (milli-
seconds) is shown on each trace. The amplitudes
of V_1 and V_2 were 52 and 26 mV, respectively.
When V_1 was maintained for longer than 125 msec
$I_2(0)$ was less thant $I_2(\infty)$. Notice the large
after-currents.
Calibration: 5 mV 1 mV=3.79 x 10^{-6} Amp/cm^2.

b) The open circles show $I_2(0)$ as a function of
the duration of V_1. The horizontal line running
across the plot indicates $I_2(\infty)$ and 0 indicates
the holding current. The two uppermost plotted
points actually indicate outward current. The
filled circles indicate the recovery of $I_2(0)$ as a
function of $\underline{t}$, when V_1 is held for a sufficient
time for I_1 to have reached a steady state. At
short times both the diminution and the recovery
processes have timecourses that closely approxi-
mate exponentials with time constants of 100
milliseconds (plotted lines) but slow considerably
at later times.
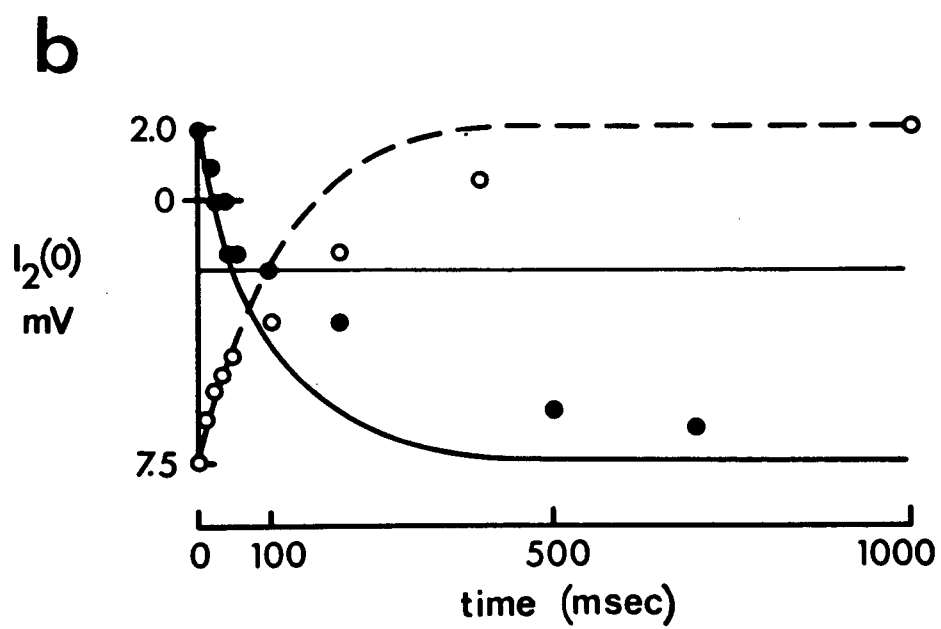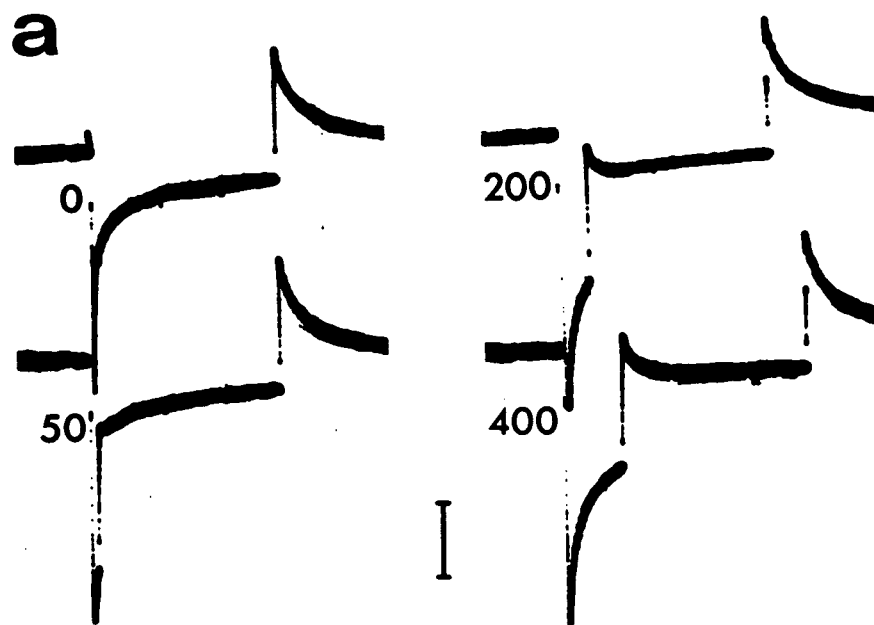
Figure 2.3.11 Effects of duration of the conditioning potential

(V_1) on the kinetic time constant of the test current

(I_2) in a fiber at pH 8.4 (the same fiber as Fig.2.3.10:

holding potential, -20 mV, solution Ed).

Abscissa is the duration of V_1 and ordinate is the

time constant of the test current. Open circles

denote falling currents and filled circles, rising

currents.

When the duration of V_1 was very brief, the test current

(I_2) fell to the steady stat with an initially fast

time constant (open circles) and then a slower one

(open squares). The fast time constant was dependent

on the duration of V_1 whereas the slower one was

independent. As the duration of V_1 increased, the

test current became biphasic: first rising, with a time

constant indicated by the filled circles, and then

falling toward the steady state (the uppermost circles).

When the durations of V_1 was lying between 200 and

400 milliseconds, the biphasic responses were too

small for accurate resolution of the time constants.
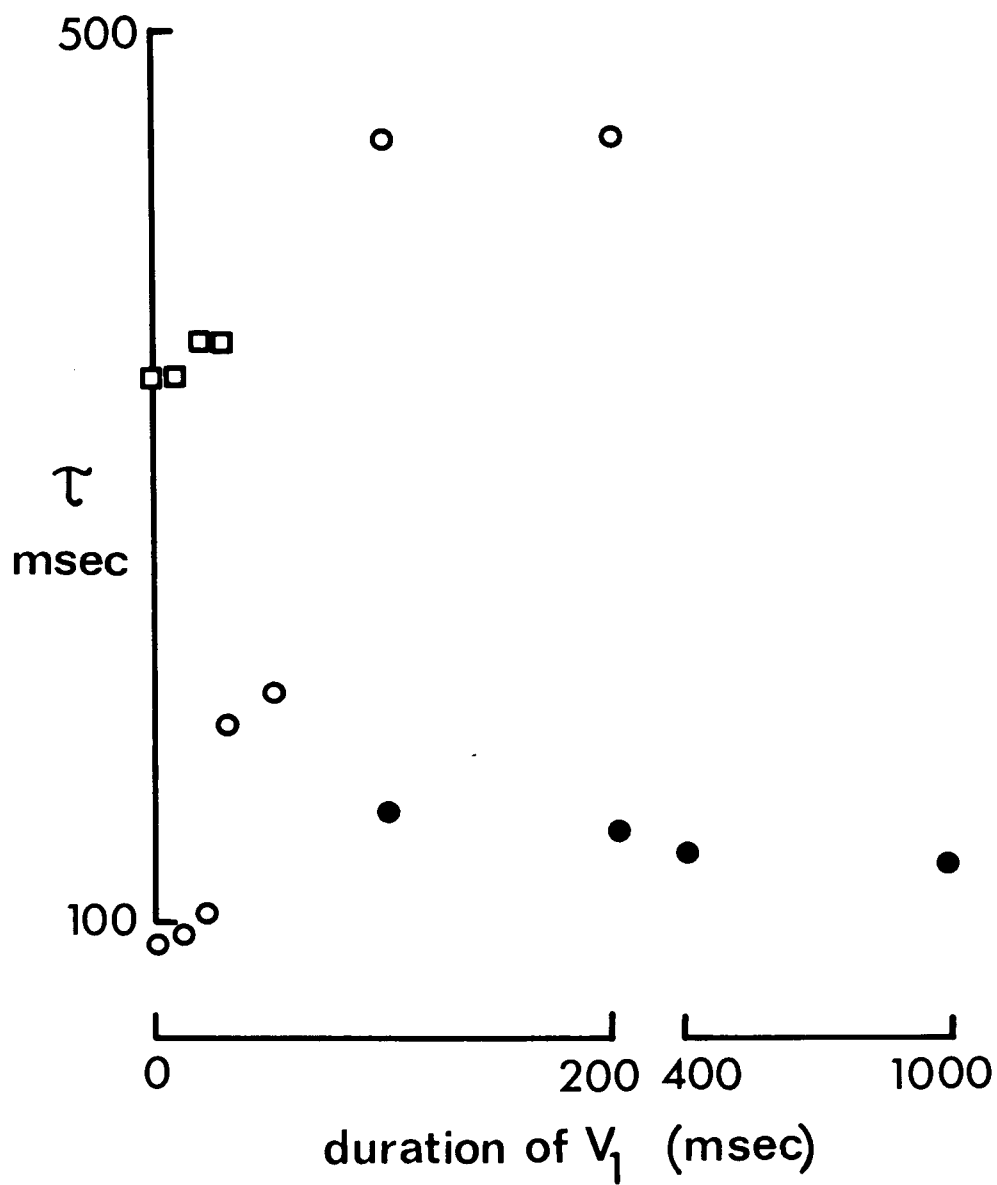
of the conductance prior to the application of the test potential.
The experiments were conducted on depolarized fibers in alkaline
solutions (solution Ed, pH 8.4).

Fig.2.3.10a shows the current traces from such an experiment
on a fiber held at -20 mV. V_1 and V_2 were hyperpolarizing pulses of
52 and 26 mV, respectively (absolute membrane potentials were -72
and -40 mV). I_2 fell from the initial to the steady level when V_1
was less than 125 msec in duration, whereas $I_2(0)$ was less than
$I_2(\infty)$ for V_1 longer than this duration. The initial current became
outwards in this fiber for V_1 exceeding 260 msec. The open circles
of Fig.2.3.10b show the dependence of $I_2(0)$ on the duration of the
conditioning pulse.

The dependence of the time constants of the test current I_2
is shown in Fig.2.3.11. When the duration of V_1 was increased from
10 msec to 125 msec, the rate of fall of I_2 decreased. When the
step to V_1 exceeded 125 msec the rate of rise of I_2 increased with
increasing conditioning time. The current relaxations were resolved
for V_1 durations less than 30 msec into an initial fall whose time
constant depended sigmoidally on the duration of V_1 (open circles)
and delayed fall that was independent of the conditioning period
(open squares). As the conditioning period approached 1 second,
the initial fall reached minimum rate.

Comparison of the rates of inactivation and recovery.

To further probe the underlying processes involved in current

relaxation both the time dependence of the inactivation and recovery
of initial test currents, and the time dependence of the inactiva-
tion and recovery of the test current time constants were compared.

The dependence of initial test current $I_2(0)$ on $\underline{t}$ (from the
same fiber as Fig.2.3.10a) is plotted as solid circles on Fig.2.3.
10b. The dashed and solid lines are exponential fits to the initial
currents from inactivation and recovery experiments. The lines have
the same time constants (100 msec). It thus appears that the
initial phase of the recovery and inactivation of initial currents
follow the same time course.

Waveforms of the test current as $\underline{t}$ was increased are shown in
Fig.2.3.12a. When $\underline{t}$ was within 60 msec, the recovery of the initial
time constant (Fig.2.3.12b) appeared sigmoid, although the maximum
asymptote was not always seen because the rising transient became too
small for time constants to be resolved at longer times (Fig.2.3.12a).
For periods between 60 and 200 msec, the waveform was biphasic,
current rising to a maximu, then falling toward the steady state.
The amplitudes of the transients were too small for accurate analy-
sis. For longer times the waveform had only a decaying phase that
was seen to be a single exponential (open circles, Fig.2.3.12b).

Qualitatively, the recovery of the time constants in Fig.2.3.12b
and the initial segment (first 60 msec) of Fig.2.3.11 are similar.
This observation, together with the similarity of the rates of inacti-
vation and recovery of instantaneous currents, suggests a symmetry

Figure 2.3.12 a) Current transients in a recovery experiment
performed on the same fiber as Fig. 2.3.10. The
duration of recovery $\underline{t}$, in milliseconds, is indicated
on top of each sweep. The straight lines on the
left indicate the relative position of the holding
currents for each of the successive sweeps. In the
waveforms corresponding to $\underline{t}$ = 200 and 100 milli-
seconds, the current was outwards when the membrane
potential was stepped back to the holding potential.

b) This figure shows the dependence of the relaxation
time constants of the test current on $\underline{t}$. The solid
circles are time constants for rising currents and
the open circles are for falling currents.
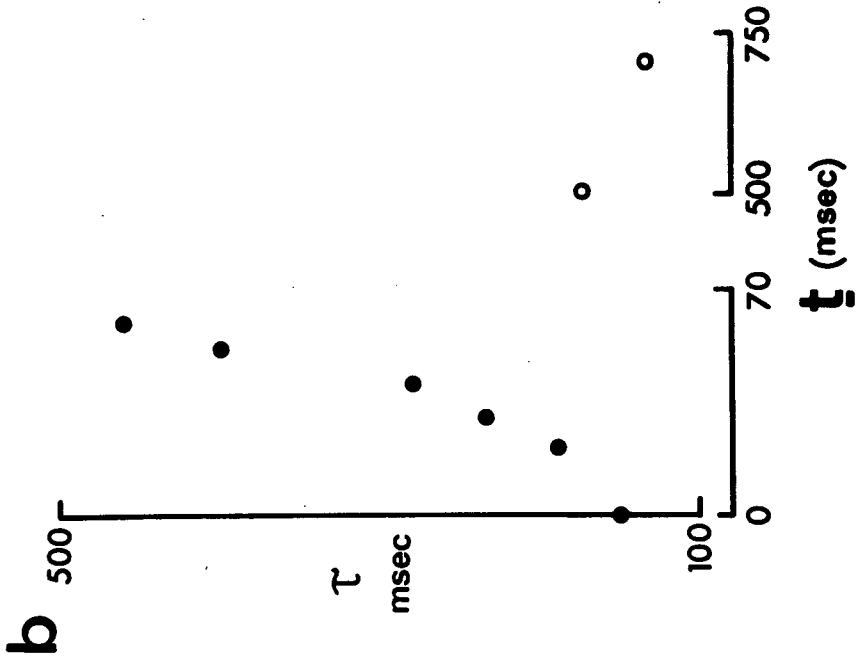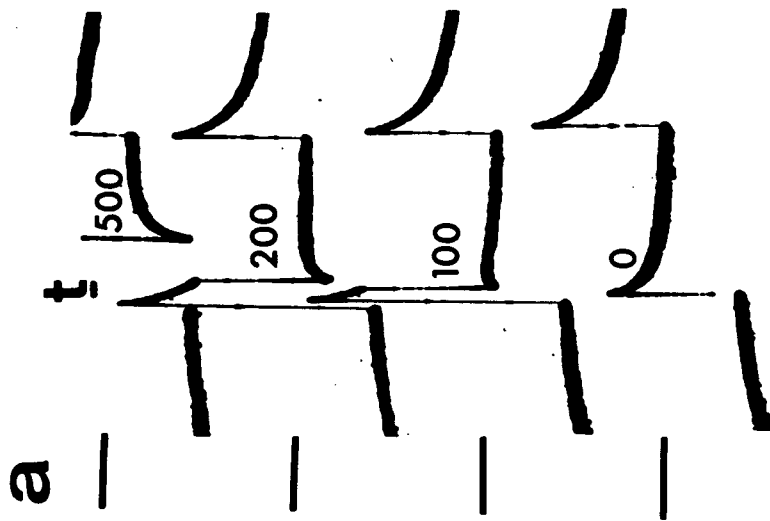
between the inactivation and recovery processes.

Discussion

Dependence of kinetics on initial conditions

One of the main conclusions in this section is that the rate of diminution of initial current during hyperpolarizing conditioning is approximately equal to the rate of its recovery at the resting potential. Moreover, the dependence of instantaneous current on initial conditions is paralleled by a similar dependence of the relaxation rate constants on initial conditions. A dependence of conductance kinetics on previous history has also been reported in the potassium channel in <u>Xenopus</u> myelinated nerve fibers (Frankenhaeuser, 1963) and more recently in the potassium channel in frog node (Palti, Ganot and Stampfli, 1976). The mechanism responsible for this is obscure as it is not predicted by first order (cf. Hodgkin and Huxley, 1952) kinetics.

We have shown, in the preceding experimental section, that kinetics of current transients depend on the voltage step between conditioning and test voltages $|V_2-V_1|$. This dependence on $|V_2-V_1|$ (the amount of energy input into the transport system) is the most puzzling and difficult aspect of the chloride conductance to understand. It will be shown in the following chapter that this is so even in non-steady conditions. That is, even during non-stationary conditions, it is possible to define an equivalent 'V_1' upon which

kinetics depend.

Slow currents under 'primed' conditions

Throughout the three experimental sections, references have
been made to a current that arose as the result of 'priming' in
chronically depolarized fibers. The necessary condition for its
appearance was a step from a large negative potential to potentials
more positive than about -50 mV; it was particularly noticeable in
fibers in alkaline solutions.

The observation that this component is absent in negative-going
steps from the holding potential suggests that the channel mechanism
controlling this current exists in three states: (1) an inactivated
state in which it cannot conduct. At potentials near -20 mV (the
resting potential for depolarized fibers in alkaline solutions) most
channels are inactivated. (2) an activated, but non-conducting state.
The transition from inactivated to activated state requires less
than 50 msec for potentials more negative than -100 mV. At -50 mV
a significant fraction of the channels is reactivated, since steps
from the steady state at this voltage to the holding potential
elicited inward aftercurrents. (3) A conducting state. Activated
channels are made to conduct by applying a positive-going step from
V_1 (depolarization).

A simple kinetic scheme relating these states is depicted in
Fig.2.3.13. At large negative potentials inactivated channels are
rapidly activated and conducting channels made non-conducting, but

activated (dashed arrows). Depolarization (solid arrows) would cause rapid opening of activated channels (conducting state) as well as very slow inactivation that would presumably proceed with and without a transient conducting state (total inactivation has been seen to require more than one minute).

No attempt was made to test whether these currents were due to chloride. However, the experimental evidence does not support the other candidates, rubidium and calcium. A contribution by rubidium ions seems unlikely since there would be no net driving force on ions that permeate K^+-channels, at the resting potential. The evidence supporting calcium is conflicting: Beaty and Stefani (1976) have presented evidence for inward calcium current triggered by depolarization, that inactivates slowly. Such a current would normally be short-circuited by a much larger chloride shunt (Beaty and Stefani, 1976). However, in our experiments the 'primed' currents were as large as those recorded in the absence of priming.

Figure 2.3.13   Schematic relating the postulated states of the
                conductance mechanism of the 'primed' current
                to membrane potential. Solid arrows indicate the
                direction of changes of the state of the mechanism
                in response to depolarization; dashed arrows show
                the direction of changes when the membrane potential
                is made more negative. For more explanation, see
                text.
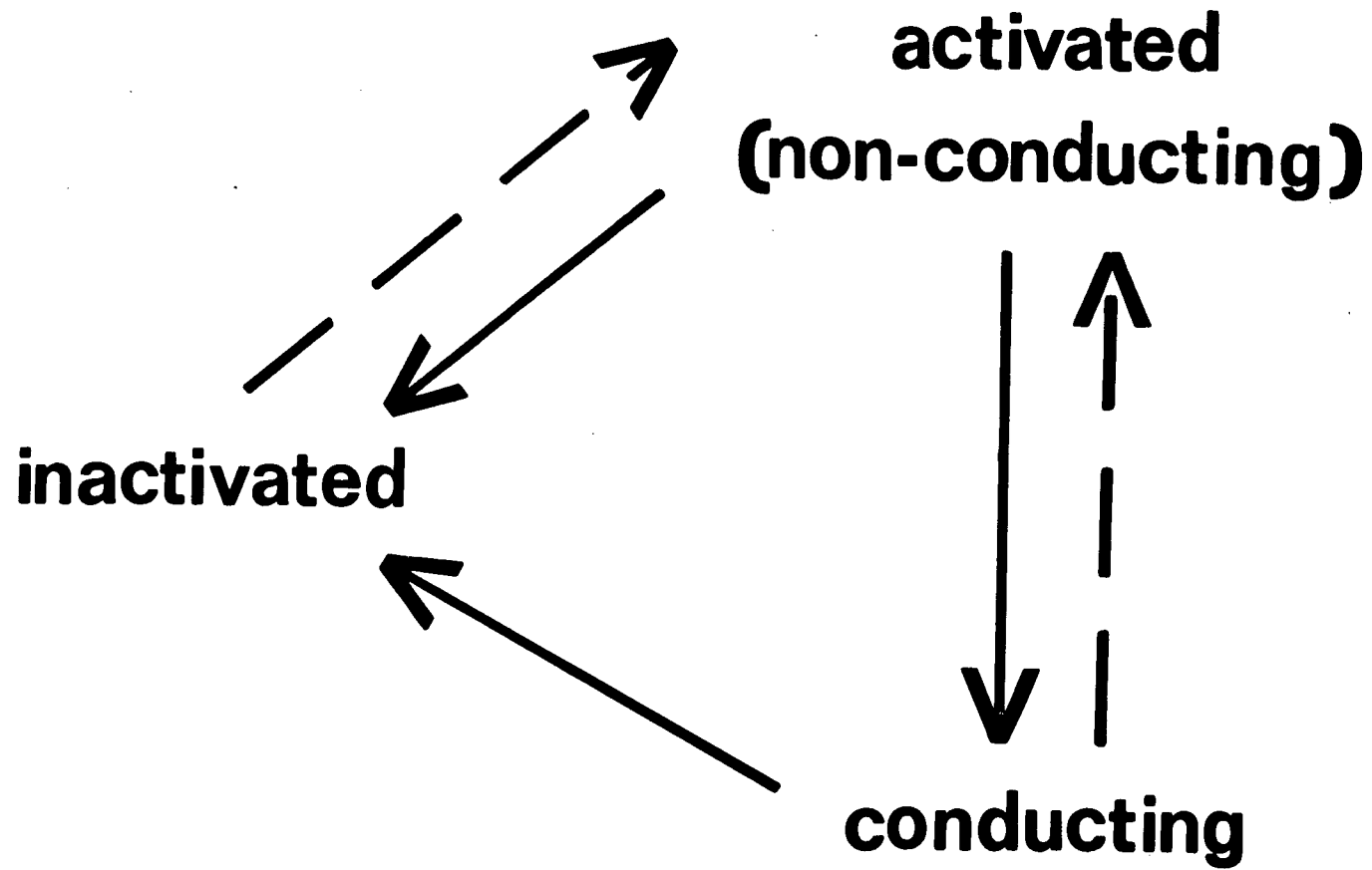
Chapter III

The Initial Current-Voltage Manifold

In the preceding chapter, data from experiments on fibers at different pH's and under different resting potentials were presented. Among various aspects of chloride conductance that were described and summarized in the appropriate sections were: the steady state conductance as a function of voltage, pH, and resting potential; the instantaneous conductance as a function of pH, the voltage of the conditioning (V_1) and test potentials (V_2), and concentration; the dependence of current transients on pH and voltage; and the time course of inactivation and recovery of conductance as well as the dependence of kinetics on initial conditions. An essential observation was that the instantaneous chloride currents and relaxation kinetics depend on the magnitude and 'state' of the prepulse (conditioning potential).

In this chapter, we will show that an overall perspective of much of the experimental data can be obtained. The idea is to represent the dependence of instantaneous test currents $I_2(0)$ as a function of the conditioning potential (V_1) and test potential (V_2) in a three dimensional rectangular coordinate system where the independent variables are V_1 and V_2 and the dependent variable is initial test current $I_2(0)$.

The result of the representation, called a manifold (two dimensional), provides us with an overall perspective of the experimental results and enables us to compare and relate diverse experimental protocols such as the inactivation and recovery of conductance and the dependence of current transients on a voltage step and on initial conditions.

The representation requires that values of $I_2(0)$ be specified

on families of mutually perpendicular planes--the $I_2(0) \times V_1$ (when V_2

is constant) and the $I_2(0) \times V_2$ (when V_1 is constant) planes. The

forms of these relations are as described in the results (for example,

Fig. 2.2.4a and Fig. 2.2.4b). In the event that experimental data

are available, these should be obtained from a single cell. In

other words, detailed analytical expressions for the dependence of

$I_2(0)$ on V_1 and V_2 are required. We were unable to obtain such exten-

sive data from a single fiber to construct an experimental manifold

but we did obtain sufficient experimental evidence to provide a strong

framework for a theoretical synthesis. Since $I_2(0)$ depends on both

V_1 and V_2, information from variable V_2 (amplitude of V_1 held fixed)

experiments provides information on variable V_1 (amplitude of V_2

held fixed) experiments. More precisely, any specified current,

$I_2(0)(V_1^o, V_2^o)$ is on the intersection of the planes $I_2(0) \times V_1$ (at constant

V_2^o) and $I_2(0) \times V_2$ (at constant V_1^o).

Assumptions

The approach used in developing the manifold relies heavily

on the sigmoid dependence of $I_2(0)$ on V_1 (at a constant V_2). We

will focus our construction on fibers in alkaline solutions (using

a shape parameter of .087, z=2, Fig. 2.2.18c). Linear $I_2(0)$ versus

V_2 (for constant V_1) relations will be used throughout. These relations

are highly non-linear (even saturating, see Fig. 2.2.3b) in polarized

fibers in alkaline solutions (pH 8.4) but in depolarized fibers

128

at the same pH, were much more linear. However, since

analytical expressions describing them over a wide voltage range

were not obtained, the assumption of linearity was adopted. Finally

an additional relation requiring the dependence of the instantaneous

test currents $I_2(0)$ on V_2 for different conditioning voltages V_1

is required. The assumption that we used was that when these relations

(the dependence of $I_2(0)$ on V_2) are plotted in the same plane, regard-

less of V_1 (as in Fig. 2.2.4), they intersect in the same point

(see step 4 below). It is interesting at this moment to note that

despite the approximate nature of the last two assumptions, the

qualitative predictions of the representation will be seen to account

for much of our experimental data.

The synthesis is perfomed as follows:

1. A reference sigmoid relation $(I_2(0)(V_1,V_2^o))$ is placed in

    the plane (open circles, Fig. 3.1a). The choice of V_2^o

    and the position of the relation in the plane are arbitrary.

    The value of $V_2^o = (V_h-70)$mV was selected for convenience,

    since it is the largest value used in our experiments.

    (When $V_1=V_2$, the instantaneous test current $I_2(0)$ is equal

    to the steady state conditioning current and the point at

    A represents the steady state current corresponding to a

    hyperpolarization voltage step of 70 mV). There would have

    been no loss of generality had any other V_2^o been chosen.

    The slope of the relations is appropriate to currents in

    alkaline solutions (k=.087,Fig.2.2.1b,c). The qualitative

properties of the construct would not be altered if the steeper slope of the acid-derived data had been used.

2. The points (open circles of Fig.3.1a) are replotted on the $I_2(0) x V_2$ plane (open circles, Fig.3.1b and c).

3. A family of $I_2(0) x V_2$ relations (fixed V_1) (Fig.3.1c) is generated by first projecting a line from the smallest current value plotted (point A, Fig.3.1a and c) through the holding-current axis at a voltage negative to the holding potential. A value of -20 mV was used in Fig.3.1c as this value was approximately the largest value obtained for the shift in equilibrium potential with hyperpolarization. Secondly, a line is then drawn through the reference point (V_h, I_h) and open circle B, at which $V_1 = V_h$. This line is the instantaneous current-voltage relation for steps from the holding potential.

4. The family of $I_2(0) x V_2$ relations is completed by locating all P_j (Fig.3.1b) in the plane. Lines are then drawn through AP and BQ to intersect in 0 (the point of intersection of all the rays in Fig.3.1c, this point is not shown in Fig.3.1c). OAB and OPQ are similar triangles and $PP_j/AA_j = PQ/AB$. PP_j is the only unknown. Once all P_j are located, the lines through $A_j P_j$ complete the family (Fig.3.1c).

5. A family of $I_2(0) x V_1$ relations is now obtained by repeatedly reversing step 2: for each of a number of chosen values of V_2 data points are replotted from the $I_2(0) x V_2$ plane onto

the $I_2(0)xV_1$ plane. The filled circles (P_j) are given as
an example.

It is seen by construction that the $I_2(0)xV_1$ curve passing through
the holding potential at the holding current (V_h,I_h) gives outward
currents for V_1 more negative than the holding potential (when V_2
is equal to the holding potential),the recurring observation in all
our experiments.

The manifold is drawn in Fig.3.2. The left-hand abscissa is
V_2, the right-hand abscissa V_1, and the vertical axis, current.
When $V_1=V_2$, instantaneous and steady state currents are equal,
indicated by filled circles in Fig.3.2. They will be referred to
as stationary points. Contrary to the sense of our other figures,
current plotted in the upward direction here is inward. The plane
containing the abscissae represents holding current: when the manifold
rises above it, currents are inward relative to the holding current,
and when the manifold falls beneath the plane, currents are outwards.

Applications of the Manifold

Prediction of the instantaneous currents

The surface enables us to predict the instantaneous current
that will be recorded when the voltage is changed from one value, at
which a steady state has been attained, to another. An example
is given in Fig.3.3. In a three of the S-relations of Fig.3.2 have
been replotted. The lines with arrows indicate the direction of a
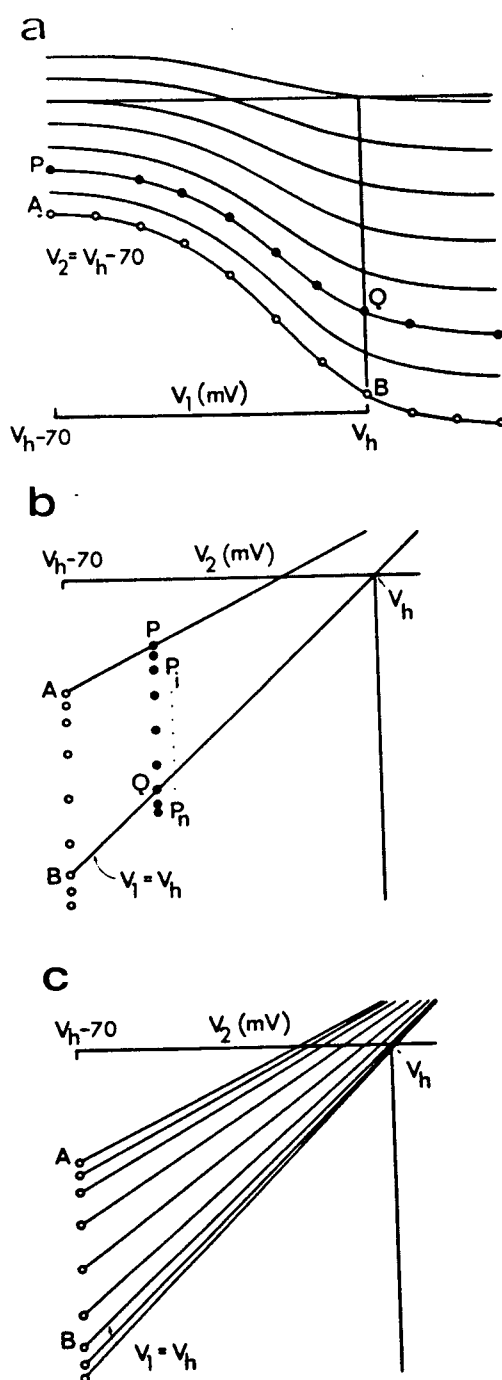
Figure 3.1   Steps in the construction of the current-voltage
manifold (see text).
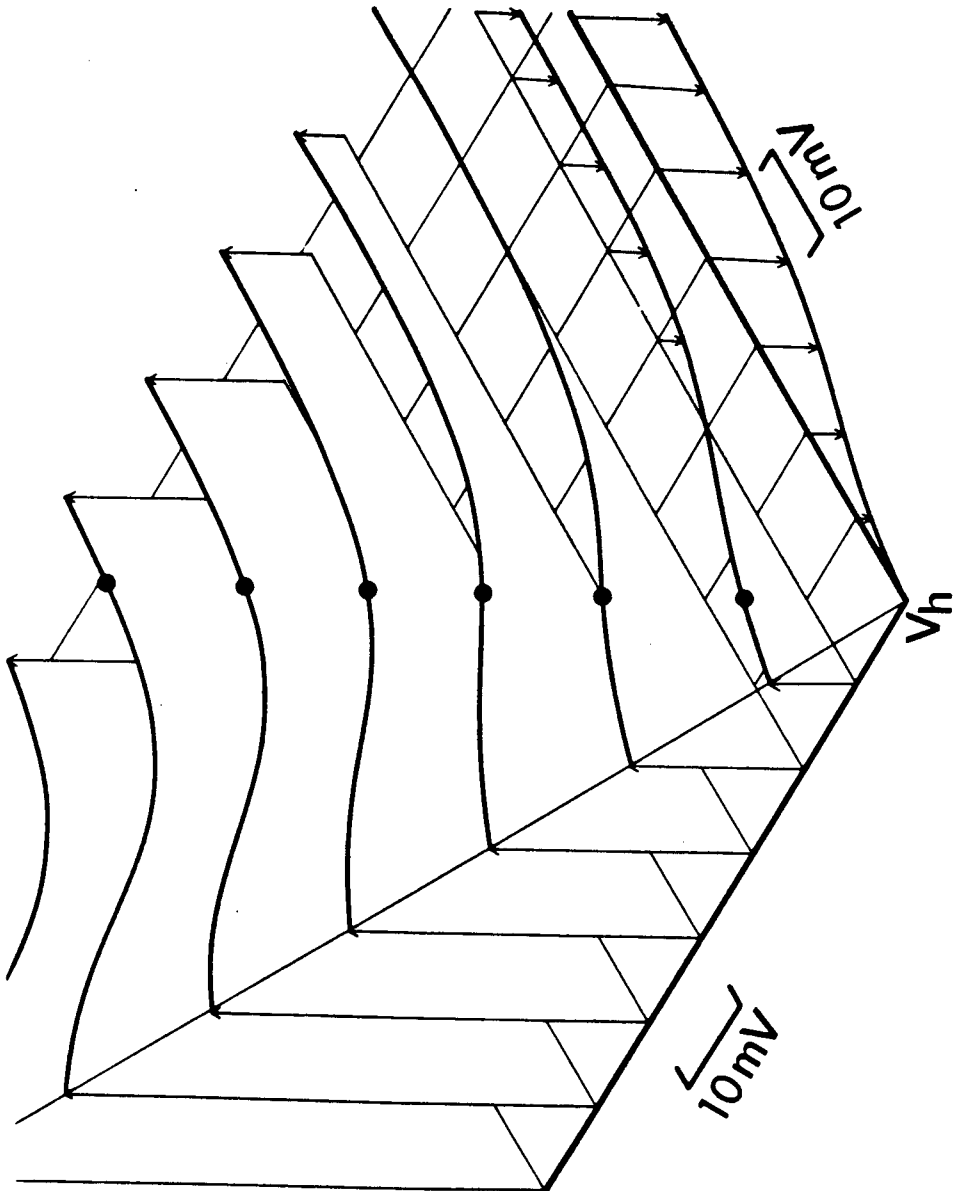
Figure 3.2   The current-voltage manifold.
For description, see text.
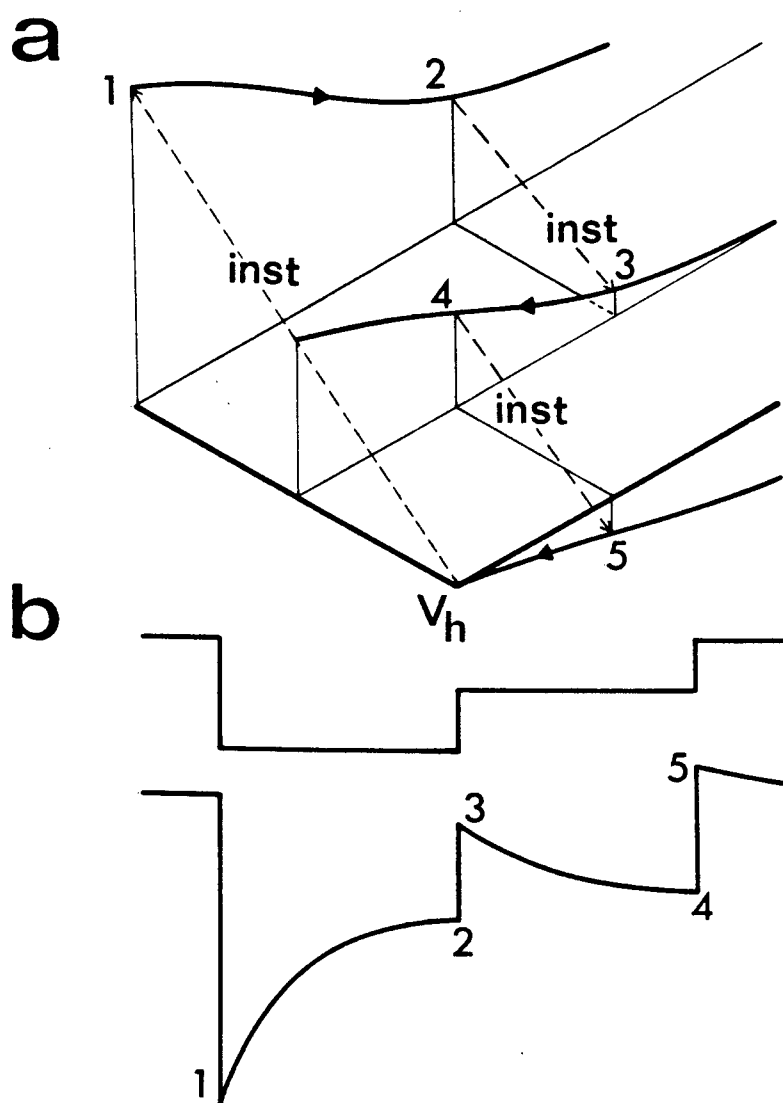
Figure 3.3 Use of the manifold to predict the responses to a
sequence of voltage steps. For details, see text.

Figure 3.4 (a) and (b) demonstrate the use of the manifold in predicting currents when voltage steps are made after steady state conditions have been reached.

(c) and (d) simulate a case in which the voltage step from V_2 to V_2' is made before the current at V_2 has decayed to the steady state (2'). From data obtained on the voltage dependence of time constants, it is possible to predict the time constants of the transitional currents.
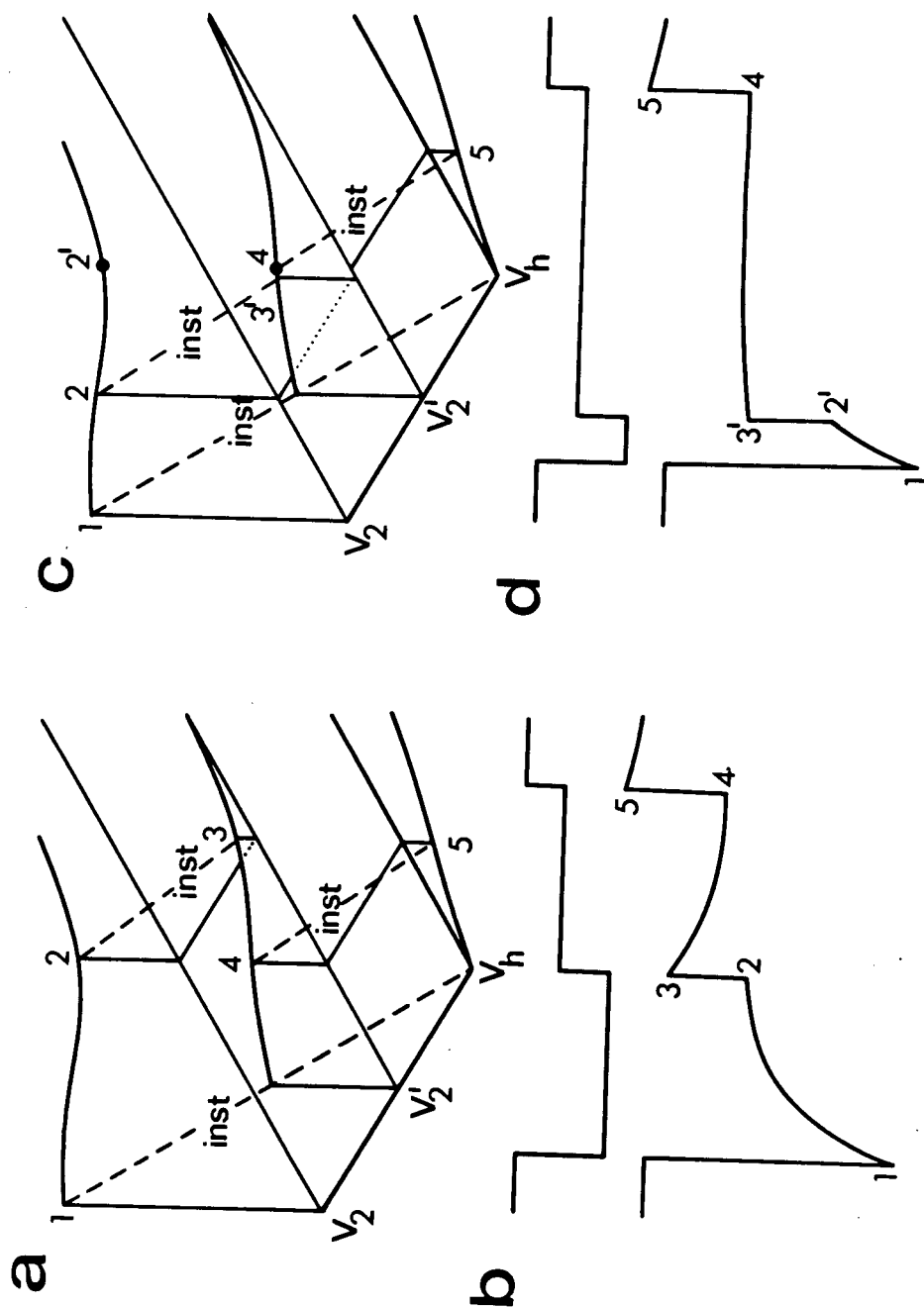
cycle of voltage changes and in <u>b</u> the currents observed at the onset

of the steps of voltage are plotted, measured directly from <u>a</u>, and

joined by 'transient currents' with similar timecourses to those

observed in alkaline solution. When the membrane potential is suddenly

stepped to and held at a new value (V_2) the current changes with time

until it settles at the stationary point of the S-curve corresponding

to that V_2.

It can be seen from Fig.3.1c that as V_1 (the holding potential)

is made more negative the slope of the instantaneous (V_2) current-

voltage relation of negative-going steps decreases. This is consistent

with the observed reduction in a one pulse experiment when the holding

potential is made more negative. It is also clear that as V_1 is made

more negative the shift of the $I_2(0) \times V_2$ intercept on the voltage axis

approaches a limiting value.

The dependence of instantaneous currents on initial conditions

in non-steady states can be explained qualitatively using the instantane-

ous current manifold.

We shall first describe the results of an experiment in which the

membrane potential is stepped from the holding potential (V_h) to a

more negative voltage (V_2), then to an intermediate voltage (V_2').

Two conditions are compared: one in which the initial pulse is

sufficiently long for a steady state to have been reached before the

step is made, the other in which the step to the intermediate voltage

is made before the steady state is reached (an experimental example

is given in Fig.3.4). In both cases, the second pulse is sufficiently

long that steady conditions are attained before the step back to the holding potential.

These transitions are shown in Fig.3.4a. The same manifold segment is used as was employed in Fig.3.3a. For the first case, the membrane potential, V_2, is kept constant and the current declines until the stationary point is reached, at 2. The step to V_2' is associated with an initial current, 3; current rises to 4 (stationary point) and the return to V_h elicits the outward current at 5, and so on. The initial currents are joined by arbitrarily drawn transients in Fig.3.4b.

For the second sequence the initial current at 1 is the same, but at 2' it has not declined to the stationary value. At this point, a step from V_2 to V_2' gives the current at 3' that decays to the steady state at 4, and so on as shown in Fig.3.4d.

The results of recovery experiments (eg. Fig.2.3.12) can also be accounted for using the manifold as seen in Fig.3.5. The same initial step from V_h to V_2 is used as in Fig.3.4. After the current has reached steady state at 2 the membrane potential is returned to the holding potential for a period $\underline{t}$ before being stepped to V_2'. The initial current at the holding potential (3) is followed by a decay to 4. The membrane voltage is now stepped to V_2' and the current at 5, which is a stationary point as the manifold is constructed, is recorded. The initial and steady state currents are identical; the potential is then switched back to V_h (6). The currents are sketched in Fig.3.5b. If the duration of the transient

step to the holding potential were less than t_o there would be a

rising transient during the next step, a falling transient if it

were longer than t_o.

Dependence of kinetics on initial conditions

We have seen experimentally that the rate of relaxation from

initial to steady state currents is dependent on the size of the voltage

step. That is, in Fig.3.6, the rate of relaxation from 1 to 2 depends

on the distance between their projections on the V_1V_2 plane: precisely

$$\left| V_2 - V_1 \right| .$$

A simple extension of this principle is to predict the time

constants of relaxations when voltage steps are made from non-steady

states, using the manifold and the measured dependence of time

constants on $\left| V_2 - V_1 \right|$. We do not take into account the contributions

of voltage independent transients.

Linear regression analysis of the dependence of relaxation

time constants on $\left| V_2 - V_1 \right|$ (ΔV) showed that time constants (τ) can

be closely approximated by

(1) $\qquad \tau = -1.5 \, \Delta V + 125 \quad \text{(msec)}$

A 60 mV step from V_h to V_2 in Fig.3.6 gives an instantaneous

current at 1 that falls toward the steady condition at 2 with a time

constant of 35 msec (from equation 1). After one time constant

current has decayed to 3 and the membrane potential is suddenly

stepped to 30 mV more positive potential, V_2'. Current, initially

at 4, rises to the steady state at 5. The distance between the pro-

jections of 4 and 5 in the V_1, V_2 plane is approximately 9 mV.

Alternatively, point 5 could be reached from the stationary point

on a trajectory intermediate between V_2' and V_2 , 9 mV more negative

than V_2' . This potential $(V_2'-9)$ mV could be considered as the effective

conditioning voltage in an experiment in which the conditioning pulse

is sufficiently long for steady state current to have been reached.

Thus $(V_2'-9)$ mV may be considered an 'equivalent V_1' for purposes

of interpretation of the manifold. Current will rise to the steady

state with a time constant of

$$-1.5 \times 9 + 125 \text{ msec}$$

$$= 111 \text{ msec}$$

Had the step to V_2' been made directly from V_h (a 30 mV step) the

falling transients would have had a time constant of 80 msec. These

results are in qualitative agreement with experimental observations.

<center>Discussion</center>

Relationships between steady state and instantaneous current-voltage

relations

In the discussion to section 2 of Chapter 2, (Fig.2.2.8), the

discrepancy between the steady state current-voltage relations and

the family of sigmoid $(I_2(0)$ versus $V_1)$ relations was quantitatively

analyzed using the standard formulation:

(1) $I_{Cl} = g \cdot (V_m - V_{Cl})$

It was observed that this description of chloride conductance was

inadequate to relate the steady state conductance to the subsequent

conductance (or vice versa) in two pulse voltage clamp experiments.

The reason for this inability to relate the two conductances was that

it did not take into account the shift of the zero current potential

V_{Cl} with conditioning voltage V_1. In this discussion, it will be

shown that the steady state relations and the family of instantaneous

current-voltage relations are related, but the relationship is much

more complex than the simple expression (1). Moreover, it will be

shown that one cannot understand the steady state chloride current-

voltage characteristics without an overall comprehensive understanding

of all the characteristics (both instantaneous and steady state).

Fig.3.7 shows the stationary points on a manifold generated

by a family of characteristics with the slope parameter k=.087,

the common value obtained in alkaline solutions. The dashed line

connecting the stationary points is the steady state current-voltage

relation. It can be seen that this steady state current-voltage

relation is governed by the shifting or spacing of the S-curves

in the plane (current voltage plane). When the dispersion (or separation

between the sigmoid curves) increases with increasingly negative

V_2, the steady state current-voltage relation shows downward concavity,

as in acid solutions. As the dispersion decreases with increasingly

negative V_2, saturation or a region of negative slope may be observed

in the current-voltage relations, as in alkaline solutions.
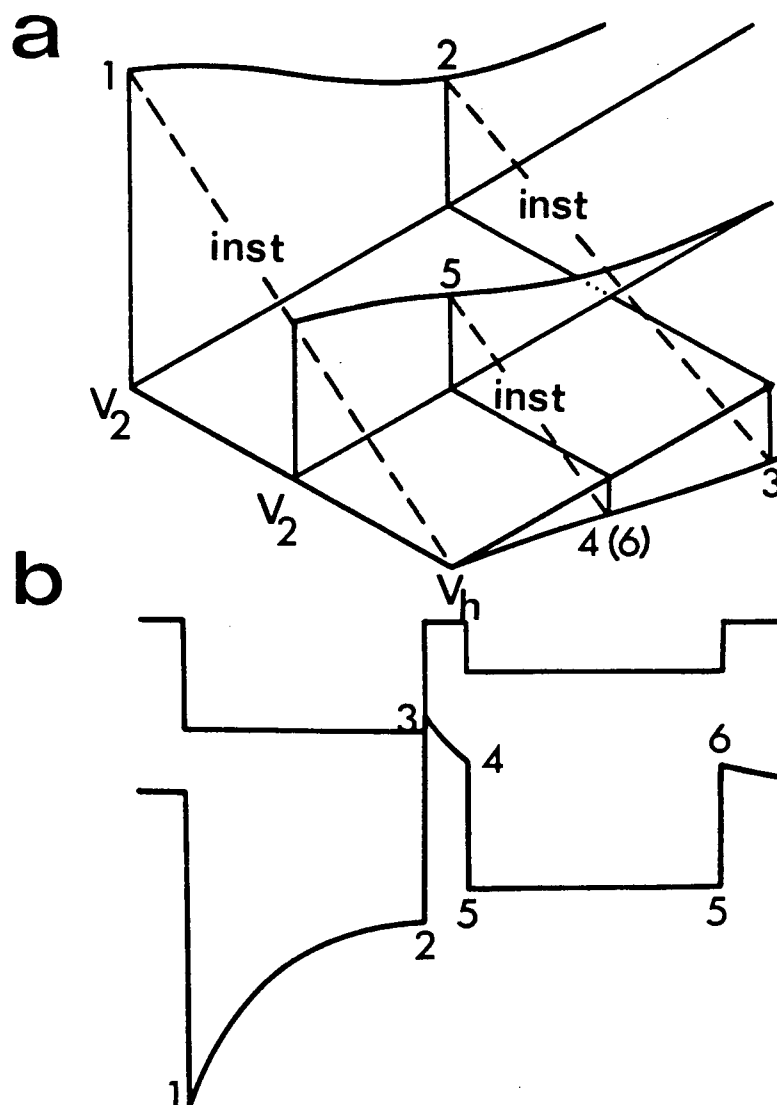
Figure 3.5 Representation of a recovery experiment on the current-
voltage manifold. Since the amplitude of the step
from the holding potential to V_2 is the same as that
from V_2 back to the holding potential, the time constants
of relaxation from 1 to 2 and from 3 to 4 should be
the same. For details, see text.

Figure 3.6 Prediction of instantaneous currents and relaxation
time constants from the current-voltage manifold when
steps are made during non-steady conditions. An initial
step from V_h to $(V_h-60$ mV$)$ is held for one time constant
(35 msec) before the membrane potential is stepped back
to $(V_h-30$ mV$)$. The time constant of the relaxation from
4 to 5 (a stationary point) is dependent on the distance
between their projections on the voltage scale. For
details, see text.
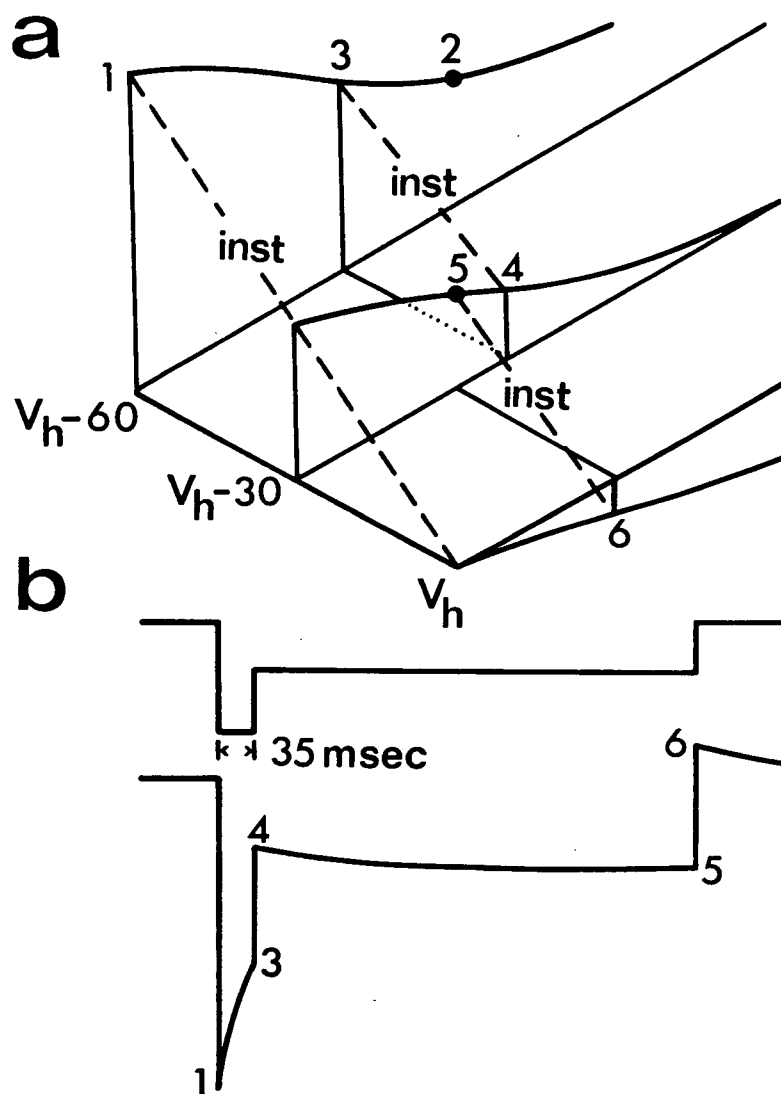
Figure 3.7   Relationship between the steady state current-voltage
             relation and the dispersion of the S-curves. The points
             on the S-curves are the stationary points and the broken
             lines joining them are the steady state relations.
             When the dispersion increases with increasingly negative
             V_2, as in the top panel, the steady state current-
             voltage relation shows downward concavity, as in acid
             solutions. With uniform dispersion (center panel)
             the relation tends toward saturation and as dispersion
             decreases with increasingly negative V_2 (bottom panel)
             there is a rapid approach to saturation or possibly a
             region of negative slope.
             Note the effect of dispersion on the resting conductance.

V_1 (mV)

V_h-70

V_h
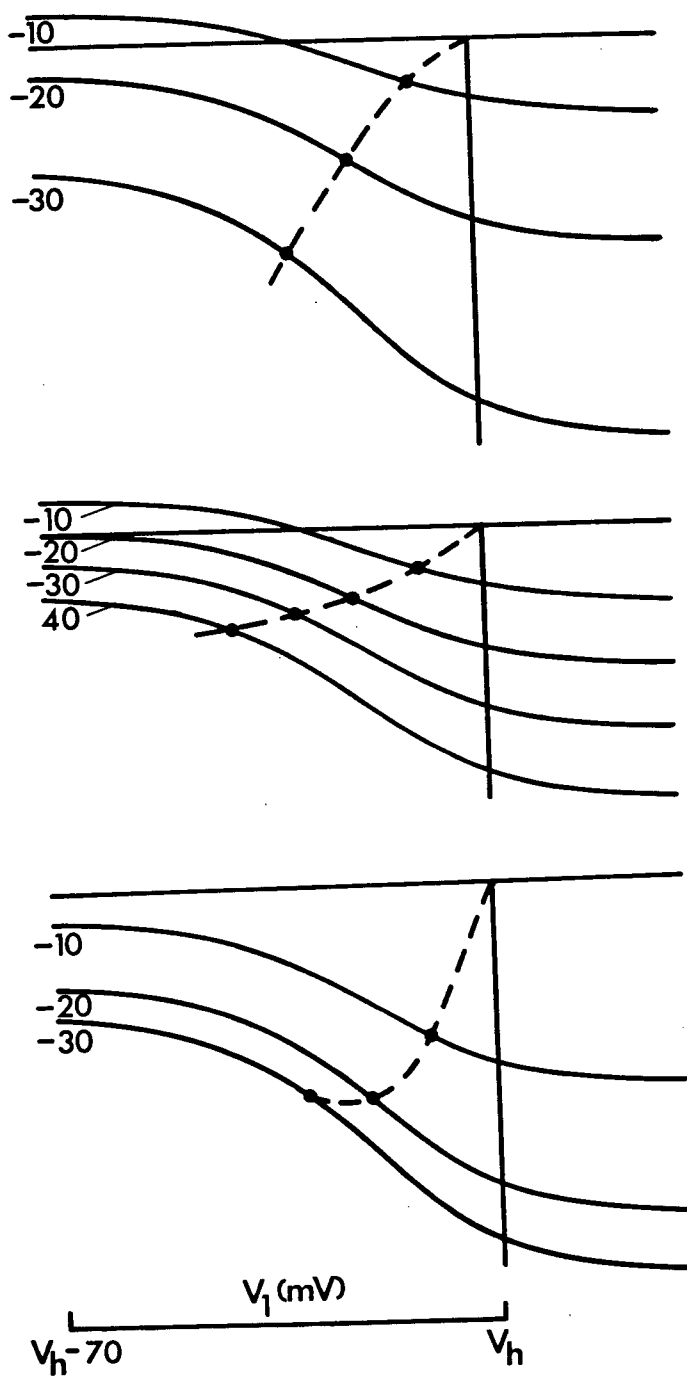
Chapter IV

Theoretical Considerations: Models of Membrane Permeation Process

Introduction

The purpose of this chapter is to present a number of simple
models of ion movement through membranes to determine if they share
any of the properties that have been observed for chloride permeation.
Particular attention is given to relations predicted between steady-
state currents and voltage and the dependence of conductance changes
on time and voltage. As mentioned in Chapter 1, current-voltage
relations that are non-linear and conductance changes depending on vol-
tage and time are the rule rather than the exception in studies from a
wide variety of biological membranes. Many different kinds of mechanisms
have been proposed to account for steady state rectification in membranes.
Two of these mechanisms we have mentioned in Chapter 1 involve changes
in the number of conducting channels or in the conductance of a single
channel. On the other hand, satisfactory theories for the voltage
dependence of conductance changes for ionic channels in cell membranes
(for instance, the sodium and potassium channels in nerve) are lacking,
and this remains one of the least well understood aspects of
ion transport across membranes.

Of the models that have been proposed for chloride transport in
amphibian fibers (Hodgkin and Horowicz, 1959; Spurway, 1970; Venosa,
Ruarte, and Horowicz, 1972; Warner, 1972; Woodbury and Miles, 1973) only
two types have been considered: classical electrodiffusion models as
exemplified by constant field theory (Hodgkin and Horowicz, 1959), and
channel models (Spurway, 1970; Woodbury and Miles, 1973). Electro-
diffusion systems have been much studied (Cole, 1968) and their steady-

state conductance properties are well known (Adrian, 1969; Hope, 1971).

Moreover, the pH-dependence of the steady state chloride current-voltage

relations cannot be accounted for by electrodiffusion theory in the

manner of its formulation in the past (Hutter and Warner, 1972). But

in our view, it is of interest to review the behavior of the electro-

diffusion model with regards to rectification ratio or the dependence of

conductance on concentration; to determine whether the chloride permeation

system is mimicked by electrodiffusion in any aspect other than the

steady state I-V relation near neutrality (Hodgkin and Horowicz, 1959;

Adrian, 1961; Hutter and Warner, 1972). The chloride system has been

seen to exhibit voltage dependent transients and time and voltage depen-

dent recovery of conductance after experiencing changes of membrane

potential (conditioning steps); the transient properties of constant

field theory under voltage clamp during stationary and non-stationary

conditions will be investigated for comparison.

The evidence for chloride translocation via ionic channels or pores

has been reviewed in Chapter 1. Our aim in the present chapter is not to

perform an exhaustive analysis of the properties of ionic channels but

only to point out some of the more salient features of channel transport

and discuss these features in view of the data on chloride transport.

Most of the material in the chapter is well known, as our present under-

standing of transport processes across membranes involves very simple

concepts. It will be seen that some of the models considered are too

idealized and are clearly inadequate to account for the observed

behavior of chloride conductance, but only through the understanding

gained from a succession of simple models can we eventually arrive at a model which could perhaps account for our observations.

Throughout the discussion, ionic activities will be assumed to be equal to concentrations. Because physiological concentrations of chloride are low (from $3-10^2$ mM/ℓ) and no estimate of chloride activity coefficients inside cells is available, there is no loss of generality in setting the chloride activity coefficients at one.

Models of membrane permeation process

A. Electrodiffusion models

Definitions and symbols; typical dimensions

d = membrane thickness, typical dimension 50-80 A^o.

x = distance coordinate within the membrane. x lies between
 0 and d.

z = valence of the permeating ion.

$c(x)$ = concentration of the permeating ion within the membrane
 phase.

c_I , c_{II} are the concentration of ions in the extracellular and
 intracellular compartments respectively. Physiological
 concentrations are c_I = 120 mM/ℓ ; c_{II} = 4 mM/ℓ

$\tilde{\mu}(x)$ = electrochemical potential of the permeating ion within
 the membrane phase.

u = electrophoretic mobility of the permeating ion within
 the membrane phase. u has the dimensions cm $sec^{-1}volt^{-1}$.

 u will be assumed to be related to diffusion coefficient
 via Einstein's relation $D = uRT/|z|F$

ε = dielectric constant of the lipid phase of the membrane,

approximately (4-5).

β = oil/water partition coefficient.

$V(x)$ = potential profile within the membrane, in Volts.

$V = (V_{II} - V_{I})$ is the difference in potential between intracellular

and extracellular compartments. In experimental

situations V can vary between +100 and -200 mV without

dielectric breakdown of the membrane.

V_o = zero current potential.

zF/RT : F is the Faraday; R is the gas constant and T is

absolute temperature. For z=1, at room temperature

$(293^{\circ}K)$, zF/RT = 39.6 $Volts^{-1}$.

$I(t)$ = transmembrane current density $(Amp.cm^{-2})$ measured in voltage

clamp experiments. t is usually referenced from the onset

of a voltage clamp step.

P_{Cl} = chloride permeability coefficient, defined by

$$P_{Cl} = \beta u_{Cl} RT/d |z_{Cl}| F \quad , \quad z_{Cl} = -1 \quad .$$

Consider a membrane of thickness d separating two well-stirred
solutions, designated as compartment I and II. The membrane will be
assumed to be the rate limiting step for the flow of ions. This flow
is proportional to the gradient of the electro-chemical potential
$\tilde{\mu}(x)$ of the ions.

The electrochemical potential is given by the sum of the
electrical potential $zFV(x)$ and a concentration potential $RT \cdot \log(c(x))$.

The transport equations relating the concentration of permeant ions in the membrane and the potential are obtained using the conservation of mass:

(1) $$\frac{\partial c}{\partial t} = \frac{\partial}{\partial x} \left\{ \frac{uRT}{zF} \frac{\partial c}{\partial x} + uc \frac{\partial V}{\partial x} \right\}$$

and the electrostatic (Poisson's) relation:

(2) $$\frac{\partial^2 V}{\partial x^2} = \frac{4\pi}{\varepsilon} (zFc)$$

At the boundaries between the aqueous and membrane phases, the concentrations of ions will be assumed, for simplicity, to obey the partition relation (Hodgkin and Katz, 1948):

(3) $$c(0) = \beta c_I$$
$$c(d) = \beta c_{II}$$

β is a partition coefficient independent of voltage. c_I and c_{II} are the concentrations in the extracellular and intracellular compartments. Equations (1-3) are the classical electro-diffusion equations for a single permeant ion. It is explicit that the time scale of the equilibrium at the boundaries is much shorter than that for diffusion within the membrane. In order to integrate equations (1-3), the approximate assumption that has frequently been made is that the potential gradient throughout the membrane is approximately constant (Goldman, 1943; Hodgkin and Katz, 1949). The relatively low dielectric constant of cell membranes suggests that the intramembrane

concentration of mobile ions would have to be small for the assumption of constant field to be a good approximation (Adrian, 1969), or equivalently, space charge effects are negligible.

The transmembrane current that is measured in voltage clamp experiments is the average current:

$$(4) \qquad I(t) = \frac{zF}{d} \int_0^d (\frac{uRT}{zF} \frac{\partial c}{\partial x} + uc \frac{\partial V}{\partial x}) \, dx$$

It can be expressed as a sum of currents due to diffusion and migration:

$$(5) \qquad I(t) = \beta uRT(\frac{c_{II} - c_I}{d}) + zFu \frac{V}{d^2} \int_0^d c(x) \, dx$$

V is the transmembrane voltage.

Steady state properties

The steady state properties of constant field theory have been well reviewed (Adrian, 1969; Hope, 1971). At a given transmembrane potential V, there is a steady state concentration profile (maintained by the energy stored in the electric field) given by

$$(6) \qquad c(x) = \beta \{ \frac{c_I e^{FV/RT} - c_{II}}{e^{FV/RT} - 1} + (\frac{c_{II} - c_I}{e^{FV/RT} - 1}) e^{FVx/RTd} \}$$

This is illustrated in Fig.4.1a,b for various values of V. The membrane conductance according to equation 5, is the average charge of ions within the membrane phase. The steady state current-voltage relation

Figure 4.1 a) and (b) are concentration profiles of permeant
anion within the membrane for various values of the
membrane potential, shown on the relations. In (a)
the resting (zero current) potential is -90 mV and in
(b) it is -30 mV. The scales are normalized so that
at the extracellular boundary the concentration is 1.

c) shows current-voltage relations for different zero
current potentials (shown on the relations). The
dotted lines represent the independent inward (below
the zero current axis) and outward (above the axis)
currents. The solid lines are total currents obtained
by the addition of the inward and outward currents.

d) The rectification ratio, defined by equation 10,
in constant field electrodiffusion theory . The
numbers on the lines indicate the zero current potentials.

e), (f) and (g) are current-voltage relations of modified
constant field theory incorporating surface charge
(equation 11). In (e) the resting potential is -90 mV,
in (f) it is -30 mV and in (g) it is 0 mV. The (outside)
surface charge, in mV, is indicated on each relation.
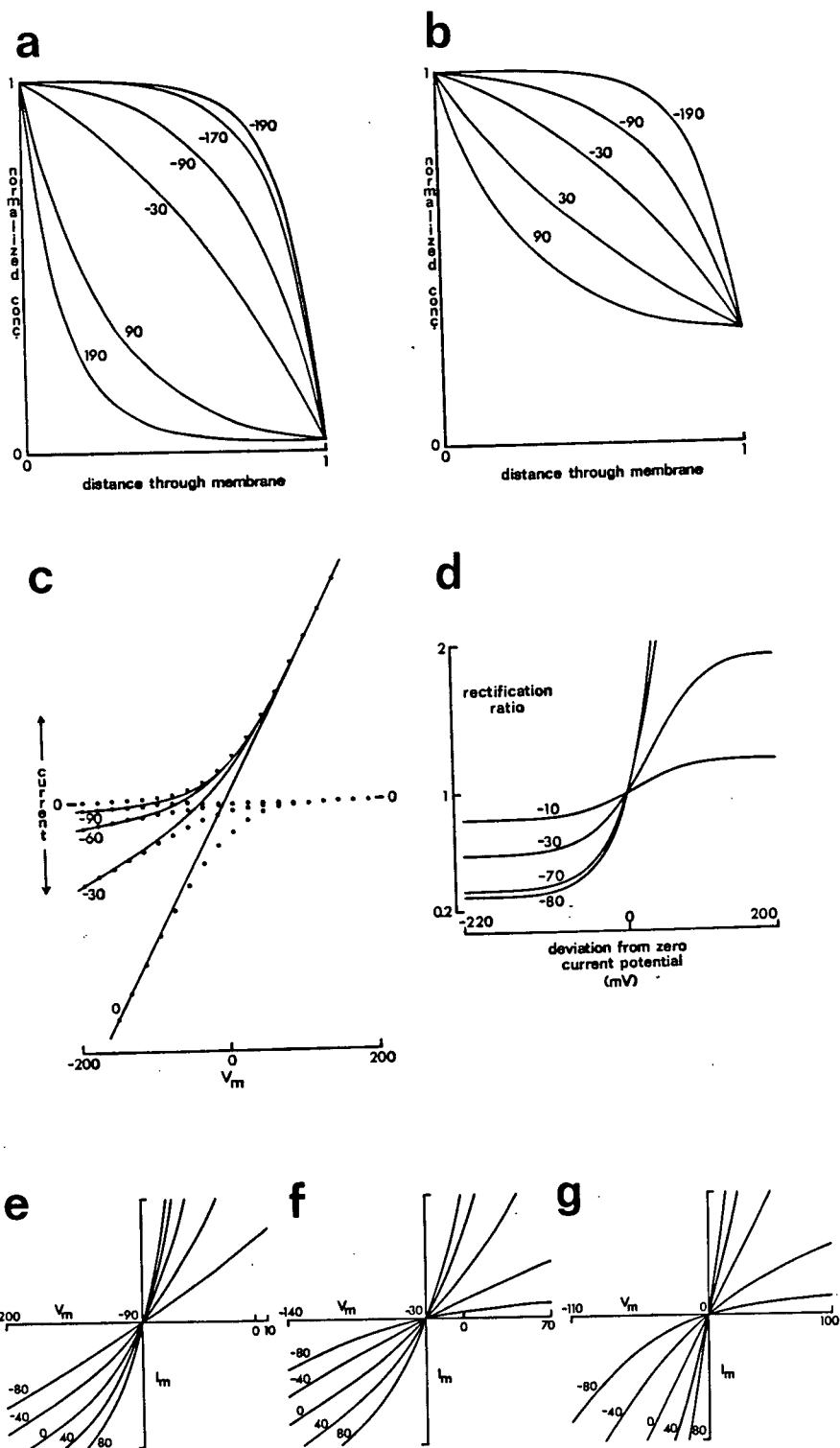
$$(7) \qquad I(V) = - \frac{PF^2V}{RT} c_I \frac{1 - (c_{II}/c_I) e^{-VF/RT}}{1 - e^{-VF/RT}}$$

obeys the independence principle: Ionic current inwards (anion efflux)

$$I_{in}(V) = + \frac{PF^2V}{RT} c_{II} \frac{e^{-VF/RT}}{1 - e^{-VF/RT}}$$

and outwards (anion influx)

$$I_{out}(V) = - \frac{PF^2V}{RT} c_I \frac{1}{1 - e^{-VF/RT}}$$

are independent.

Asymptotically, for large transmembrane potentials, the current is proportional to voltage:

$$I \simeq I_{in} = - \frac{PF^2}{RT} c_{II} V \qquad VF/RT \ll 0$$

(8)

$$I \simeq I_{out} = - \frac{PF^2}{RT} c_I V \qquad VF/RT \gg 0$$

This property of limiting conductances being proportional to the internal and external concentrations of permeating ions will be referred to as ' rectification of the electrodiffusion type'. The terminology will also be applied to channels.

An experimental situation of special interest to us is when the external chloride concentration is maintained while its internal concentration is varied. By the independence principle, only the outward movement of chloride is affected. The resultant current-

voltage relations are shown in Fig.4.1c   Linearization of the current-voltage relations with decreasing concentration gradients is a characteristic of 'rectification of the electrodiffusion type'.

An alternate quantitative method of studying the nature of rectification is to investigate the rectification ratio (Lauger, 1973) defined as the ratio of the slope conductance at a given membrane potential V to the zero current potential V_o:

$$(9) \qquad \lambda(V) = \frac{\frac{dI}{dV}(V)}{\frac{dI}{dV}(V_o)}$$

Experimentally, this is a useful device in comparing experiments from different cells that exhibit large variations in current density. Moreover, if there are uncertainties in the calibration of membrane current densities because of uncertainties in cable parameters such as the internal resistivity (see, for instance, equation 1, chapter I), then they are removed as the rectification ratio is independent of cable parameters. In the chloride system in Xenopus, we find experimentally that the rectification ratio is independent of the resting potential as $\lambda(V)$ for both polarized and depolarized fibers are similar. However, it is highly dependent on external pH: $\lambda(V)$ is greater than 1 in acid solutions (downwards concave) in the hyperpolarizing range, and is less than 1 in alkaline solutions (upwards concave).

The expression for $\lambda(V)$ from constant field electrodiffusion theory is:

$$(10) \quad \lambda(V) = \frac{(-1)(1 - e^{-FV_o/RT})^2}{(FV_o/RT)e^{-FV_o/RT}(1 - e^{-FV/RT})} \left\{ (1 - e^{F(V_o-V)/RT}) - \right.$$

$$\left. (FV/RT) \; e^{-FV/RT} \; \frac{(1 - e^{FV_o/RT})}{(1 - e^{-FV/RT})} \right\}$$

It can be seen from Fig.4.1d that $\lambda(V)$ is always less than one when the internal chloride concentration is less than the external. Hence it clearly fails to account for experimental observations.

Electrodiffusion theory may be modified to change the rectification ratio at a given resting potential. An explicit assumption of the model is that the rates for entry into the membrane are much greater than the membrane limited diffusion. Hutter and Warner (1972) have attempted to adapt Frankenhaeuser's (1960) modification of the constant field equation incorporating surface charges to account for constant field rectification at different pH's. Here, the steady state current voltage relation is modified by a surface voltage term V_s:

$$(11) \quad I(V) = -\frac{PF^2}{RT}(V-V_s)c_I \left\{ \frac{e^{V_sF/RT} - (c_{II}/c_I) \; e^{-(V-V_s)F/RT}}{1 - e^{-(V-V_s)F/RT}} \right\}$$

The direction of the current voltage rectification depends on the difference between potential V_s and the zero current potential $V_o = (RT/F) \log_e (c_{II}/c_I)$ (Frankenhaeuser , 1960; Adrian, 1969; Hutter and Warner, 1972).

Asymptotically,

$$I(V) \simeq -\frac{PF^2}{RT}(V-V_s) \, c_{II} \qquad FV/RT \ll 0$$

(12)

$$I(V) \simeq -\frac{PF^2}{RT}(V-V_s) \, c_I e^{FV_s/RT} \qquad FV/RT \gg 0$$

If $(V_o-V_s) < 0$, rectification is in the direction that the conductance

for outward current is greater than for inward current.

If $(V_o-V_s) = 0$, there is no rectification (the current-voltage relations

are linear).

If $(V_o-V_s) > 0$, rectification is in the direction that the conductance

for inward current is greater than the conductance

for outward current.

It is seen (Fig.4.1e,f,and g) that the direction of the rectification

changes depending on the surface potential. However, the current-

voltage characteristics do not cross or intersect each other if the

conductances are appropriately scaled so that the effects of pH on the

resting conductance are taken into account (Hutter and Warner, 1972).

It is also noteworthy that the current-voltage relations are

always conductance limited (equation 12), and therefore cannot

account for observations in alkaline solutions, where saturation and

negative slope conductance is sometimes observed.

An extension of electrodiffusion model

An alternate formulation which we have studied is the generalization

of the Nernst-Planck equations (equations 1-3) by the introduction

of an invariant barrier function $w(x)$ into the expression for the

electrochemical potential $\overset{\sim}{\mu}(x)$ (Hall, Mead and Szabo, 1973; Neumcke
and Lauger, 1969):

(13) $\overset{\sim}{\mu}(x) = RT \log(c(x)) + zFV(x) + w(x)$

w(x) represents the energetic cost of moving an ion from place to

place inside the membrane. The form of such a barrier function can

either be calculated from the energy required to move an ion from a

region of high dielectric constant to one of low dielectric constant

(Neumcke and Lauger, 1969) or it can be empirically fitted from a

study of current-voltage characteristics (Hall, Mead and Szabo,

1973).

The steady state current-voltage relation is obtained by inte-

grating the current relation $I(x) = -zFuc(x)\nabla\overset{\sim}{\mu}(x)$

(14) $I(V) = -|z|Fu \dfrac{e^{F(V_{II} + w_{II})/RT}c_{II} - e^{F(V_I + w_I)/RT}}{\displaystyle\int_0^d e^{F(V + w)(x)/RT}dx}$

The subscripts I and II denote the values of the parameters c, V, and

w in the compartments I and II respectively. The I-V relation (equation

14) was studied assuming different potential energy profiles w(x)

(triangular, trapezoidal, parabolic) and various asymmetric profiles

that may represent membrane sites which chloride might interact with

as it crosses the membrane. Our conclusion (assuming constant electric

field within the membrane) is that the current-voltage relations are

always conductance limited in an asymptotical fashion, regardless of

the potential energy profile w(x). The transmembrane electric field

will ultimately be the dominant force and the limiting conductances
are proportional to the internal and external concentrations of the
permeating ions. The current-voltage relations are highly dependent
on the ionic concentration gradients across the membrane and the I-V
relation is the sum of two effects: one due to concentration gradients
across the membrane ('electrodiffusion' effect) and the other to the
asymmetric barrier function.

Transient properties

    When a test voltage V_2 is applied across a membrane previously
in a steady state under conditioning voltage V_1, the concentration
of permeant ions within the membrane will redistribute to a new equili-
brium profile. The time course of this redistribution is obtained
from the solution of the initial value problem:

$$\frac{\partial c}{\partial t} = (\frac{uRT}{zF})\{\frac{\partial^2 c}{\partial x^2} + z\frac{FV}{RT}\frac{\partial c}{\partial x}\} \qquad 0 < x < d$$

(15) $c(x,0) = c_o(x)$

$c(0,t) = \beta c_I$, $c(d,t) = \beta c_{II}$

    $c_o(x)$ is the initial concentration profile prior to the onset

    of the voltage V_2 at $t=0$, and is given by equation (6) with

    V replaced by V_1 if the membrane is initially in a steady state.

Equation (15) describes diffusion in a constant force field or diffusion
with a constant drift velocity. The formal solution can be obtained
by many standard methods. The relaxation spectrum is most easily

obtained from the eigenvalue problem associated with equation (15) by separation of variables. The solution, written as a sum of a steady state $c_\infty(x)$ and a transient term $c_{tr}(x,t)$ is:

(16) $c(x,t) = c_\infty(x) + c_{tr}(x,t)$

$$c_\infty(x) = \beta \frac{c_I e^{FV_2/RT} - c_{II}}{e^{FV_2/RT} - 1} + \beta \frac{c_{II} - c_I}{e^{FV_2/RT} - 1} e^{FV_2 x/RTd}$$

(17) $$c_{tr}(x,t) = \sum_{n=1}^{\infty} A_n \sin n\pi(x/d) \, e^{-\lambda_n^2 t}$$

$$A_n = (1/2) \int_0^d e^{zFV_2 x/RTd} (c_\infty(x) - c_0(x)) \sin n\pi(x/d)dx$$

(18) $$\lambda_n^2 = \frac{(n\pi)^2 + (zFV_2/RT)^2}{4} \frac{D}{d^2} \qquad , \quad n \geqslant 1$$

It is well known that the principal characteristic time constant (n=1, equation 18) of diffusion with no drift in a finite domain is $4d^2/\pi^2 D$. Under the influence of drift (the imposed transmembrane potential V_2), the characteristic time constant is modified to $4d^2/(\pi^2 + (FV_2/RT)^2)D$. The macroscopic current measured in voltage clamp experiments, defined by equation (5), is then expressed as:

(19) $I(t) = I_\infty + I_{tr}(t),$ where

(20) $$I_\infty = \beta \frac{uRT}{d}(c_{II} - c_I) + zFu \frac{V_2}{d^2} \int_0^d c_\infty(x)dx$$

(21) $$I_{tr}(t) = zFu \frac{V_2}{d^2} \sum_{n=1}^{\infty} \int_0^d A_n e^{-\lambda_n^2 t} \sin n\pi(x/d)dx$$

The conclusion that can be drawn from equation (21) is that

the kinetics of current relaxations depend only on the absolute membrane

potential, and are independent of the initial state (that is, the

conditioning potential V_1).

The principal time constant for chloride may be estimated from

P_{Cl} values obtained from steady state current-voltage relation (7).

$P_{Cl} = \dfrac{\beta uRT}{d\ zF} = \dfrac{\beta}{d} D$. Therefore

$$\tau = \frac{4d^2}{\pi^2 + (FV_2/RT)^2} \frac{\beta}{Pd}$$

If $d = 60$ Å

$\qquad P_{Cl} = 8.0 \times 10^{-6}$ cm sec^{-1} (Table II.1.1)

$\qquad V_2 = -90$ mV

$\qquad \beta = 10^{-5}$

then $\tau = 1.3 \times 10^{-7}$ sec

The above estimate of the time constant (τ) may not be valid

since it depends on a priori knowledge of the partition coefficient

β , a value difficult to obtain for cell membranes. However, an

alternate estimate , of the ratio of the principle time constants at

$V=0$ (τ_0) and $V= -90$ mV (τ_{-90}), is independent of β :

$$\frac{\tau_{-90}}{\tau_0} = \frac{4d^2/(\pi^2 + (3.8)^2)}{4d^2/(\pi^2)} = .64$$

This implies that if chloride transport were to be described

be electrodiffusion, as has been shown in neutral solutions by

many authors (Hodgkin and Horowicz, 1959; Adrian, 1961; Adrian and

Freygang, 1962a; Harris, 1963, 1965; Hutter and Warner, 1972), then

the time constants for current decay for small hyperpolarizing pulses

from the holding potential in polarized and depolarized fibers would

differ by a factor of 2. This is not observed in experiments in

Xenopus laevis.

Instantaneous currents and aftercurrents

The expression for the instantaneous current $I(V_2,0)$ corresponding

to a test voltage applied to a membrane which had been in a steady

state corresponding to a conditioning pulse V_1 is:

$$(22) \qquad I(V_2,0) = \frac{\beta uRT}{d} (c_{II} - c_I) + \frac{zFuV_2}{d^2} \int_0^d c(x,V_1,\infty) \, dx$$

This instantaneous current is an affine function of the test voltage

(V_2).

On return to the zero current potential V_o after an exploratory

test step V_1, there is an after-current due to the restoration of

the concentration profile to the equilibrium position. This transient

aftercurrent , given by

$$(23) \qquad I_{tr}(t) = \frac{zFu}{d^2} V_o \sum_{n=1}^{\infty} \int_0^d (c_0(V_1,x) - c_\infty(V_o,x)) \, e^{-\lambda_n^2(V_o)t} \sin n\pi(x/d)dx$$

is the mirror image of the decay of the current starting from the

zero current potential except that the driving force is $V_o (\neq 0)$.

The magnitude of the shift in equilibrium potential V_{shift} can be

obtained by setting the instantaneous current to be zero:

$$I_{aft}(0) = 0 = \frac{\beta uRT}{d}(c_{II} - c_I) + \frac{zFu}{d^2} V_{shift} \int_0^d c(x,V_1,\infty) \, dx$$

to obtain

$$(24) \qquad V_{shift} = -\frac{RT}{zF} \frac{\beta d(c_{II} - c_I)}{\int_0^d c(x,V_1,\infty)dx}$$

The shift of zero current potential, V_{shift}, is proportional to the concentration differences across the membrane. Hence in the case of decreasing concentration gradients across the membrane (as in depolarized fibers), the magnitudes of the shift in zero-current potential should disappear. Experimentally, this was not observed.

Summary

Some aspects of electrodiffusion and experimental results can be related while others cannot. When a voltage is applied to a membrane in a steady state, the instantaneous current is proportional to the applied voltage. Current transients then relax to the steady state with infinitely many time constants depending on the absolute membrane potential. The steady state current-voltage relation always exhibits a limiting conductance that depends on the internal and external ionic concentrations. On return to the zero current potential after a test pulse, there is an aftercurrent opposite in direction to the test current. The magnitude of this aftercurrent depends linearly on the difference between the ionic concentration between the two sides of

the membrane. Kinetics of current relaxations depend absolutely on membrane potential even when the initial conditions are not steady.

B. Channel or pore models

Apart from a geometric or structural description, a channel may be characterized by a series of potential energy barriers. When an ion enters a channel, it undergoes a series of random walks or discrete jumps over successive potential barriers. The forward and backward jump rates over any barrier depend on the electric field within the membrane. When the transmembrane voltage is changed, there are current relaxations that depend on the relaxation of the potential profile within a single channel to a new equilibrium. The time scales for these processes are very fast. If the jump rates are also time dependent, since they are probably due to macromolecular movements within the membrane, they are expected to be slower.

The initial current-voltage manifold may be used to illustrate a possible relationship between the above and experimental results as follows: each point (current density) in the manifold is described by the number of open channels and the conductance of a single channel (for simplicity, channels will be assumed either 'open' or 'closed'). Coordinates with the same conditioning potential V_1 have the same number of open channels and those with the same V_2 have the same conductance for each channel.

Starting from a stationary state, when a voltage across the membrane is altered to a new value, the initial current depends on the activating

barrier profile at the previous steady state. Since the relaxation of the conductance of a single channel is very fast (faster than the resolution of our experiments), the instantaneous current measured is a product of the number of open channels during steady V_1 and the single channel conductance at V_2. In time, the current undergoes a relaxation due to changes in the number of open channels. Alternatively, the current transients may be due to a time dependent molecular relaxation within the channel and consequently the conductance of a single channel is changed. The purpose of this section is to explore some qualitative predictions of the ideas expressed above.

The first objective of the present section is to describe the general formulation for a pore model.

General formulation for a pore model

It is assumed that the membrane contains N identical pores/cm^2. The pores are independent (do not interact with each other), and only ions of the same sign (anions) are able to enter the pore. A potential energy diagram for the situation of an ion diffusion across a pore is shown in Fig.4.2. The rate constants for the jump from the nth minimum to the right and to the left is denoted by k_n and k_{-n}. According to the Theory of Absolute Rates (Glasstone, Laidler and Eyring, 1941) the following expressions for the rate constants are obtained:

$$(25) \qquad k_n = \kappa_n (kT/h) \exp(-(f_n^{max} - f_n^{min})) \qquad n = 0, 1, 2, \ldots n.$$

$$k_{-n} = \kappa_{-n} (kT/h) \exp(-(f_{n-1}^{max} - f_n^{min}))$$

163
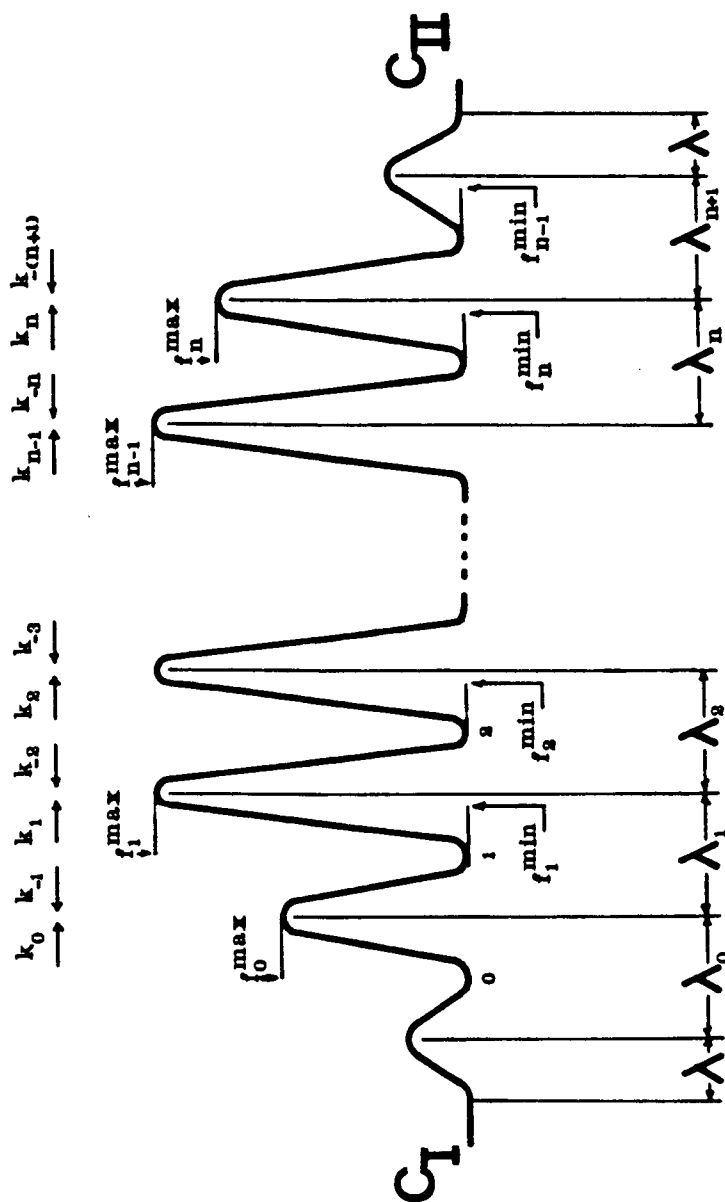
Figure 4.2 A potential energy diagram for diffusion within an
ionic channel. Energy is plotted vertically and
distance horizontally. Symbols are as defined in the
text.

f_n^{min}, and f_n^{max} are the non-dimensionalized free energies (free energy divided by RT) in the nth minimum and at the top of the barrier to the right of the nth minimum. k, T , R, and h are the Boltzmann constant, absolute temperature, the gas constant and Planck's constant respectively. The term (kT/h), which is an attempt rate (Stephens, 1978) is 6.2 X 10^{12} sec^{-1} (298 ^oK) and has the dimensions of a frequency, the translational vibrational frequency of the activated complex (Glasstone, Laidler and Eyring, 1941). The transmission coefficient κ_n and κ_{-n} will be set equal to one.

The λ_j's (Fig.4.2) may be thought of as the mean jump distances for the ion. If c_j is the concentration of ions per cubic centimeter at the jth minimum, then N_j, the number of molecules which are candidates to jump across the barrier in a square centimeter of area normal to the direction of diffusion, is $N_j = \lambda_j c_j$.

In the derivation of the equations, the pore will be assumed to contain no more than one ion. However, even though the model is based on single occupancy, it is not a restrictive assumption as the analytical expressions derived reduce to the situation when more than one ion is allowed inside the pore. Moreover by studying the model under what appears initially as unnecessarily restrictive assumptions, the required conditions for possible saturation and blocking effects can be derived.

The pore is assumed to be accessible to two ionic species A, and B. Let A_j and B_j represent states of the channel with ionic species A and B at the jth minimum (j=1, 2,.. n). The state 0 represents the channel when

it is free of an occupied ion. k_n^A, k_j^B, k_{-j}^A and k_{-j}^B are the forward and backward rate constants of A and B respectively at the jth minimum.

Let p_j^A and p_j^B be the probabilities that a single channel is occupied by A or B at the jth minimum ($1 \leqslant j \leqslant n$). p_0 is the probability that the channel is unoccupied, and is equal to

(26a) $$p_0 = (1 - \sum_{j=1}^{n} (p_j^A + p_j^B)).$$

N_0, the number of unoccupied channels per square cm is

(26b) $$N_0 = Np_0$$

The outer or inner minimum (at positions 0 and n+1, Fig.4.2) will not be considered as pore positions, and we assume that the concentrations N_I and N_{II} in these positions to be proportional to the bulk concentrations c_I and c_{II} :

$$N_I = \nu c_I \quad , \quad N_{II} = \nu c_{II}$$

The constant of proportionality ν is equal to the volume from which an ion may enter the pore in a single jump (Lauger, 1973). It can be expressed as the product ($\nu = \lambda \sigma$) of the distance λ between the first energy barrier in the outer (or inner) mouth of the pore and the entrance barrier to the membrane, and σ, the effective cross sectional area of the pore (Lauger, 1973).

All the transitions and states of the channel are connected by the diagram shown in Fig.4.3 where the rate constants have equivalent interpretations as conditional probabilities.

For the present discussion, the rate constants $k_{\pm j}$ are assumed to be independent of time but depend on the electric field within the membrane. N_j^A and N_j^B, the number of channels per square centimeter with ions A or B in the jth minimum, are $N_j^A = N p_j^A$ and $N_j^B = N p_j^B$ and also depend on the membrane potential. When the transmembrane potential is changed, as in voltage clamp experiments, the occupational densities p_j^A and p_j^B and consequently N_j^A and N_j^B relax to new stationary values depending on the membrane potential. The time evolution of this relaxation is described by the matrix equation:

$$(27) \quad \frac{d}{dt}
\begin{bmatrix}
p_0 \\
p_1^A \\
p_1^A \\
\cdot \\
\cdot \\
\cdot \\
p_n^A \\
p_1^B \\
p_2^B \\
\cdot \\
p_n^B
\end{bmatrix}
=
\begin{bmatrix}
-(k_0^A + k_{-(n+1)}^A + k_0^B + k_{-(n+1)}^B) & k_{-1}^A & \cdot & \\
k_0^A & -(k_{-1}^A + k_1^A) & k_{-2}^A & \cdots \\
\cdot & k_2^A & k_{-3}^A + k_3^A & \cdots \\
\cdot & & & \\
\cdot & & & \\
\cdot & & & \\
k_{-(n+1)}^A & & & \\
k_0^B & & & \\
\cdot & & & \\
k_{-(n+1)}^B & & &
\end{bmatrix}
\begin{bmatrix}
p_0 \\
p_1^A \\
p_2^A \\
\cdot \\
\cdot \\
\cdot \\
p_n^A \\
p_1^B \\
p_2^B \\
\cdot \\
p_n^B
\end{bmatrix}$$

The rows are not independent since

$$(28) \quad p_0(t) + p_1^A(t) + \ldots + p_n^A(t) + p_1^B(t) + \ldots + p_n^B(t) = 1$$

The matrix equation (27) is the Chapman-Kolmogorov equation for a temporally homogeneous and spatially inhomogeneous birth and death process.

The equations for the fluxes J_j^A of A across the potential energy maximum f_j^{max} ($0 \leqslant j \leqslant n$) are:

$$J_0^A = \lambda_0 k_0^A P_0 - \lambda_1 k_{-1}^A P_1^A$$

$$J_1^A = \lambda_1 k_1^A P_1^A - \lambda_2 k_{-2}^A P_2^A$$

(29)
$$\vdots$$

$$J_n^A = \lambda_n k_n^A P_n^A - \lambda_{(n+1)} k_{-(n+1)} P_0$$

There are similar equations for B.

Steady state properties

The steady state current-voltage relations for a single ionic species can be obtained either by solving the flux equations (29) by successive elimination (Lauger, 1973) or by graph theoretic means (King and Altman, 1956; Hill, 1966; Heckmann et al, 1972; Macey and Oliver, 1967). For our purposes, the relation as first expressed by Lauger (1973) is adequate:

$$I = zFN\nu k_0 \frac{(c_I - \kappa c_{II})}{1 + \sum_{j=1}^{n} S_j + \nu c_I Q_I + \nu c_{II} \kappa Q_{II}}$$

$$\kappa = \prod_{j=1}^{n+1} \frac{k_{-j}}{k_{(j-1)}}$$

$$S_j = \prod_{\ell=1}^{j} \frac{k_{-\ell}}{k_\ell}$$
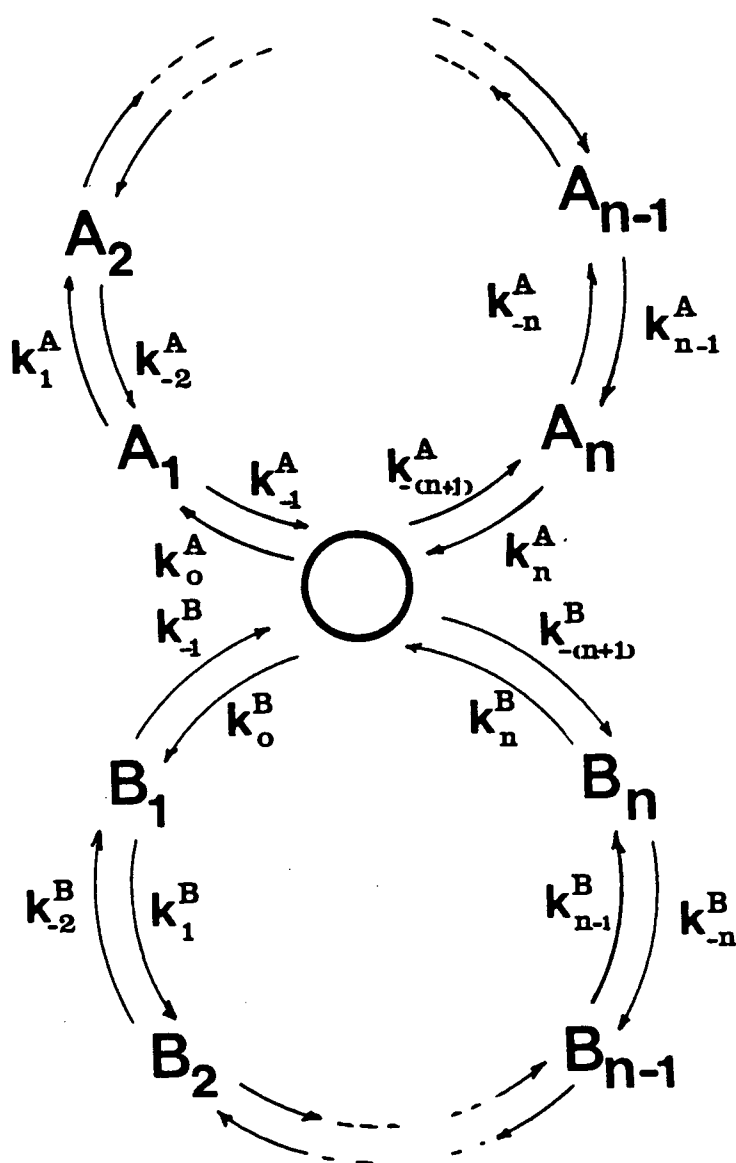
Figure 4.3 A schematic diagram illustrating all the states of a
channel which permits the entrance of one of two ionic
species A or B into the channel but only one ion
is allowed to occupy a channel at one time.

$$R_j = \prod_{\ell=1}^{j} \frac{k_{(\ell-1)}}{k_{-\ell}}$$

$$Q_I = \sum_{j=1}^{n} S_j \sum_{u=1}^{j} R_u$$

$$Q_{II} = \sum_{j=1}^{n} R_j + \sum_{j=2}^{n} R_j \sum_{u=1}^{j-1} S_u$$

The I-V relation (30) was derived on the restrictive assumption of single occupancy. However, in the event that most of the pores are empty of ions, that is,

$$(32) \qquad \nu(c_I Q_I + c_{II} Q_{II} \kappa) << \quad (1 + \sum_{j=1}^{n} S_j)$$

the relation reduces to

$$(33) \qquad I = NzF\nu k_0 \frac{c_I - \kappa c_{II}}{1 + \sum_{j=1}^{n} S_j}$$

Equation (33) was first derived by Zwolinski, Eyring and Reese (1949) and was first extended to equation (30) by Lauger (1973). Special cases of the equation for specific profiles of the rate constants $k_{\pm j}$'s have been extensively analyzed (Johnson , Eyring and Polissar, 1954; Parlin and Eyring, 1954; Woodbury, 1971).

Alternatively, current-voltage relations may be obtained in the case of interactions of ions within channels (Hladky, 1965; Hladky and Harris, 1967) or single file diffusion of ions within channels (Sandblom et al, 1977; Eisenman et al, 1976, 1978).

Recently, evidence (French and Adelman, Jr., 1976) has been gathered for multiple occupancy and interference of ions in the

sodium (Hille et al, 1973; Woodhull, 1973; Hille, 1975b; Cahalan

and Begenisich,1976)and potassium channels in nerve and muscle (Cahalan

and Armstrong, 1972;Gay and Stanfield, 1977; Hille and Schwarz, 1978)

and in compounds that form channels (Gramicidin A) in lipid bilayers

(Bamberg and Lauger, 1977; Sandblom et al, 1977; Eisenman et al,

1978; Schragina et al, 1978).

At the present , there is some evidence supporting the possibility

of single occupancy of chloride channels, as will be discussed in

the following section. However, to consider possible multiple

occupancy or interactions within the chloride channel would be premature.

Specifications for a possible chloride channel

In the preceding section, the equations for a channel model were

derived on very general assumptions. Single occupancy of ionic

channels was considered because of the possible relevance to the chloride

channel. It is plausible that the interference of chloride movement

by Br^-, I^-, NO_3^-, and SCN^- may be due to the occupancy of a site within

the channel excluding the entrance or passage of chloride. In addition

the independence of resting conductance on internal chloride concentration

could also be due to a saturation of the channels by chloride even

at very low concentrations. This would be the case if the chloride

channel densities within the membrane are low (equation 32).

A first approximation for a simple model of a chloride channel

is a symmetric pore with identical internal barriers but different

surface barriers. There are several reasons why these approximations

might be pertinent:

Woodbury and Miles (1972) have suggested that there is only one

rate limiting step at the outer surface (Parker and Woodbury, 1976) of

the membrane in the chloride channel. The rate limiting step at the

surface will be represented by a surface barrier on the external side

of the channel and the interior step in jumping from the cytoplasm into

the membrane is also represented by a surface barrier. Since the available

experimental evidence on the internal pH has shown that it is fairly

constant (Hill, 1955; Caldwell, 1956, 1958; Kostyuk and Sorokina, 1960;

Waddel and Bates, 1969) while the external pH and transmembrane potential

can have large variations, one of the effects of changing the external

pH could be a change of the external barrier potential to anion

permeation.

The near 'constant field like' current-voltage relations at neutral

solutions suggests that perhaps the channel might exhibit some form of

regularity with respect to the internal potential energy profiles. That

is, under some conditions, the model exhibits constant field behavior.

Hence the model envisages n potential energy minima equally spaced

within the membrane. The distance between successive maximum and

minimum is denoted by $1/2(n+1)$.

Let $\hat{v} = FV/RT$ be the normalized transmembrane potential and

$v = \hat{v}/(n+1)$. The voltage dependence of the rate constants k_n and k_{-n}

is a function of the electric field within the membrane. The simplifying

assumption of a constant electric field will be used. Then the voltage

dependence of the rate constants are expressed in the form:

$$(34) \quad k_n = k_j^o \exp(\hat{v}/2(n+1)) = k_j^o \exp(v/2)$$

$$k_{-n} = k_j^o \exp(-\hat{v}/2(n+1)) = k_j^o \exp(-v/2)$$

Notice that with hyperpolarization, the backward rate constants

(rate constants for chloride efflux) increase. The voltage independent terms

$$(35) \quad k_j^o = (kT/h) \exp(-(f_j^{max} - f_m^{min})) = (kT/h) \exp(-(f^{max} - f^{min}))$$
$$k_{-j}^o = (kT/h) \exp(-(f_{j-1}^{max} - f_j^{min})) = (kT/h) \exp(-(f^{max} - f^{min}))$$
$$1 \leqslant j \leqslant n$$

At the inner and outer mouths of the channel:

$$(36) \quad k_0 = k_0^o \exp(v/2)$$

$$k_{-(n+1)} = k_{-(n+1)}^o \exp(-v/2)$$

The non-voltage dependent terms k_0^o and $k_{-(n+1)}^o$ are expressed as:

$$(37) \quad k_0^o = (kT/h)\exp(-f^I)$$

(There is no loss of generality in assuming that the free energies in the compartments I and II to be zero)

$$k_{-(n+1)}^o = (kT/h)\exp(-f^{II})$$

When the channels are mostly unoccupied, the current-voltage relation

(33) becomes:

$$(38) \quad I = FNvk_0^o c_I \frac{(1 - (c_{II}/c_I)e^{-VF/RT})\, e^{v/2}}{[\, 1 + (e^v + e^{2v} + e^{3v} + .. + e^{(n-1)v})\, e^{-(f^I - f^{max})} + e^{nv} e^{-(f^I - f^{II})} e^{f^{max}}\,]}$$

The dependence of the current-voltage relation (38) on the number of internal barriers, the concentration of the permeant anion, and on the differences between f^I, f^{max} and f^{II} is shown in Fig. 4.4. Fig.4.4a shows the linearization effect of increasing the number of internal barriers: the current-voltage relations are more linear for a greater polarizing range (Woodbury, 1971; Lauger, 1973).

The current-voltage relations rectify either inwards or outwards depending on the difference between the activation energies of the surface step and the internal potential energy maxima. This is illustrated in Fig.4.4b for a channel with symmetrical internal (5 internal minima) and surface barriers (inner and outer activation energies are equal). The degree of rectification is dependent on a single parameter, which is expressed as a function of the difference between the surface activating energy f^I and the activating emergy of any one of the internal maxima f^{max}.

(39) $q = \exp(-(f^I - f^{max}))$

When $q > 1$ ($f^I < f^{max}$), ie. internally rate limited, the current-voltage relation bends downwards for hyperpolarizations and upwards for depolarizations. Conversely when $q < 1$ ($f^I > f^{max}$, the rate limiting step is at the surface), the current-voltage curves are concave upwards for hyperpolarizations and bend towards the voltage axis with depolarization.

In the extrme case when $q = 0$, the surface rate limiting step becomes completely dominant. The rectification reaches a limiting degree as the ratio q approaches zero. In Fig.4.4b these rectifications are not complicated by a concentration component because the resting

or zero current potential is zero.

The dependence of the current-voltage rectification on concentration gradients across the membrane is shown in Fig. 4.4c. The linear current-voltage relation of Fig.4.4b becomes a constant field rectification. Depending on whether the surface or interior of the membrane is the rate limiting step,the effect of concentration varies (Fig.4.4d and 4.4e). When the zero current potential (or concentration gradient across the membrane) is decreased in the situation where the interior is the rate limiting step, the degree of rectification increases.

In contrast, when the surface is the rate limiting step, decreasing the concentration gradient of the permeant ion greatly linearizes the I-V relations.

In Fig.4.4d and 4.4e the current-voltage characteristics are normalized so that the chord conductances at the resting potential are equal.

In Fig.4.4f the effect of changing the surface potential f^{II} on the inside mouth of the channel is shown. Here, the energy of the first maximum is decreased. It can be seen that the hyperpolarizing current is greatly increased. Instead of the linear current-voltage relation when q = 1.0, it becomes downwards concave whereas in the depolarization direction, there is no change in the characteristics.

Variations in the number of conducting channels

Steady state current-voltage relations measured from a collection of channels could be complicated by voltage dependence of the number of conducting channels.

In this section, the current-voltage relations of some cases will be examined. The current-voltage relation is in the form:

(40) $I(V,\infty) = n(V,\infty)\ I_{ch}(V,\infty)$

where $n(V,\infty)$ is the dependence of the number of open channels on voltage (in the steady state) and $I_{ch}(V,\infty)$ is the steady state current-voltage relation of a single channel.

The analysis of the steady state relations also requires a hypothesis on the dependence of the channel parameters on pH to account for the pH dependence of the steady state current-voltage rectification. Moreover, it is clear that reduction of single channel conductances by a constant amount that is pH dependent or reduction of the number of channels by a constant amount with pH is inadequate to account for the degree of rectification since they would only yield families of parallel characteristics.

Parker and Woodbury (1976) have reported a shift of the S-curves of resting conductance with pH as a function of resting potential, and have suggested that a titratable group located about one-quarter of the distance from the outer mouth of the channel controls resting conductance.

The equation:

(41a) $g(V) = \dfrac{1}{1 + 10^{-(pH-pK)}\exp(zFV/4RT)}$

satisfies this condition (Fig.4.5a,b). An interpretation is that such a group distributes two states to control the open and closed

states of the channel. At a fixed membrane potential, changing the pH

shifts the half-potential of the distribution.

In order to obtain the required current-voltage relations, a

knowledge of the driving force is necessary. In the absence of such

knowledge, the simplest assumption is that current is obtained from

conductance by the multiplication of a linear factor $\underline{g}(V_m-V_{Cl})$. Then

(41b) $I = \underline{g} \, n_o (V-V_{Cl}) g(V)$

where $\underline{g}(V_m-V_{Cl})$ is the conductance of a single channel and n_o is the total

number of channels. V_{Cl} is zero current potential.

Current-voltage relations are shown in Fig.4.5c for pH 5 and 8.

These relations are always upwards concave at the zero current potential

V_{Cl}.

If the exponential term is made to increase more rapidly with

voltage (eg. $\exp(zFV/2RT$ rather than $\exp(zfV/4RT))$, a saturating

current-voltage relation, or one that exhibits negative slope, is generated

(Fig.4.5d).

The model using the empirical expression (41a) clearly cannot account

for chloride currents because the I-V relations predicted are not

downwards concave (inward rectification) at any pH. The relations of

Fig.4.5c and 4.5d were obtained assuming that a single channel conductance

is proportional to (V_m-V_{Cl}) ($\underline{g}$ is the constant of proportionality).

We have studied the model using the more complex expressions for

single channel conductance defined by equation 38 and illustrated in

Fig.4.4. Since the asymptotic behavior of the I-V relations is governed

by the exponential expression in g(V) (equation 41a), in order for

inward rectification to occur (as in acid solutions) the growth rate

of the single channel conductance ($I_{ch}(V)$) with voltage needs to be

greater than this exponential. This is implausible, based on the

model of channel behavior expressed by equation (38) and illustrated

in Fig.4.4.

An alternate hypothesis, suggested by the curves of Fig.4.5d is

that as the pH of the external solution is lowered, the groups do not

sense as much of the electric field as they do in more alkaline solutions.

It is even conceivable that the group changes valence and sign as

a function of the local pH. Such an empirical relationship between

current and voltage is:

$$(42a) \qquad I = g \cdot \frac{1}{1 + \exp(pK-pH)FV/RT} \cdot (V_m - V_{Cl})$$

g is a constant of proportionality.

A special interpretation may be given to equation (42a). The

fraction $1/(1+\exp(pK-pH)FV/RT))$ may be interpreted as the fraction

of channels 'blocked' by a particle within it. In alkaline solutions,

the channel is blocked during hyperpolarizations and is 'unblocked' in

acid solutions.

Plots of I-V relations (from equation 42a) are shown in Fig.4.6a and

b for zero current potentials of -90 mV and -30 mV respectively. The

curves are normalized at the zero current potential so that the resting

conductance at pH 8.0 is three times the resting conductance at pH 6.0

(Fig.2.1.4). In agreement with experimental observations: the curvature

of the I-V relations depends continuously on pH, from upwards concave

and negative slope conductance in alkaline solutions to downwards con-

cavity in acid solutions; the relations do not depend on concentration

gradients (resting or zero current potential) to any appreciable

extent.

The expression (42a) may be modified by the more complex expression:

$$(42b) \qquad I = \frac{1}{1 + \exp(pK-pH)FV/RT} \; I_{ch}(V)$$

where $I_{ch}(V)$ is the single channel current-voltage relation of equation 38.

However, the qualitative behavior of equations 42a and 42b remain

unchanged.

Transient properties

In this section, the voltage and time dependence of channel

transport is considered. When the transmembrane potential is suddenly

perturbed, the evolution of the occupation densities N_1, N_2, ...,N_n

to a stationary distribution with a single channel is described by

the matrix equation:

$$(43) \qquad \frac{d}{dt} \begin{bmatrix} N_1 \\ N_2 \\ . \\ . \\ . \\ N_n \end{bmatrix} = \begin{bmatrix} -(k_1+k_{-1}) & k_{-2} & . & . & . \\ k_1 & (k_2+k_{-2}) & k_{-3} & . & . \\ . & & & & \\ . & & & & \\ . & & & & \end{bmatrix} \begin{bmatrix} N_1 \\ N_2 \\ \\ \\ N_n \end{bmatrix} + \begin{bmatrix} k_0 N_0 \\ 0 \\ . \\ . \\ . \\ k_{-(n+1)} N_{n+1} \end{bmatrix}$$

Figure 4.4 The qualitative behavior of the current-voltage equation
(equation 38).

a) If the number (n) of internal barriers is increased,
the current-voltage relation is linearized. All the
other parameters remain fixed. The numbers indicate the
number of barriers.

b) This graph illustrates the effect of different
rate limiting steps in the case of a 'homogeneous'
channel with symmetrical surface barriers at the inner
and outer mouths of the channel. The numbers beside
each curve indicate the value of q (equation 39).

c) This graph shows the influence of concentration
gradients on current-voltage rectification. Note that
the direction of the (I-V) rectification remains un-
changed, but the magnitude of the normalized current
density for hyperpolarization (as compared to (b)) is
reduced.

d) The purpose of these two graphs is to illustrate the
effect of concentration gradients on (I-V) rectification
when the rate-limiting step is either at the interior
(d) or surface (e) of the membrane. Both graphs are
normalized so that all curves have equal chord conductances
at the zero current potential. In both graphs, the
interior surface step is assumed to be equal to the
external step. The results with asymmetrical barriers
at the interfaces are similar except that the rectification
in the inward direction (with hyperpolarization) is much
larger with a smaller internal barrier. In (d) it is
seen that with decreasing zero-current potential, the
degree of rectification increases. In (e), as the
zero current is decreased, the degree of rectification
decreases. The numbers on the lines are the zero-
current potentials. In (d) the curves have all been
shifted to superimpose the -50 mV relationship at
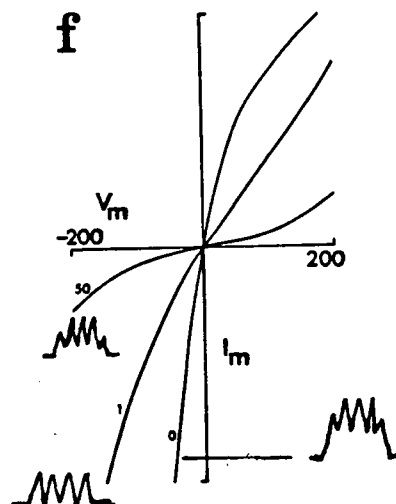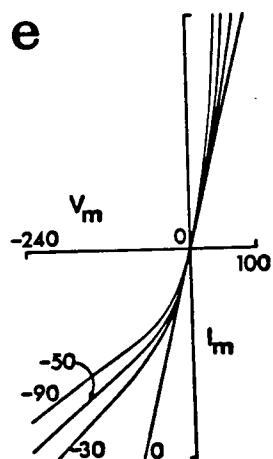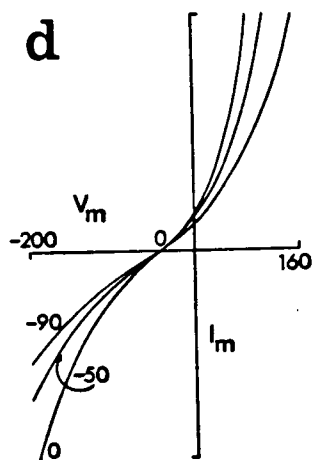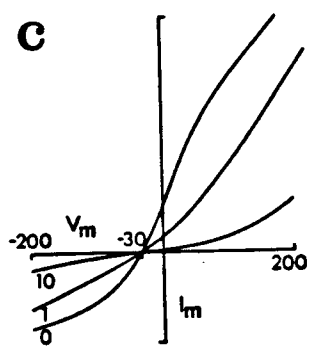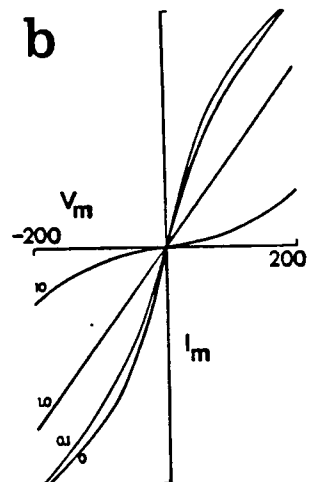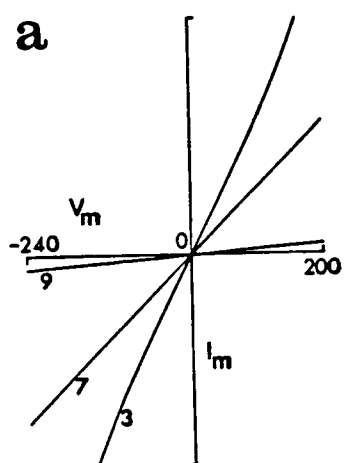
zero current and in (e) they have all been shifted to superimpose the 0 mV relationship.

f) This figure illustrates the effect of asymmetrical potential barriers at the inner and outer mouths of the channel (with the internal barrier heights f^{max} kept at the same value in all the curves). The small figure inset beside each curve illustrates the relative heights of the activating energy barriers.

Curve 0 (q=0). The value of $e^{f^I-f^{II}}$ = .4 (see text, equations 37, 38). That is, the barrier at the external surface is larger than at the internal surface. f^I is also greater than f^{max} in this graph (hence the downwards concavity of the curve).

Curve 1 ($e^{f^I-f^{II}}$ = 1.0) . The internal barrier height f^I is the same as the external barrier height f^{II} and $f^{II} = f^{max}$.

Curve 50   ($e^{f^I-f^{II}}$ = 50.0) . The internal barrier height is very small ($f^{max} > f^I > f^{II}$).

with initial distribution
$$\begin{bmatrix} N_1(0) \\ \vdots \\ N_n(0) \end{bmatrix}$$

Set the matrix A to be :

$$(44) \quad A = \begin{bmatrix} -(k_1+k_{-1}) & k_{-2} & \cdot & & \\ k_1 & (k_2+k_{-2}) & k_{-3} & & \\ & k_2 & -(k_3+k_{-3}) & k_{-4} & \\ & \vdots & & & \end{bmatrix}$$

In the following discussion, most of the channels will be assumed to be unoccupied so that single occupancy effects are not present. The barriers within the channel will also be assumed to be symmetric and regular.

The characteristic times for the relaxation (of occupation densities) in such a channel is obtained by solving the characteristic polynomial $\det(A - \lambda I) = 0$. Seshadri (1971), using the method of generating functions and Frehland&Lauger (1974) , using orthogonal polynomials, have solved the problem when there is no voltage gradient across the membrane. We have extended the solution of Frehland and Lauger (1973) to include non-zero potential gradients across the membrane. However, the conclusions that can drawn is exactly analogous to the extension of diffusion to incorporate drift. This is not surprising as the channel model with regular internal barriers is a discretization of continuous electro-diffusion (Woodbury, 1971;

Figure 4.5   a)   Families of S-shaped curves shifted by voltage

(equation 41a).

b)   Plots of the conductance from (a) when the pH is

remained constant and the membrane potential is varied.

The numbers beside each curve indicate the pH.

c)   Current-voltage relations using equation 41a and a

linear channel conductance voltage (equation 41b).

The currents at pH 5.0 have been multiplied by 100 to

make them visible against those at pH 8.0

d)   Current-voltage relations with the 'group' at

various distances within the membrane.   The number

beside each curve indicates the distance within the

membrane.
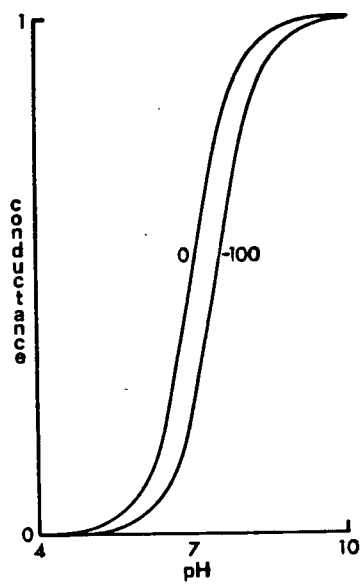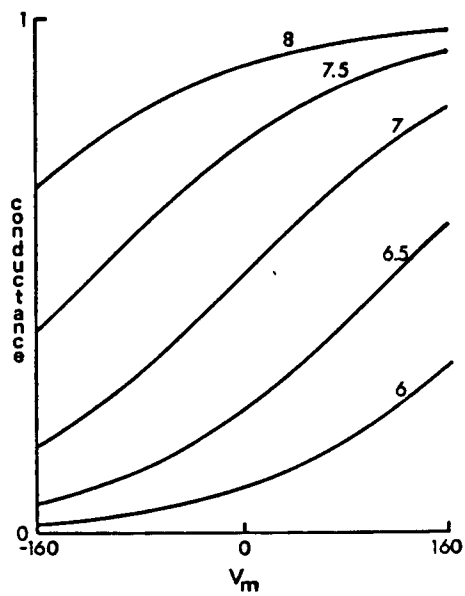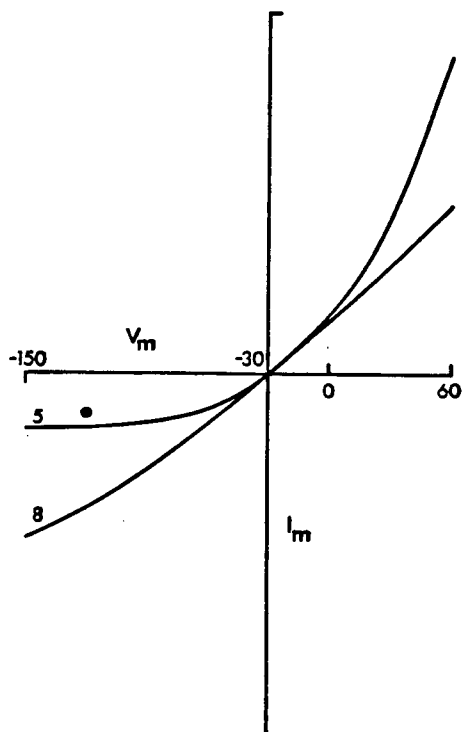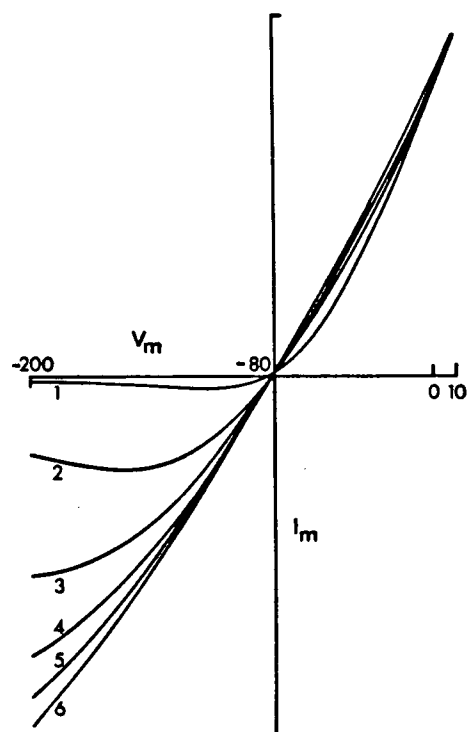
Frehland and Lauger, 1973). Hence the details will not be presented and we will consider only the qualitative behavior:

When the voltage across a membrane (with n internal potential energy minima) is changed, the current relaxes with a spectrum of n characteristic time constants depending on the absolute membrane potential. The magnitudes of these relaxation time constants depend on whether the surface or the interior of the membrane is the rate limiting step. This is summarized in Table IV.1 for the largest and smallest time constants.

Our discussion has been based on the assumption of no single occupancy effects, primarily for simplicity. If single occupancy is incorporated into this model with regular internal barriers, its effect is to introduce a delay into the relaxation transients of the occupation densities and hence membrane currents (Macey and Oliver, 1967). This may be qualitatively observed as follows: a channel with single occupancy may be viewed as a chain of reactions $N_1 \rightleftharpoons N_2 \rightleftharpoons N_3 \rightleftharpoons \cdots \rightleftharpoons N_n \rightleftharpoons N_0$, where N_j denote the state of the channel with an ion in the jth minimum, and N_0 is the channel free of ions. Hence a delay would be expected between the entrance of an ion into a channel and its eventual exit. However, in spite of this delay, since the relaxations are ionic in nature, observed kinetics are expected to be much faster (microseconds) then experimentally observed relaxations (milliseconds).

When the rate constants $k_{\pm j}$'s are time dependent as a result of relaxation of membrane bound molecules within a channel, the matrix

equation (43) becomes non-autonomous (equation of a temporally

inhomogenous birth and death process). Without further experimental

evidence on the local field inside the membrane and the nature of

these movements, it will not be fruitful to pursue these matters further.

But it is of interest to note that if the matrix $A(t)$ (equation 44)

is decomposed into:

$$(45) \qquad A(t) = A(0) + \sum_{j=1}^{n} A_j(t) \qquad\qquad A(t) = A(0) + (A(t) - A(0))$$

where $A_j(t)$ is the matrix whose entries a_{ik}^{j} are

$$a_{ik}^{j} = \begin{cases} 0 & \text{when } k \neq j \\ -(k_{-j}(t) - k_{-j}(0)) & , \ i = j-1, \ k = j \\ -((k_j(t) - k_j(0)) + (k_{-j}(t) - k_{-j}(0))), & i=j, \ k=j \\ (k_j(t) - k_j(0)) & , \ j=j+1 \ , \ k=j \end{cases}$$

then the solution of (43) is

$$(46) \qquad N(t) = N(0) \, e^{A(0)t} \prod_{j=1}^{n} e^{\int A_j(t)dt}$$

The expression (46) indicates that formally, current relaxations

within a single channel may be equivalently viewed as changes in the

number of conducting channels. Here the product $\prod_{j=1}^{n} e^{\int A_j(t)dt}$

is equivalent to changes in the number of channels. Hence subsequent

discussions will be restricted to changes in the number of channels.

Table IV.1

Dominant fast and slow time constants for channel
model with n identical internal barriers (from
Frehland and Lauger, 1974).

Rate limiting step	Smallest time constant	Largest time constant
interior rates are the same as the surface rates $(k^o = k^o_{-1} = k^o_{n+1})$	$1/k^o(1+\cos\pi/(n+1))$	$1/2k^o(1+\cos n\pi/(n+1))$
interior rate limited $(k^o \ll k_{-1} \; ; \; k^o \ll k_{n+1})$	$1/2k^o(1+\cos 2\pi/n)$	$1/2k^o(1+\cos(n-1)\pi/n)$
surface rate limited $(k^o \gg k^o_{-1}; \; k^o \gg k^o_{n+1})$	$1/2k^o(1+\cos\pi/n)$	$1/(k^o_{-1} + k^o_{n+1})$

For definition of the symbols, refer to Fig.4.2 and equation 35
$(k^o_j = k^o$ for $1 \leqslant i \leqslant n)$. k^o, k^o_{-1} and k^o_{n+1} are voltage independent.

The dependence of the number n(V,t) of conducting channels on voltage and time has been found to be very varied. In the sodium and potassium channels of nerve and muscle (Hodgkin and Huxley, 1952; Adrian, Chandler and Hodgkin, 1970a) it is described by first order kinetics but satisfactory theories accounting for the voltage dependence of conductance changes in both of these channels are lacking.

Understanding of the transient properties of the chloride permeation poses several problems. The most outstanding problem is the dependence of kinetics on differences between conditioning and test potentials (or differences between initial and the newly imposed voltage). In ChapterIII when the manifold was constructed, this also was extended to non-stationary initial conditions as it was shown that when voltage steps are made during recovery or inactivation of conductance, there is an equivalent voltage from which the current transients may be considered as starting. A second problem is the independence of current transients on external pH in spite of the wide variations in steady state rectification. Since the equilibria of chemical reactions depend on the rate constants it is difficult to reconcile the steady state and transient properties of chloride conductance.

In view of these difficulties, only a brief discussion is considered. It will be clear that traditional models that have been proposed for other ionic channels (such as sodium and potassium channels in nerve and muscle) are inadequate to account for the observations for chloride current transients.

The simplest model is that of a channel distributing between two states, open and closed, depending on the transmembrane voltage. When the voltage is changed, a redistribution into a new equilibrium occurs. If the redistribution is a first order (unimolecular) process:

$$\text{Open} \xrightleftharpoons[k_{-1}]{k_1} \text{Closed}$$
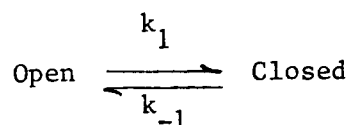
then the relaxation kinetics follow an exponential time course

$$c(t) = (c(0) - c(\infty))e^{-t/\tau} + c(\infty)$$

($c(t)$ is the concentration of either open or closed channels).

The rate constant $= 1/(k_1(V) + k_{-1}(V))$ depends on voltage but is independent of the initial concentration $c(0)$. The independence of kinetics of initial conditions also applies to linear chains of first order reactions:

$$\text{Open} \rightleftharpoons I_1 \rightleftharpoons I_2 \rightleftharpoons \cdots \cdots \cdots \rightleftharpoons I_n \rightleftharpoons \text{Closed}$$
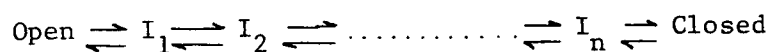
Kinetics depend as well on the absolute membrane potential since the eigenvalues of the transition matrix for such a chain depend only on the rate constants $k_{\pm j}$ $(1 < j < n)$. For instance, the sodium and potassium channel kinetics of nerve have been modeled primarily by a sequence of first order steps (Hoyt, 1963; Goldman, 1964,1965; Armstrong, 1969; Jain et al, 1970; Fishman et al, 1971; Moore and Jakobsson, 1971; Moore and Cox, 1976).

The dependence of kinetics on initial conditions cannot be explained by first order reactions.

Chemical reactions whose rates show a dependence on initial concentrations usually involve higher order (multi-molecular) reactions or catalytic reactions (Benson, 1960). But the kinetics of higher order reactions in in general non-exponential. For instance, the simple combination of two Gramicidin A molecules

$$G + G \rightleftharpoons 2G$$
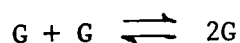
to form a conducting channel has a sigmoid dependence on time (Bamberg and Lauger, 1974) and the rate constants of current relaxations in response to a step change in transmembrane voltage depend on the difference between initial and final currents.

In the chloride channel, the dependence of kinetics on a step change in voltage is more difficult to understand. The best approximate model that we have been able to find and accounting qualitatively for some of the experimental observations is that conversion from open to closed states of a channel(or from a higher to a lower conducting state in a single channel) involves the participation of a molecule A which acts in a catalytic role controlling the rate of the conversion. Such a role has been postulated for calcium in the sodium channel in nerve (Moore and Cox, 1976). The availability or concentration of A depends on membrane potential. For instance, in the kinetic schemes (1) and (2):

(1) $\text{Open} \xrightarrow{k_1 A} \text{Closed}$

(2) $\text{Active} \underset{k_{-2}}{\overset{k_2}{\rightleftharpoons}} \text{Inactive}$
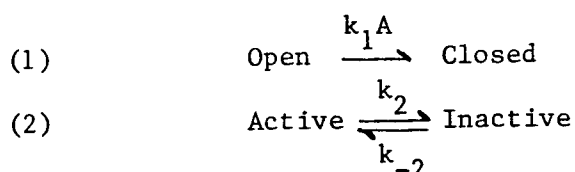
Figure 4.6 The current-voltage relations according to equation

(42a). The curves are normalized so that the resting

conductance at pH 8.0 is 3 times greater than at

pH 6.0 . The numbers beside each curve indicate the

pH. The zero current potentials V_{Cl} for (a) and (b)

are -90 mV and -30 mV respectively.
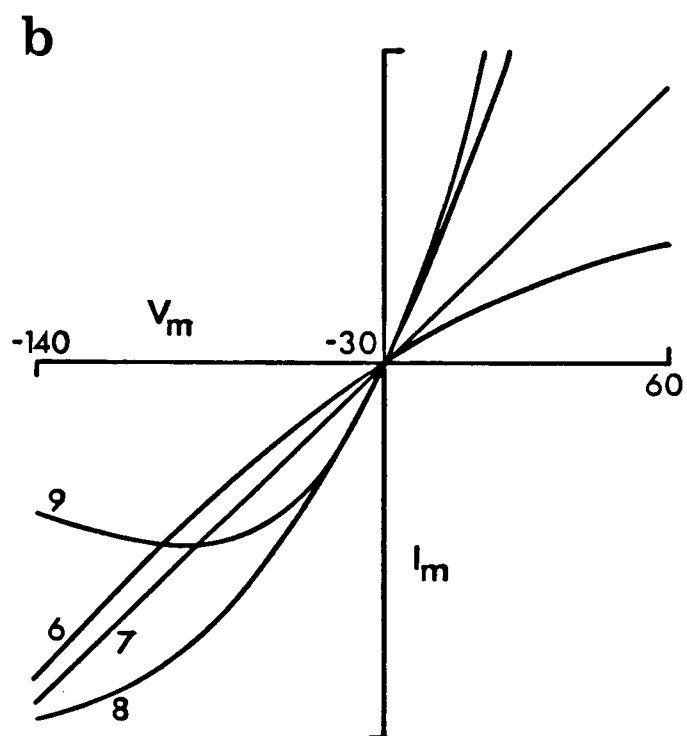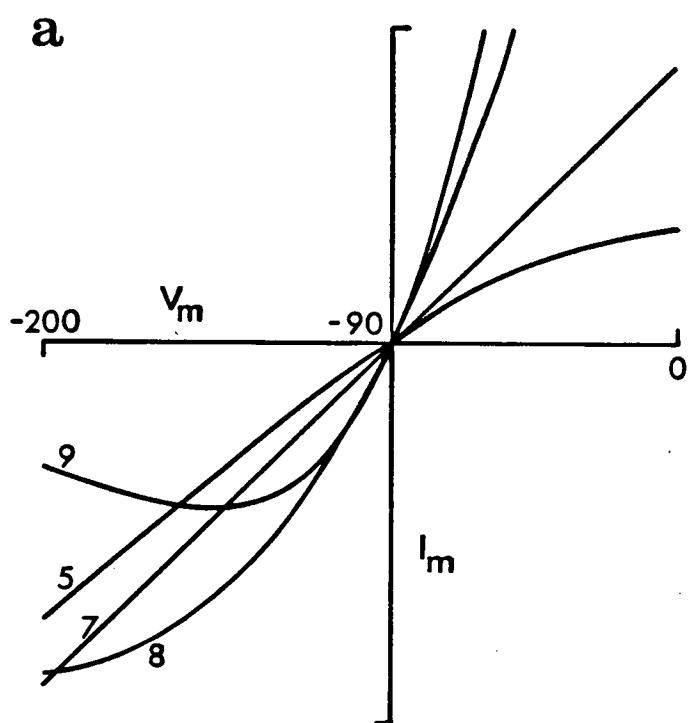
The concentration $c_o(t)$ of open channels after a change in voltage

from a steady state at V_1 (conditioning voltage) to a new voltage V_2

at $t = 0$ is

$$c_o(t) = c_o(0)e^{-k_1(A_0(V_1)-A_\infty(V_2))}e^{-(t/\tau + k_1 A_\infty(V_2)t)}$$

$A_0(V_1)$ and $A_\infty(V_2)$ are the initial and steady state concentrations

of the active form of the molecule A, and $\tau = 1/((k_2(V_2) + k_{-2}(V_2))$

is the rate constant for reaction (2).

and shows a dependence on the initial and final concentrations of A.

The kinetics do not depend simply on the voltage step $|V_2-V_1|$.

We have investigated more complex schemes than (1) and (2) , but they

have all failed to account for the simple dependence of kinetics on

the voltage step.

Discussion

In this chapter, we have reviewed some of the qualitative behavior

of electrodiffusion and channel transport with the hope of finding

some properties of the chloride permeation system that might be

described by standard models for ion transport. The heuristic view

of the chloride permeation system that we have assumed is that instan-

taneous conductances reflect single channel conductance whereas steady

state conductances are the result of changes either in the number of

of conducting channels or in the conductance of a single channel or

possibly both situations. In this discussion we will consider in more

detail the applicability of this hypothesis.

Instantaneous current-voltage relations

The instantaneous conductance is postulated to reflect the conductance of a single channel. In polarized fibers, the instantaneous current-voltage relations are linear in acid solutions, conductance limiting in neutral solutions, and exhibit saturation and negative slope conductance in alkaline solutions. When the internal chloride concentration is increased, and the chloride concentration gradient is decreased (in depolarized fibers), the instantaneous current-voltage relations become downwards concave in acid solutions, and linear for a greater voltage range in neutral and alkaline solutions. This linearization behavior indicates the conductance of single channels may be describable by the 'electrodiffusion' type of channel models (For instance, Fig.4.4 of this chapter).

However, the observation that resting conductances of both polarized and depolarized fibers are of the same magnitude is not compatible with these views since single channel conductances are highly concentration dependent in 'electrodiffusion' models. Perhaps an explanation for the independence of concentration would be that channels are saturated with permeating anions in polarized fibers, and any further increase of the internal concentration would have no significant effect on the currents. If this were the case, then the negative slope conductance observed in some polarized fibers in alkaline solutions would be attributed to mutual interference of ions. It is

surprising then, that with a ten-fold increase in concentration in depolarized fibers, there is no observation of negative slope conductance.

Effect of pH on current-voltage relations

In order to understand the action of external pH, a satisfactory explanation would have to be given to the rectification of the steady state current-voltage characteristics. Amongst all the simple models that we have studied, some of which are reviewed in this chapter, the one that qualitatively yields the current-voltage relations most similar to those observed in experiments is the model of Fig.4.6 where changing pH changes the electrical sign and charge of a group that controls chloride permeation. However, the appearance of a more pronounced negative slope conductance in depolarized fibers than in polarized fibers (in the steady state current-voltage relations in alkaline solutions), if it is not an artefact, is not predicted.

In ionic channels, selectivities depend on dynamic parameters such as the rate constants for surmounting the activating energy barriers (Bezanilla and Armstrong, 1972; Lauger, 1973; Armstrong, 1975a; Hille, 1975a). If there is a change in the effective charge of the group controlling chloride permeation, then a change in the selectivity pattern of the anion channel would be anticipated with changes in external pH and membrane potential.

Shifts in zero-current potential

Shifts of zero-current potential are predicted (see equation 24)

in electrodiffusion and 'electrodiffusion' channel models. But the magnitude of these shifts depend on the steady state channel conductance of the preceding pulse. This is contrary to experimental observations. The source of these shifts remains unresolved.

Dependence of current transients on voltage and on initial conditions

The most plausible explanation for the dependence of kinetics on initial conditions is that current transients involve the mediation of a moiety whose presence determines the rate of a reaction, in this instance, the translocation of chloride across the membrane. If this moiety distributes also in two states such that only one state can mediate the channel inactivation process, then the rate constants will depend on the difference between the initial and final concentrations of this moiety. If this dependence is on the membrane electric field, then the time constants will depend on the difference between initial and final voltage, but this dependence is more complex than the dependence of $|V_2-V_1|$ that we have described from experiments.

Final Discussion

Final Discussion

Channel versus carrier transport

One of the objectives of these experiments was to investigate

the carrier and channel hypotheses for chloride transport in Xenopus

laevis muscle membrane. The results obtained in this study, like

those that we have reviewed in Chapter I, support a channel hypothesis

more favourably than a carrier for chloride transport. Although

there is no compelling single piece of evidence that completely excludes

a carrier, various observations tend to make the adoption of this

hypothesis implausible: The carrier hypothesis as suggested by Warner

(1972) based on the model studied by Sandblom, Eisenman and Walker

(1967) cannot account for the dependence of rectification on concentration

gradients, nor the negative slope conductances observed in alkaline

solutions. Perhaps an alternate formulation of a carrier model based

either on position dependent mobilities of the carrier within the membrane

(Agin, 1972) or on more ad hoc assumptions such as the carrier concentration

on one side of the membrane being constant (Adrian, 1969) will account

for the negative slope conductance, but introduction of these assumptions

at the present time would be largely empirical.

The nature of the chloride channel

Diverse experimental evidence indicates that the internal structure

of the chloride channel may be very complex: as we have mentioned,

the blocking action of Br^-, NO_3^-, I^- and SCN^- and the non-interference

of F^- and the family of 'benzoate-like' anions (Woodbury and Miles, 1973) suggests that the rate limiting steps for different anions may differ.

Additional evidence on the possible multi-component nature of the chloride channel is obtained from studies on the reduction of chloride and permeability by the disulphonic stilbene derivative, SITS (4-acetamido-4'-isothiocyano-2,2'-stilbene disulphonic acid), which has been found to inhibit chloride flux in mammalian red blood cells (Knauf and Rothstein, 1971) and barnacle muscle fibers (Russel and Brodwick, 1976). At concentrations of .2 mM and 1 mM, SITS has been found to reduce resting chloride conductance by 50% and 75% respectively regardless of the external pH (Vaughan and Fong, 1978). Unlike the irreversible action of SITS on red blood cells and barnacle fibers, in Xenopus the reduction of chloride conductance by SITS is reversible. The pH independent actions of SITS suggest that the membrane site affected by SITS is different from the pH dependent site. Parker and Woodbury (1976) have found two temperature dependent but correlated components of chloride conductance and have suggested that the pH dependent site and the conductance activating site are close together. A study of the temperature dependence of the action of SITS will aid us in determining whether the SITS binding site is the conductance activating site.

The reduction of chloride conductance with repeated polarization in permanently depolarized fibers in alkaline solutions also suggests a multi-component channel for chloride permeation. But the observations pose two unsolved problems. The first is whether this is a voltage

or current effect. That is, is the conductance reduced by current passing through the channel or do channels disintegrate or become less stable by repeated changes in transmembrane potential?

The second problem is whether a variable number of channels is inactivated or the conductance of a single channel is reduced.

Some unsolved problems

Although we have clarified the phenomenon of instantaneous aftercurrents, their source and mechanism remain to be resolved.

Another interesting and important aspect of chloride conductance is its independence of absolute membrane potential. In our experiments, families of S-shaped curves (the manifold) are translated in the $I_2(0)$ versus V_1 plane with changes in resting potential. The kinetics of current transients (as described in Chapter III) remain <u>invariant</u> relative to this family of S-curves as it is shifted along the plane. An elucidation of this translation would greatly aid us in understanding chloride permeation.

An understanding of the current transients was one of the main objectives of our experiments. Although the dependence of kinetics on voltage and pH is clarified, the molecular mechanisms of the current transients remain unresolved.

The construction of the initial current-voltage manifold and its ability to account for diverse experimental protocols (such as instantaneous and steady state current-voltage rectification, the dependence of current transients on the difference between conditioning and test voltages, and the dependence of kinetics on initial conditions) suggests

that there is a fundamental unity in the molecular mechanism governing chloride transport at different external pH and different chloride concentration gradients across the membrane.

Finally, for an eventual understanding of chloride permeation, we require a demonstration that the channel hypothesis is really applicable to chloride permeation and a clarification of whether the current transients are due to reduction of single channel conductance or the reduction of the number of conducting channels (or possibly both). Microscopic measurements, possibly noise analysis, may help us answer these questions.

References

Adrian, R.H. (1961). Internal chloride concentration and chloride efflux of frog muscle. J. Physiol. 156, 623-632.

Adrian, R.H. (1964). The rubidium and potassium permeability of frog muscle membrane. J. Physiol. 175, 134-139.

Adrian, R.H. (1969). Rectification in muscle membrane. Prog. Biophys. Molec. Biol. 19, 341-369.

Adrian, R.H., Chandler, W.K.,and Hodgkin, A.L. (1969). The kinetics of mechanical activation in frog muscle. J. Physiol. 204, 207-230.

Adrian, R.H., Chandler, W.K., and Hodgkin, A.L. (1970a). Voltage clamp experiments in striated muscle fibers. J. Physiol. 208, 607-644.

Adrian, R.H., Chandler, W.K., and Hodgkin, A.L. (1970b). Slow changes in potassium permeability in skeletal muscle. J. Physiol. 208, 645-658.

Adrian, R.H. and Freygang, W.H. (1962). The potassium and chloride conductance of frog muscle membrane. J. Physiol. 163, 61-103.

Agin, D. (1972). Negative conductance and electrodiffusion in excitable membrane systems. Chapter 5 in : Perspectives in Membrane Biophysics (Ed. Adelman, Jr.), pp. 240-265. Gordon and Breach, New York.

Almers, W. (1972a). Potassium conductance changes in skeletal muscle and the potassium concentration in the transverse tubules. J. Physiol. 225, 57-83.

Almers, W. (1972b). The decline of potassium permeability during extreme hyperpolarization in frog skeletal muscle. J. Physiol. 225, 57-83.

Almers, W. and Levinson, S.R. (1975). Tetrodotoxin binding to normal and depolarized frog muscle and the conductance of a single sodium channel. J. Physiol. 247, 483-509.

Anderson, C.R. and Stevens, C.F. (1973). Voltage clamp analysis of acetylcholine produced end-plate current fluctuations at frog neuromuscular junction. J. Physiol. 235, 655-692.

Armstrong, C.M. (1969). Inactivation of the potassium conductance and related phenomena caused by quaternary ammonium ion injection in squid axons. J. Gen. Physiol. 54, 553-575.

Armstrong, C.M. (1971). Interaction of tetraethylammonium ion derivatives with the potassium channels of giant axons. J. Gen. Physiol. 58, 413-437.

Armstrong, C.M. (1975a). Potassium pores of nerve and muscle membranes. In: Membranes--A series of Advances, Vol. 3, Artificial and Biological Membranes. (Ed. Eisenman, G.), Dekker, New York, Chapter 5.

Armstrong, C.M. (1975b). Ionic pores, gates and gating currents. Quart. Rev. Biophys. 7, 179-210.

Armstrong, C.M. and Hille, B. (1972). The inner quaternary ammonium receptor in potassium channels of the node of Ranvier. J. Gen. Physiol. 59, 388-400.

Bamberg, E. and Lauger, P. (1973). Channel formation kinetics of gramicidin A in lipid bilayer membranes. J. Membrane Biol. 11, 177-194.

Bamberg, E. and Lauger, P. (1974). Temperature-dependent of gramicidin A channels. Biochim. Biophys. Acta 367, 127.

Bamberg, E. and Lauger, P. (1977). Blocking of the Gramicidin Channel by divalent cations. J. Memb. Biol. 35. 351-375.

Barry, P.H. and Adrian, R.H. (1973). Slow conductance changes due to potassium depletion in the transverse tubules of frog muscle fibers during hyperpolarizing pulses. J. Membrane Biol. 14, 243-292.

Beaty, G.N. and Stefani, E. (1976). Calcium dependent electrical activity in twitch muscle fibers of the frog. Proc. R. Soc. Lond. B. 194, 141-150.

Benson, S.W. (1960). The foundations of chemical kinetics. McGraw-Hill Book Co., Inc., New York.

Bezanilla, F. and Armstrong, C.M. (1972). Negative conductance caused by entry of sodium and cesium ions into the potassium channels of squid axons. J. Gen. Physiol. 60, 588-608.

Boyle, P.J. and Conway, E.J. (1941). Potassium accumulation in muscle and associated changes. J. Physiol. 100, 1-63.

Cahalan, M. and Begenisich, T. (1976). Sodium channel selectivity: Dependence on internal permeant ion concentration. J. Gen. Physiol. 68, 111-125.

Caldwell, P.C. (1956). Intracellular pH. In: Intern. Review of Cytology, edited by G.H. Bourne and J.F. Danielli. New York: Academic, Vol. V. pp. 229-277.

Caldwell, P.C. (1958). Studies on the internal pH of large muscle and nerve fibres. J. Physiol. 142, 22-62.

Chandler, W.K. and Meves, H. (1964a). Voltage-clamp experiments on internally perfused giant axons. J. Physiol. 180, 788-820.

Chandler, W.K. and Meves, H. (1965b). Ionic selectivity in perfused giant axons. J. Cell. Comp. Physiol. pt. 2, 66, 65-70.

Chandler, W.K. and Schneider, M.F. (1976). Time-course of potential spread along a skeletal muscle fiber under voltage clamp. J. Gen. Physiol. 67, 165-184.

Ciani, S. (1965). A rate theory analysis of steady diffusion in a fixed charge membrane. Biophysik 2, 368-375.

Cole, K.S. (1968). Membranes, Ions and Impulses. University of California Press, Berkeley, 1968.

Colquhoun, D., Rang, H.P. and Ritchie, J.M. (1974). The binding of tetrodotoxin and bungarotoxin to normal and denervated mammalian muscle. J. Physiol. 240, 199-226.

Eaton, D.C. and Brodwick, M.S. (1978). Barium block of potassium currents. Biophys. J. 21, no. 3. 164a.

Edwards, C., Harris, E.J. and Nishie, K. (1957). The exchange of frog muscle Na and K in the presence of anions Br^-, NO_3^-, and CNS^-. J. Physiol. 135, 560.

Eisenman, G. (1961). On the elementary atomic origin of equilibrium ionic specificity. In: Membrane Transport and Metabolism, ed. Kleinzeiler, A. and Kotyk, A. Acad. Press, London, p. 163.

Eisenman, G., Sandblom, J. and Neher, E. (1976). Ionic selectivity, saturation, binding, and block in the gramicidin A channel: A preliminary report. In: 9th Jerusalem Symposium on Metal-Ligand interactions in Organic and Biochemistry. B. Pullman, editor.

Eisenman, G., Sandblom, J. and Neher, E. (1978). Interactions in cation permeation through the Gramicidin channel. Cs, Rb, K, Na, Li, Tl, H and effects of anion binding. Biophys. J. 22, 2. 307-340.

Eisenman, G., Sandblom, J.P. and Walker, J.L. Jr. (1967). Membrane structure and ion permeation. Science vol. 155, 965-974.

Falk, G. and Fatt. P. (1964). Linear electrical properties of striated muscle fibres observed with intracellular electrodes. Proc. Roy. Soc. B. 160, 69-123.

Fatt, P. (1964). An analysis of the transverse electrical impedance of striated muscle. Proc. Roy. Soc. B. 159, 606-651.

Fatt, P. and Katz, B. (1951). An analysis of the end-plate potential recorded with an intracellular electrode. J. Physiol. 115, 320-370.

Fenn, W. (1936). Electrolytes in muscle. Physiol. Rev. 16: 450-487.

Fishman, S.N., Chodorov, B.I. and Volkenstein,M.V. (1971). Molecular mechanisms of membrane ionic permeability changes. Biochim. Biophys. Acta 225, 1-10.

Frankenhaeuser, B. (1960). Sodium permeability in toad nerve and in squid nerve. J. Physiol. 152, 159-166.

Frehland, E. and Lauger, P. (1974). Ion transport through pores: Transient phenomena. J. Theor. Bio. 47, 189-207.

French, R.J. and Adelman, W.J. Jr. (1976). Competition; saturation and inhibition--ionic interactions shown by membrane ionic currents in nerve, muscle, and bilayer systems. In: Current Topics in Membranes and Transport. Vol. 8, 1976. Ed. Broneer, F. and Kleinzeller, A. Academic Press, New York.

Gage, P.W. and Eisenberg, R.S. (1969a). Capacitance of the surface and transverse tubular membrane of frog sartorius muscle fibers. J. Gen. Physiol. 53, 265-278.

Gay, L.A. and Stanfield, P.R. (1977). Cs^+ causes a voltage-dependent block of inward K currents in resting skeletal muscle fibres. Nature vol. 267, 169-170.

Glasstone, S., Laidler, K.J. and Eyring, H. (1941). The theory of rate processes. New York: McGraw-Hill.

Goldman, D. (1943). Potential, impedance and rectification in membrane. J. Gen. Physiol. 27, 37-60.

Goldman, D.E. (1964). A molecular structural basis for the excitation properties of axons. Biophys. J. 4, 167-188.

Goldman, D.E. (1965). Gate control of ion flux in axons. J. Gen. Physiol. 48, 75-79.

Hagiwara, S. and Takahashi, K. (1967). Surface density of calcium ions and calcium spikes in the barnacle muscle fiber membrane. J. Gen. Physiol. 50, 583-601.

Hagiwara, S., Toyama, K., and Hayashi, H. (1971). Mechanisms of anion and cation permeations in the resting membrane of a barnacle muscle fiber. J. Gen. Physiol. 57, 408-434.

Hall, J.E., Mead, C.A., and Szabo, G. (1973). A barrier model for current flow in lipid bilayer membranes. J. Memb. Biol. 11, 75-97.

Harris, E.J. (1958). Anion interaction in frog muscle. J. Physiol. 141, 351-365.

Harris, E.J. (1963). Distribution and movement of muscle chloride. J. Physiol. 166, 87-109.

Harris, E.J. (1965). The chloride permeability of frog sartorius. J. Physiol. 176, 123-135.

Haydon, D.A. and Hladky, S.B. (1972). Ion transport across thin lipid membranes: A critical discussion of mechanisms in selected systems. Q. Rev. Biophys. 5, 187-282.

Heckmann, K. (1972). Single file diffusion. Biomembranes 3, 127-153.

Heckmann, K., Lindemann, B. and Schnakenberg, J. (1972). Current-voltage curves of porous membranes in the presence of pore-blocking ions. I. Narrow pores containing no more than one moving ion. Biophys. J. 12, 683-702.

Hestenes, J.D. and Woodbury, J.W. (1972). Anomalous position of fluoride in the halide conductance of frog sartorius muscle membrane. The Physiologist 15, 166.

Hestenes, J.D. and Woodbury, J.W. (1973). Anion binding to anion channels of frog sartorius: Estimates of dissociation constants. Abstr. Biophys. Soc., 17th Ann. Meeting, 243a.

Hill, A.V. (1955). The influence of the external medium on the internal pH of frog muscle. Proc. R. Soc. B. 144, 1-22.

Hill, T.L. (1966). Studies in irreversible thermodynamics:IV. Diagrammatic representations of steady state fluxes for unimolecular systems. J.Theor. Biol. 10, 442-460.

Hille, B. (1970). Ionic channels in nerve membranes. Progress in Biophys. Molec. Biol. 21, 1-32.

Hille, B. (1971). The permeability of the sodium channel to organic cations in myelinated nerve. J. Gen. Physiol. 58, 599-619.

Hille, B. (1975a). Ionic selectivity of Na and K channels of nerve membranes. In: Membranes--A series of Advances, Vol. 3, Artificial and Biological Membranes, ed. Eisenman, G., Dekker, New York, Chapter 4. pp. 255-323.

Hille, B. (1975b). Ionic sensitivity, saturation, and block in sodium channels. A four-barrier model. J. Gen. Physiol. 66, 535-560.

Hille, B., Woodhull, A.M. and Shapiro, B.I. (1975). Negative surface charge near sodium channels of nerve: divalent ions, monovalent ions, and pH. Phil. Trans. Roy. Soc. Biol. 270, 301-318.

Hille, B. and Schwarz, W. (1978). K channels of nerve and muscle: Single file, multi-ion pores. Biophys. J. Vol. 21, no. 3, 164a.

Hladky, S.B. (1965). The single file model for the diffusion of ions through a membrane. Bull. Math. Biophys. 27, 79-86.

Hladky, S.B. and Harris, J.D. (1967). An ion displacement membrane model. Biophys. J. 7, 535-543.

Hladky, S.B. and Haydon, D.A. (1972). Ion transfer across lipid membranes in the presence of gramicidin A. I. Studies of the unit conductance channel. Biochim. Biophys. Acta. 274: 294-312.

Hober, R. (1904). Uber den Einfluss der Salze auf den Ruhestrom des Froschmuskels. Pflugers Arch, ges. Physiol. 106, 599-635.

Hodgkin, A.L. and Horowicz, P. (1959). The influence of potassium and chloride ions on the membrane potential of single muscle fibers. J. Physiol. 148, 127-160.

Hodgkin, A.L. and Horowicz, P. (1960a). The effect of sudden changes in ionic concentration on the membrane potential of single muscle fibres. J. Physiol. 153, 370-385.

Hodgkin, A.L. and Huxley, A.F. (1952). A quantitative description of membrane current and its application to conduction and excitation in nerve. J. Physiol. 117, 500-544.

Hodgkin, A.L. and Katz, B. (1949). The effect of sodium ions on the electrical activity of giant axon of the squid. J. Physiol. 108, 37-77.

Hodgkin, A.L. and Keynes, R.D. (1955). The potassium permeability of a giant nerve fibre. J. Physiol. 128, 61-88.

Hope, A.B. (1971). Ion transport and membranes. University Park Press, Baltimore. 1971.

Horowicz, P. (1964). The effects of anions on excitable cells. Pharmac. Rev. 16, 193-221.

Hoyt, R.C. (1963). The squid giant axon: Mathematical models. Biophys. J. 3: 399-431.

Hutter, O.F., deMello, W.C. and Warner, A.E. (1969). An application of the field strength theory. In: Molecular basis of membrane function, ed. D.C. Tosteson, pub. Prentice-Hall, 391-400.

Hutter, O.F. and Noble, D. (1960). The chloride conductance of frog skeletal muscle. J. Physiol. 151, 89-102.

Hutter, O.F. and Padsha, S.M. (1959). Effect of nitrate and other anions on the membrane resistance of frog skeletal muscle. J. Physiol. 146, 117-132.

Hutter, O.F. and Warner, A.E. (1967a). The pH sensitivity of the chloride conductance of frog skeletal muscle. J. Physiol. 189, 403-425.

Hutter, O.F. and Warner, A.E. (1967b). The effect of ^{36}Cl from skeletal muscle. J. Physiol. 189, 427-443.

Hutter, O.F. and Warner, A.E. (1967c). Action of some foreign cations and anions on the chloride permeability of frog muscle. J. Physiol. 189, 445-460.

Hutter, O.F. and Warner, A.E. (1972). The voltage dependence of the chloride conductance of frog muscle. J. Physiol. 227, 275-290.

Jain, M.K., Marks, H.L. and Cordes, E.H. (1970). Kinetic model of conduction changes across excitable membranes. Proc. Natl. Acad. Sci., U.S.A. 67, 799-806.

Johnson, F.H., Eyring, H. and Polissar, M.I. (1954). The kinetic basis of molecular biology, Chapter 14, John Wiley and Sons, Inc., New York.

Katz, B. (1948). The electrical properties of the muscle fibre membrane. Proc. R. Soc. B. 135, 506-534.

Keynes, R.D., Ritchie, J.M. and Rojas, E. (1971). The binding of tetrodotoxin to nerve membrane. J. Physiol. 213, 235-254.

King, E.L. and Altman, C. (1956). A schematic method of deriving the rate laws for enzyme-catalyzed reactions. J. Phys. Chem. 60, 1375-1381.

Knauf, P.A. and Rothstein, A. (1971). Chemical modification of membranes. I. Effects of sulfhydryl and amino reactive reagents on anion and cation permeability of the human red blood cell. J. Gen. Physiol. 58, 199-210.

Kostyuk, P.G. and Sorokina, Z.A. (1960). On the mechanism of hydrogen ion distribution between cell protoplasm and the medium. In: Membrane Transport and Metabolism, edited by A. Kleinzeller and A. Kotyk. New York: Academic, 1960. pp. 193-203.

Krasne, S., Eisenman, G. and Szabo, G. (1971). Freezing and melting of lipid bilayers and the mode of action of nonactin, valinomycin, and gramicidin. Science 174, 412.

Krawczyk, S. (1978). Ionic channel formation in a living cell membrane. Nature vol. 273, 56-57.

Laprade, R., Cian, S.M., Eisenman, G. and Szabo, G. (1974). The kinetics of carrier-mediated ion permeation in lipid bilayers and its theoretical interpretation. In: Membranes--A series of Advances, Vol. 3, G. Eisenman, Editor, Marcel Kekker, New York.

Latorre, R., Alvarez, O., Ehrenstein, G., Espinoza, M. and Reyes, J. (1975). The nature of the voltage-dependent conductance of the hemocyanin channel. J. Memb. Biol. 25, 163-182.

Lauger, P. and Stark, G. (1970). Kinetics of carrier-mediated ion transport across lipid bilayer membranes. Biochim. Biophys. Acta. 211 (1970) 458-466.

Lauger, P. (1972). Carrier-mediated ion transport. Science 178, 24.

Lauger, P. (1973). Ion transport through pores: A rate-theory analysis. Biochim. Biophys. Acta. 311, 423-441.

Macey, R.I. and Oliver, R.M. (1967). The time dependence of single file diffusion. Biophys. J. 7, 545-554.

Mathias, R.T., Eisenberg, R.S. and Valdiosera, R. (1977).
Electrical properties of frog skeletal muscle fibers interpreted
with a mesh model of the tubular system. Biophys. J. Vol. 17,
57-93.

Michaelis, L. (1926). Die Permeabilitat von Membranen.
Naturwissenschaften, 3, 33-42.

Moore, J.W. and Cox, E.B. (1976). A kinetic model for the sodium
conductance system in squid axon. Biophys. J. Vol. 16, 171-
192.

Moore, L.E. and Jakobsson, E. (1971). Interpretation of sodium
permeability changes of myelinated nerve in terms of linear
relaxation theory. J. Theor. Biol. 33, 77-89.

Moore, L.E. (1969). Anion permeability of frog skeletal muscle.
J. Gen. Physiol. 54, 33-52.

Nakajima, S. and Bastian, J. (1974). Double sucrose-gap method
applied to single muscle fiber of Xenopus laevis. J.
Gen. Physiol. 63, 235-256.

Neher, E. and Stevens, C.F. (1977). Conductance fluctuations
and ionic pores in membranes. Ann. Rev. Biophys. Bioeng.
6, 345-381

Nernst, W. (1889). Die elektromotorische Wirksamkert der Ionen.
Z. Physik. Chem. 4: 129-181.

Neumcke, B. and Lauger, P. (1969). Nonlinear electrical effects
in lipid bilayer membranes. II. Integration of the generalized
Nernst-Planck equations. Biophys. J. 9, 1160.

Palade, P.T. and Barche , R.L. (1977). Characteristics of the
chloride conductance in muscle fibers of the rat diaphragm.
J. Gen. Physiol. 69, 325-342.

Palti, Y., Ganot, G. and Stampfli, R. (1976). Effect of conditioning
potential on potassium current kinetics in the frog node.
Biophys. J. 16, 261-273.

Parker, M.G. and Woodbury, J.W. (1976). Titratable sites of Cl^-
channels of frog muscle are near the outside of the membrane.
Biophys. J. 16, 157a.

Parlin, B. and Eyring, H. (1954). Membrane permeability and
electrical potential In: Ion Transport Across Membranes
(Clarke, H.T., Ed.). pp.103-118, Academic Press, New York.

Planck, M. (1890). Uber die Erregung von Elektricitat und
    Warme in Elektrolyten. Ann. Physik. Chem. 39: 161-186.

Russel, J.M. and Brodwick, M.S. (1976). Chloride fluxes in
    the dialyzed barnacle muscle fiber and the effect of SITS.
    Biophys. J. 16, 156a.

Sandblom, J., Eisenman, G. and Neher, E. (1977). Ionic selectivity,
    saturation and block in gramicidin A channels. I. Theory
    for the electrical properties of ion selective channels
    having two pairs of binding sites and multiple conductance
    states. J. Memb. Biol. 31, 383-417.

Sandblom, J., Eisenman, G. and Walker, Jr., J.L. (1967). Electrical
    phenomena associated with the transport of ions and ion pairs
    in liquid ion-exchange membranes. I. Zero current properties.
    J. Phys. Chem. 71, 3862.

Schneider, M.F. (1970) Linear electrical properties of the
    transverse tubules and surface membrane of skeletal muscle
    fibers. J. Gen. Physiol. 56, 640.

Schragina, L.V., Grinfeldt, A.E. and Lev, A.A. (1978). Interaction
    of cation fluxes in gramicidin A channels in lipid bilayer
    membranes. Nature. vol. 273, 243-245.

Seshadri, M.S. (1971). Evolution towards steady state in membrane
    transport problems. J. Theor. Biol. 31, 245-253.

Singer, S.I. and Nicholson, G.L. (1972). The fluid mosaic model
    of the structure of cell membranes. Science 175, 720-731.

Sperelakis, N. and Schneider, M. (1968). Membrane ion conductance
    of frog sartorius fibres as a function of tonicity. Am. J.
    Physiol. 215, 723-729.

Spurway, N.C. (1971). Mechanisms of anion permeation. In::
    Biomembranes, Vol.3, Passive Permeability of Cell Membranes,
    Ed. Kreuzer, F. and Slegers, J.F.G., Plenum Publ. Corp.,
    N.Y. pp. 363-380.

Startk, G. (1973) Rectification phenomena in carrier-mediated
    ion transport. Biochim. Biophys. Acta, 298, 323-332.

Stephens, C.F. (1978). Interactions between intrinsic membrane
    protein and electric field. An approach to studying nerve
    excitability. Biophys. J. 22, 295-307.

Stephenson, R.A. and Woodbury, J.W. (1976). Cl^- channels of frog
    muscle: conductance and binding constant vary similarly with
    temperature. Biophys. J. 16, 157a.

Teorell, T. (1953). Transport processes and electrical phenomena in ionic membranes. Progress in Biophys. Molec. Biol. 3, 351-375.

Valdiosera, R., Clausen, C. and Eisenberg, R.S. (1974a). Measurement of the impedance of frog skeletal muscle fibers. Biophys. J. 14, 295-315.

Valdiosera, R., Clausen, C. and Eisenberg, R.S. (1974b). Circuit models of the passive electrical properties of frog skeletal muscle fibers. J. Gen. Physiol. 63, 432-459.

Valdiosera, R., Clausen, C. and Eisenberg, R.S. (1974c). Impedance of frog skeletal muscle fibers in various solutions. J. Gen. Physiol. 63, 460-491.

Vaughan, P.C. (1975). Muscle membrane. Prog. Neurobiol. 3, 217-250.

Vaughan, P.C. and Fong, C.N. (1978). Effect of SITS on chloride permeation in Xenopus laevis. Can. J. Physiol. Pharm. (in press).

Venosa, R.A., Ruarte, A.C. and Horowicz, P. (1972). Chloride and potassium movements from frog's sartorius muscle in the presence of aromatic anions. J. Mem. Biol. 9, 37-56.

Waddel, W.J. and Bates, R.G. (1969). Intracellular pH. Physiol. Rev. 49, 285-329.

Warner, Anne E. (1972). Kinetic properties of the chloride conductance of frog muscle. J. Physiol. 227, 291-312.

Woodbury, J.W. (1971). Eyring rate theory model of the current-voltage relationships of ion channels in excitable membranes. In: Chemical Dynamics: Papers in Honor of Henry Eyring. Hirschfelder , J.O. and Henderson,D. ed. Advances in Chemical Physics. Vol 21, 601-617.

Woodbury, J.W. and Miles, P.R. (1973). Anion conductance of frog muscle membranes: one channel, two kinds of pH dependence. J. of Gen. Physiol. 62, 324-353.

Woodhull, Anne M. (1973). Ionic blockage of sodium channels in nerve. J. Gen. Physiol. 61, 687-708.

Wright, E.M. and Diamond, J.M. (1977). Anion selectivity in biological systems. Physiol. Rev. 57, 109-156.

Zwolinski, B.J. , Eyring, H. and Reese, C.E. (1949). Diffusion
and membrane permeability. J. Phys. Chem. 53, 1426-1453.

Appendix

The objective of this appendix is to describe in more detail, the interpretation of membrane current measurements using the three-microelectrode voltage clamp technique.

Electrically, the equivalent circuit of the muscle membrane is a complex branching distributive network (Falk and Fatt, 1964; Fatt, 1964; Schneider, 1970; Valdiosera et al, 1974a, b,c; Mathias et al, 1977). The complexity arises from the geometry of the transverse tubular system, which have has successively been modelled by a lumped RC (parallel resistance and capacitance) network (Fatt and Katz, 1951; Falk and Fatt, 1964); distributive disk (Falk and Fatt, 1964; Fatt, 1964; Adrian, Chandler and Hodgkin, 1969; Schneider, 1970; Valdiosera et al, 1974a,b,c) and mesh model (Mathias et al, 1977). In this appendix, we will use the disc model for illustration in the interpretation of the membrane current from 3 micro-electrode voltage clamp.

The electrical parameters of the muscle membrane, viewed as a 3 dimensional cylindrical cable (Fig.A1) are:

R_m = resistance in cm^2 of surface membrane

    = G_m^{-1} , G_m is the conductance in mho.cm^{-2}.

C_m = capacitance in Fcm^{-2} of surface membrane.

R_i = sarcoplasmic resistivity in Ωcm.

G_w = conductance of the walls of the tubular membrane (in mho.cm^{-2}).

C_w = capacity of the walls of the tubular membrane (F.cm^{-2}).

G_L = luminal resistivity of the T-system (Ω.cm).

I_m = membrane current density (Amp.cm^{-2}).

Let a be the fiber radius and b the radius of the lumen of the

T-system. The three dimensional parameters are reduced to one dimensional

parameters via the relations:

$$r_m = R_m(2\pi a)^{-1}$$

$\qquad$ = resistivity of the membrane (Ωcm)

$\qquad$ = g_m^{-1} (g_m is the membrane conductance(mho.cm^{-1}).

$$c_m = (2\pi a)C_m$$

$\qquad$ = membrane capacitance (Fcm^{-1})

$$r_i = R_i(2\pi a)^{-1}$$

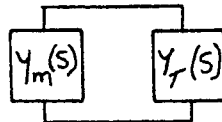$\qquad$ sarcoplasmic resisitivity (Ωcm^{-1})

$g_w = G_w(2\pi b)$ = conductance of the walls of the T-system (mho.cm^{-1})

$c_w = C_w(2\pi b)$ = tubular membrane capacitance (Fcm^{-1}).

$g_L = G_L(2\pi b)^{-1}$ = luminal resistivity of the T system in Ωcm^{-1}.

$i_m = I_m(2\pi a)$ = membrane current density (Amp.cm^{-1}).

Let Y(s) be the inside-outside admittance per cm^2 of membrane.

Y(s) is the parallel sum of the surface admittance $Y_m(s)$ and the

tubular admittance $Y_T(s)$, Y(s)=$Y_m(s)$ + $Y_T(s)$.

$\qquad$ $Y_m(s)$ = surface admittance per cm^2 of membrane. It is modeled by a

parallel RC network, $Y_m(s)= g_m + c_m s$.

$Y_T(s)$ = contribution to the membrane admittance per cm^2 from

transverse tubular system. This admittance will be taken to be

of the form (Schneider, 1970; Adrian, Chandler and Hodgkin,

1969; Valdiosera et al, 1974a, b,c)

$$Y_T(s) = \frac{G_L I_1(a/\lambda_T(s))}{\lambda_T(s) I_0(a/\lambda_T(s))}$$

where

$$a/\lambda_T(s) = a((g_w + sc_w)/g_L)^{-1/2}$$

I_0 and I_1 are the modified Bessel functions of the first kind. The resistivity of the extracellular fluid is usually assumed to be negligible.

In the domain of the Laplace transformed variable s, the cable equation is :

$$\frac{d^2 V(x,s)}{dx^2} - r_i Y(s) V(x,s) = 0$$

and the transformed boundary condition (no axial current at the end of the fiber, x=0)

$$\frac{dV(x,s)}{dx}\bigg|_{x=0} = 0$$

The other boundary condition is obtained by assuming that at the voltage (clamp) control position (see Fig.1.1).

$$V(\ell,t) = V(\ell)H(t)$$

H is the Heaviside function; $V(\ell)$ is the command or membrane potential at x= ℓ.

The solution for the voltage profile V(x,t) is:

(1) $$V(x,t) = \mathcal{L}^{-1}\left\{\frac{V(\ell)}{s} \frac{\cosh x (r_i Y(s))^{1/2}}{\cosh \ell (r_i Y(s))^{1/2}}\right\}$$

$\mathscr{L}^{-1}$ is the inverse Laplace transform operator.

Hence the difference in voltage between the electrodes at A and B (Fig.1.1) is

(2) $\qquad V(t) = V(2\ell,t)-V(\ell,t) = \mathscr{L}^{-1}\left\{\dfrac{V(\ell)}{s}\dfrac{\cosh2\ (r_iY(s))^{1/2}}{\cosh\ \ell(r_iY(s))^{1/2}} - 1\right\}$

Steady state measurements

In the steady state, the difference between the electrodes at A and B (Fig.1.1) is:

(3) $\qquad \Delta V(\infty) = V(\ell)\left\{\dfrac{\cosh2\ell(r_iY(0))^{1/2}}{\cosh\ \ell(r_iY(0))^{1/2}} - 1\right\}$

Under conditions of experimental interest, the tubular membrane conductance g_w is the sum of the tubular wall ionic conductances for sodium g_{Na}^w , potassium g_K^w and chloride g_{Cl}^w : $g_w = g_{Na}^w + g_K^w + g_{Cl}^w$.

$g_{Na}^w = 0$ because Tetrodotoxin was present in the experimental solutions, and g_K^w was negligible because rubidium replaced potassium and rubidium conductance is low. Experimental evidence (Hodgkin and Horowicz, 1959, 1960a; Eisenberg and Gage, 1969a,b) have indicated that there is no chloride conductance within the transverse tubular system $g_{Cl}^w=0$. Therefore, in the steady state, there is no contribution to the total membrane admittance from the transverse tubular system, and we have:

(4) $\qquad \Delta V(\infty) = V(\ell)\left\{\dfrac{\cosh\ 2\ell(r_ig_m)^{1/2}}{\cosh\ \ell(r_ig_m)^{1/2}} - 1\right\}$

At the command potential position x= ℓ (at A, Fig.1.1) the membrane conductance $i_m(\ell) = g_m V(\ell)$ and since $r_i g_m = 1/\lambda^2$, we have from equation (4):

$$i_m(\infty) = \Delta V(\infty) \frac{1}{r_i \lambda^2} \left\{ \frac{\cosh(\ell/\lambda)}{\cosh(2\ell/\lambda) - \cosh(\ell/\lambda)} \right\}$$

$$= (2/3 r_i \ell) \Delta V(\ell) (1 + \bigcirc (\ell/\lambda)^2)$$

If the (one dimensional) sarcoplasmic resistivity r_i is converted to R_i, via $R_i = \pi (d/2)^2 r_i$, where d is the fiber diameter, then

(5) $$i_m(\ell) = \frac{d^2}{6 R_i \ell^2} V(\ell) (1 + \bigcirc (\ell/\lambda)^2)$$

and since $I_m = i_m/\pi d$, we have equation (1) of Chapter I.

$$I_m = \frac{d}{6 R_i \ell^2} \Delta V(\infty) (1 + \bigcirc (\ell/\lambda)^2)$$

Transient properties

Analytical expressions for the transient problem (equation 1) have not been obtained. Adrian, Chandler and Hodgkin, 1970a and Chandler and Schneider, 1976 have obtained analytical solutions by discretizing the tubular model.

A rough estimate of the time required to charge the membrane capacitance network may be obtained by assuming a lumped parameter parallel RC model with $C_m = (2-3)$ F.cm^{-2} (Vaughan, 1975) and $R = G_{Cl}^{-1}$ $= 10^3 \Omega cm^2$ then the time constant is (2-3) milliseconds.

Figure A1 Diagrammatic representation of muscle fiber
and the electrical parameters defined in
the Appendix.

surface parameters

tubular system parameters